NTNU – Trondheim
Norwegian University of
Science and Technology

Vortex Induced Vibrations of Marine Risers

Geir Magnus Knardahl

Marine Technology
Submission date: June 2012
Supervisor: Carl Martin Larsen, IMT
Co-supervisor: Jo-Inge Sandell, Aker Solutions
Øystein Wærstad, Aker Solutions

Norwegian University of Science and Technology
Department of Marine Technology

M.Sc. thesis 2012

for

Stud.tech. Geir Magnus Knardahl

VORTEX INDUCED VIBRATIONS OF MARINE RISERS

(Virvelindusert respons i marine stigerør)

Vortex induced vibrations (VIV) have been studied experimentally at MARINTEK/NTNU for more than a decade. One result of this effort is the computer program VIVANA that can calculate fatigue damage caused by VIV for slender structures, and also find the influence from VIV on the global geometry of a system. The program is well suited for analysis of marine risers, anchor lines, umbilicals and free spanning pipelines. Modelling capabilities include varying riser diameter as seen in a stress joint, and also strakes for reduction of VIV.

The purpose of this project is to apply VIVANA to investigate various aspects of VIV for workover risers and drilling risers on very deep waters.

Interesting aspects of VIV for workover risers include:

- The significance of VIV for "open water workover risers" relative to "in-marine workover risers"
- The effect on VIV from variation of external diameter
- The influence on static shape of the riser caused by drag amplification, and consequences for stresses and forces in stress joint and wellhead
- Possible operational consequences from VIV

The following aspects of VIV for deepwater drilling risers should be considered:

- Varying diameter of buoyancy joints
- Use of helical strakes
- Influence on end angles from drag amplification
- VIV during installation of drilling risers

The work should be carried out in steps as follows:

1. Literature study has to some extent been reported in the pre-project report, but features like drag amplification and modelling of strakes in VIVANA need to be discussed.
2. Identify data for workover and drilling risers for use in the study.
3. Carry out case studies for investigation of consequences from VIV for selected current conditions for workover and drilling risers.

The work may show to be more extensive than anticipated. Some topics may therefore be left out after discussion with the supervisor without any negative influence on the grading.

The candidate should in her/his report give a personal contribution to the solution of the problem formulated in this text. All assumptions and conclusions must be supported by mathematical models and/or references to physical effects in a logical manner.

The candidate should apply all available sources to find relevant literature and information on the actual problem.

The report should be well organised and give a clear presentation of the work and all conclusions. It is important that the text is well written and that tables and figures are used to support the verbal presentation. The report should be complete, but still as short as possible.

The final report must contain this text, an acknowledgement, summary, main body, conclusions and suggestions for further work, symbol list, references and appendices. All figures, tables and equations must be identified by numbers. References should be given by author name and year in the text, and presented alphabetically by name in the reference list. The report must be submitted in two copies unless otherwise has been agreed with the supervisor.

The supervisor may require that the candidate should give a written plan that describes the progress of the work after having received this text. The plan may contain a table of content for the report and also assumed use of computer resources.

From the report it should be possible to identify the work carried out by the candidate and what has been found in the available literature. It is important to give references to the original source for theories and experimental results.

The report must be signed by the candidate, include this text, appear as a paperback, and - if needed - have a separate enclosure (binder, DVD/ CD) with additional material.

Supervisor at NTNU is Professor Carl M. Larsen

Trondheim, January 2012

Carl M. Larsen

Submitted:	16 January 2012
Deadline:	10 June 2012

Preface

This report is the result of my Master's Thesis for 5th year students at the Norwegian University of Science and Technology at department for Marine Technology, spring 2012.

The motivation for first writing the Project Thesis and later the Master's Thesis on the subject of Vortex Induced Vibrations (VIV) came from a summer internship at Aker Solutions, Department of Workover Systems the summer of 2011. A VIV analysis is one part of the global riser analysis that are executed and reported for each workover system that Aker Solutions produce.

The approach to describing the problems and interesting aspects of the topic was outlined by my advisor at NTNU.

First and foremost I would like to thank my advisor, Professor Carl Martin Larsen at the Department of Marine Technology, NTNU, for excellent follow-up and insight on the topic. I would also like to thank Jo-Inge Sandell and Øystein Wærstad for making the information used as basis in the thesis analysis accessible for me to use in my Master's Thesis.

Oslo, June 4, 2012

Geir Magnus Knardahl

Summary

This Master's Thesis goal is to present fundamental physical aspects of Vortex Induced Vibrations (VIV) of marine risers, and outline methods for suppression of VIV. Main emphasis has been given to the use of strakes, and relevant theories connected to strakes' influence on excitation of riser, riser response and drag is presented. Variation of outer diameter of the riser is also studied.

The theory has been put to test through case studies of two Aker Solutions in-marine workover systems of 321 and 1300 m water depth. The computer program VIVANA has been used. Several analyses have been performed for various different riser configurations. For the 321 m water system, the following configurations have been studied:

- Base configuration, i.e. no use of strakes
- Staggered configuration, staggered bare and buoyant joints
- Bottom strakes configuration, bottom section of riser covered with strakes
- Middle strakes configuration, middle section of riser covered with strakes
- Top strakes configuration, top section of riser covered with strakes

For the 1300 m water depth system, the following configurations have been evaluated:

- Base configuration, i.e. no use of strakes
- Staggered configuration, staggered bare and buoyant joints
- Middle strakes configuration, middle section of riser covered with strakes
- Top 50_150 strakes configuration, top 150 m of riser bare, then coverage of strakes
- Top stakes configuration, top section of riser covered with strakes

For each water depth a total of 4 different current profiles have been applied. The current profiles include both measured current profiles from the relevant oil fields, as well as several other more "theoretical" current models.

The main findings from the 321 m analyses were:

- Staggered configuration gives generally lower VIV amplitudes of the dominating frequency compared to base configuration.
- Staggered configuration gives generally lower maximum stress amplitudes compared to base configuration.
- No clear trends when comparing fatigue life of staggered and base configuration are found, however significantly better fatigue results found for the staggered configuration in measured current.
- Maximum accumulated damage is located at the WH/XMT interface.
- Top and middle strakes configurations give best VIV suppression results.
- Applying strakes to the top section of the riser gives significantly lower VIV amplitudes, stress amplitudes and higher fatigue lives across all current profiles.
- Top strakes configuration supress VIV completely for the sheared current profile.
- Very small riser deflections and corresponding low flex joint angles are found; thus no operational consequences for the 321 m water depth.

The main findings from the 1300 m analyses were:

- A significant increase in active response frequencies compared to the 321 m water depth, more than 30 active frequencies calculated.
- No clear trends in VIV amplitudes of the dominating frequency when comparing staggered and base configuration.
- Highest stress amplitudes found for the base configuration in all current profiles.
- No clear trends in calculated fatigue life when comparing the staggered and base configurations. Maximum accumulated damage found in the WH/BOP interface.
- Top 50_150 strakes configuration the most efficient in suppressing VIV.
- Significantly lower VIV amplitudes of the dominating response frequency for the top 50_150 strakes configuration. Same result found for the maximum stress amplitudes.
- Compared to the base configuration significantly better fatigue lives found for the top 50_150 strakes configuration, however for the measured current profile an increase of only 1 decade was found.
- Staggered configuration gives lowest static riser deflection for all current profiles, also after drag amplification from VIV.
- Percentage increase in riser deflection from VIV reduced by roughly 80% when comparing the top 50_150 base configuration to the base configuration.
- LFJ angles exceeded lower limits for certain drilling and workover operations, however applying the top 50_150 strakes configuration will generally give a larger operational window compared to the base configuration.

Some of the results from the 1300 m analyses revealed certain discrepancies linked to the dominating frequencies and frequencies inducing maximum stress amplitudes. These inconsistencies are probably related to the convergence limit given as input in the VIVANA module.

Table of Contents

Preface ... **iii**

Summary ... **v**

Table of figures ... **xii**

List of tables ... **xiv**

List of equations ... **xviii**

Abbreviations ... **xix**

Non-dimensional parameters ... **xx**

1 Introduction ... **1**

1.1 Motivation ... 1

1.2 Purpose and scope ... 2

Part I: Theory ... **3**

2 Short on Workover operations ... **3**

2.1 Category A – Riser less workover (light workover) ... 3

2.2 Category B – Riser well intervention ... 4

2.3 Category C – Workover using a marine riser ... 5

3 General notes on Vortex Induced Vibrations ... **7**

3.1 Current VIV analysis programs and models ... 7

4 Fundamental aspects of VIV ... **9**

4.1 Reynolds number and Strouhal number ... 9

4.2 Flow around a cylinder ... 10

4.3 In-line and cross-flow forces ... 12

4.4 Free oscillation test, added mass and response frequency ... 12

5 VIVANA ... **17**

5.1 Energy balance, CL, added mass and Strouhal number in VIVANA ... 17

5.2 Analysis method ... 19

6 Preventing VIV ... **21**

6.1 Changes to riser structural properties ... 21

6.2 VIV suppression devices ... 22

6.2.1 Radial water jet suppression ... 22

6.2.2 Other VIV suppression devices ... 23

6.3 Strakes ... 27

6.3.1 Short background ... 27

6.3.2 Function ... 27

6.3.3 Configuration 28
6.3.4 Coverage density 28
6.3.5 Pros and cons 30
6.3.6 Strakes in VIVANA 34
7 Drag forces 37
7.1 Static drag force on a fixed circular cylinder 37
7.2 Drag amplification from VIV 39
7.3 Drag amplification consequences 40
8 Methodology 43
8.1 Standards 43
8.1.1 ISO 13628 43
8.1.2 DNV-RP-C205 44
8.1.3 DNV-RP-F204 44
8.1.4 API RP 2RD 46
8.1.5 Concluding remarks on the presented standards 47
8.2 Literature review 47
8.3 Scope of case study 47
Part II: The analysis 49
9 The systems and current models 49
9.1 System description 321 m water depth 50
9.1.1 Staggered configuration, 321 m system 52
9.1.2 Bottom strakes configuration, 321 m system 53
9.1.3 Middle strakes configuration, 321 m system 54
9.1.4 Top strakes configuration, 321 m system 55
9.2 System description 1300 m water depth 56
9.2.2 Staggered configuration, 1300 m system 58
9.2.3 Middle strakes configuration, 1300 m system 59
9.2.4 Top 150 m bare, next 650 m straked configuration 60
9.2.5 Top strakes configuration, 1300 m system 61
9.3 Current models for 321 m water depth 62
9.4 Current models for 1300 m water depth 65
10 Modelling and input to RIFLEX and VIVANA 69
10.1 Boundary conditions and simplifications 69
10.2 Structure of RIFLEX AND VIVANA 72

10.3 INPMOD 72
10.4 STAMOD 74
10.5 VIVANA 75
10.6 Flex joint implementation 76
11 Results 79
11.1 321 m water depth VIV results 79
11.1.1 Dominating frequency, duration and VIV amplitudes 79
11.1.2 Stress amplitudes 81
11.1.3 Fatigue damage 84
11.1.4 Static riser deflection and VIV amplification 87
11.1.5 Lower flex joint angles 89
11.2 1300 m water depth VIV results 92
11.2.1 Dominating frequency, duration and VIV amplitudes 92
11.2.2 Stress amplitudes 94
11.2.3 Fatigue damage 97
11.2.4 Static riser deflection and VIV amplification 100
11.2.5 Lower flex joint angles 102
12 Discussion 105
12.1 Model inputs 105
12.1.1 Geometry considerations 105
12.1.2 Boundary condition considerations 105
12.1.3 Top tension considerations 105
12.2 VIVANA inputs 107
12.2.1 Convergence and convergence limit 107
12.3 Other observations 109
13 Conclusion 111
13.1 321 m water depth 111
13.2 1300 m water depth 112
13.3 Final remarks and recommendations 113
14 Further work 115
14.1 Model 115
14.2 Post-processing 115
14.3 Coverage density 115
Bibliography 117

Appendix A 119

A.1 321 m water depth VIV results 119

A.1.1 Base case 119

A.1.2 Staggered configuration 120

A.1.3 Bottom strakes configuration 121

A.1.4 Middle strakes configuration 122

A.1.5 Top strakes configuration 123

A.2 Static drag and drag amplification, 321 m water depth 124

A.2.1 Base configuration 124

A.2.2 Staggered configuration 124

A.2.3 Bottom strakes configuration 125

A.2.4 Middle strakes configuration 125

A.2.5 Top strakes configuration 125

A.3 Lower flex joint angles, 321 m water depth 126

A.3.1 Base configuration 126

A.3.2 Staggered configuration 127

A.3.3 Bottom strakes configuration 127

A.3.4 Middle strakes configuration 128

A.3.5 Top strakes configuration 129

A.4 1300 m water depth VIV results 130

A.4.1 Base configuration 130

A.4.2 Staggered configuration 131

A.4.3 Middle strakes configuration 132

A.4.4 Top 50_150 strakes configuration 133

A.4.5 Top strakes configuration 134

A.5 Static drag and drag amplification 1300 m water depth 135

A.5.1 Base configuration 135

A.5.2 Staggered configuration 135

A.5.3 Middle strakes configuration 136

A.5.4 Top 50_150 strakes configuration 136

A.5.5 Top strakes configuration 136

A.6 Lower flex joint angles, 1300 m water depth 137

A.6.1 Base configuration 137

A.6.2 Staggered configuration 137

A.6.3 Middle strakes configuration 138
A.6.4 Top 50_150 strakes configuration 138
A.6.5 Top strakes configuration 139
Apppendix B 141
B.1 Input files staggered configuration, 321 m water depth 141
B.1.1 INPMOD 141
B.1.2 STAMOD 150
B.1.3 VIVANA 152
B.2 Input files top strakes configuration, 1300 m water depth 159
B.2.1 INPMOD 159
B.2.2 STAMOD 168
B.2.3 VIVANA 170

Table of figures

Figure 1.1 Annual production rate of hydrocarbons on the Norwegian Continental Shelf 1
Figure 2.1 Category A workover 4
Figure 2.2 Category B workover 4
Figure 2.3 Category C workover 5
Figure 3.1 Helical strakes on chimney stacks to suppress VIV 7
Figure 4.1 Cylinder subjected to incident flow 10
Figure 4.2 2D flow with boundary layer thickness δ, separation illustrated (Faltinsen, 2007) 11
Figure 4.3 Flow regimes and corresponding wake at increasing Rn 11
Figure 4.4 Surface pressure from vortex shedding (Blevins, 1994) 12
Figure 4.5 Simple experiment of cylinder in incident flow 13
Figure 4.6 Added mass coefficient vs. Reduced velocity 14
Figure 5.1 Energy balance illustrated (Larsen, et al., 2009) 17
Figure 5.2 CL versus A/D from VIVANA (Larsen, et al., 2009) 18
Figure 5.3 Added mass versus non-dimensional frequency (Larsen, et al., 2009) 18
Figure 5.4 Strouhal number versus Reynolds number (Larsen, et al., 2009) 19
Figure 6.1 Response amplitude and drag coefficients from experiments with radial water jets (Lie & Larsen, u.d.) 23
Figure 6.2 Various devices for VIV suppression 23
Figure 6.3 Regular cylinder with no ribbons attached 25
Figure 6.4 Cylinder with ribbons attached to trailing edge 25
Figure 6.5 Helical strakes. Photo courtesy of VIV Solutions 27
Figure 6.6 Helical strakes controlling the vortex shedding 27
Figure 6.7 Helical strakes parameters illustrated (DNV, 2010) 28
Figure 6.8 Typical helical strake configuration with three starts (Allen, et al., 2008) 28
Figure 6.9 Strake configurations used for case study (Larsen, et al., 2005) 29
Figure 6.10 Resulting fatigue damage for uniformly current flow U=0.5 m/ 30
Figure 6.11 PSD distribution for bare riser, 40% coverage density and 70% staggered density (Vandiver, et al., 2006) 30
Figure 6.12 RMS non-dimensional CF amplitude versus Reynolds number, outer end (Allen, et al., 2008) 31
Figure 6.13 RMS non-dimensional CF amplitude vs. Reynolds number, inner end (9) 32
Figure 6.14 Fairing geometry (Allen, et al., 2008) 33
Figure 6.15 RMS non-dimensional CF amplitude vs. Reynolds number with fairings, outer end (Allen, et al., 2008) 33
Figure 6.16 Fairing installation on drilling riser. Photo courtesy of VIV Solutions 34
Figure 6.17 CF Excitation force coefficients bare riser 35
Figure 6.18 Strake excitation coefficient distribution for $f = 0.33$ 35
Figure 7.1 Drag coefficient for circular cylinder, smooth and rough surface (Schlichting & Gertsen, 2000) 38
Figure 7.2 Static displacement of drilling riser in varying current distributions (15) 40
Figure 7.3 Excerpt of Marine drilling risers Design Guidelines, ISO 13624-1 (ISO, 2009) 41
Figure 7.4 Flex joint angles for workover operations according to ISO 13628-7 (ISO, 2006) 42
Figure 8.1 Uniform velocity profile where the excitation zone is indicated (DNV, 2010) 45
Figure 8.2 (A/D) for as function of excitation length for CF response 45

Figure 9.1 System overview 321 m water depth 50
Figure 9.2 Staggered buoyant and bare joint configuration 321 m water depth 52
Figure 9.3 Bottom strake configuration 321 m water depth 53
Figure 9.4 Middle strakes configuration 321 m water depth 54
Figure 9.5 Top strakes configuration 321 m water depth 55
Figure 9.6 System overview 1300 m water depth 56
Figure 9.7 Staggered buoyant and bare joint configuration 1300 m water depth 58
Figure 9.8 Middle strakes configuration 1300 m water depth 59
Figure 9.9 Top 150 m bare, next 650 m straked config. 1300 m water depth 60
Figure 9.10 Top strakes configuration 1300 m water depth 61
Figure 9.11 2/3 current for 321 m water depth 62
Figure 9.12 Sheared current for 321 m water depth 63
Figure 9.13 Uniform current distribution for 321 m water depth 63
Figure 9.14 Measured current distribution for 321 m water depth 64
Figure 9.15 2/3 current distribution for 1300 m water depth 65
Figure 9.16 Sheared current distribution for 1300 m water depth 66
Figure 9.17 Measured current distribution for 1300 m water depth 67
Figure 10.1 Boundary conditions used for all systems 71
Figure 11.1 Stress amplitudes for measured current, base configuration 81
Figure 11.2 Stress amplitudes for measured current, staggered configuration 82
Figure 11.3 Stress amplitudes for measured current, top strakes configuration 83
Figure 11.4 Fatigue damage for mesured current, base configuration 84
Figure 11.5 Fatigue damage for measured current, staggered configuration 85
Figure 11.6 Fatigue damage for measured current, top strakes configuration 86
Figure 11.7 Stress amplitudes for measured current profile, base configuration 94
Figure 11.8 Stress amplitudes for measured current, staggered configuration 95
Figure 11.9 Stress amplitudes for measured current, top 50_150 strakes configuration 96
Figure 11.10 Fatigue damage for measured current, base configuration 97
Figure 11.11 Fatigue damage for measured current, staggered configuration 98
Figure 11.12 Fatigue damage for measured current, top 50_150 strakes configuration 99
Figure 12.1 Bending stress form curvature (Larsen, 2009) 107

List of tables

Table 4-1 Flow regimes 9
Table 9-1 Stack-up data 321 m water depth 51
Table 9-2 Flex joint data 321 m water depth 51
Table 9-3 Staggered configuration data 321 m water depth 52
Table 9-4 Bottom strakes configuration data 321 m water depth 53
Table 9-5 Middle strakes configuration data 321 m water depth 54
Table 9-6 Top strakes configuration data 321 m water depth 55
Table 9-7 Stack-up data 1300 meter water depth 57
Table 9-8 Flex joint data 1300 m water depth 57
Table 9-9 Staggered configuration data 1300 m water system 58
Table 9-10 Middle strakes configuration data 1300 m water depth 59
Table 9-11 Top 150 m bare, next 650 m straked 1300 m water depth 60
Table 9-12 Top strakes configuration data 1300 m depth 61
Table 9-13 2/3 current data 62
Table 9-14 Sheared current data 62
Table 9-15 Uniform current data 63
Table 9-16 Measured current data 64
Table 9-17 2/3 current data 65
Table 9-18 Sheared current data 65
Table 9-19 Measured current data 66
Table 9-20 Ormen Lange 2 data 67
Table 9-21 Extended Ormen Lange 2 current distribution for 1300 m water depth 68
Table 10-1 CRS0 riser components, 321 m water depth 73
Table 10-2 CRS1 riser components, 321 m water depth 73
Table 10-3 Additional input for CRS1 riser components, 321 m water depth 73
Table 10-4 Flex joint data as given in INPMOD 74
Table 10-5 Drag coefficient for bare and straked components 74
Table 10-6 Added mass coefficient for bare and straked components 74
Table 10-7 Top tension 321 m water depth 74
Table 10-8 Top tension 1300 m water depth 75
Table 10-9 Flex joint data 77
Table 11-1 Dominating frequencies, durations and VIV amplitudes for base configuration, 321 m water depth 79
Table 11-2 Dominating frequencies, durations and VIV amplitudes for staggered configuration, 321 m water depth 79
Table 11-3 Dominating frequencies, durations and VIV amplitudes for top strakes configuration, 321 m water depth 80
Table 11-4 Stress amplitudes, base configuration 81
Table 11-5 Stress amplitudes, staggered configuration 82
Table 11-6 Stress amplitudes, top strakes configuration 83
Table 11-7 Fatigue damage, base configuration 84
Table 11-8 Fatigue damage, staggered configuration 85
Table 11-9 Fatigue damage, top strakes configuration 86
Table 11-10 Static riser deflection, base configuration 87

Table 11-11 Static riser deflection, staggered configuration 87
Table 11-12 Static riser deflection, top strakes configuration 88
Table 11-13 Lower flex joint angles, base configuration 89
Table 11-14 Lower flex joint angles after VIV amplification, base configuration 89
Table 11-15 Lower flex joint angles, staggered configuration 90
Table 11-16 Lower flex joint angles after VIV amplification, staggered configuration 90
Table 11-17 Lower flex joint angles, top strakes configuration 90
Table 11-18 Lower flex joint angles after VIV amplification, top strakes configuration 91
Table 11-19 Dominating frequencies, durations and VIV amplitudes, base configuration 92
Table 11-20 Dominating frequencies, durations and VIV amplitudes, staggered configuration 92
Table 11-21 Dominating frequencies, durations and VIV amplitudes, top 50_150 strakes config. 92
Table 11-22 Stress amplitudes, base configuration 94
Table 11-23 Stress amplitudes, staggered configuration 95
Table 11-24 Stress amplitudes, top 50_150 strakes configuration 96
Table 11-25 Fatigue damage, base configuration 97
Table 11-26 Fatigue damage, staggered configuration 98
Table 11-27 Fatigue damage, top 50_150 strakes configuration 99
Table 11-28 Static riser deflection, base configuration 100
Table 11-29 Static riser deflection, staggered configuration 100
Table 11-30 Static riser deflection, top 50_150 strakes configuration 101
Table 11-31 Lower flex joint angles, base configuration 102
Table 11-32 Lower flex joint angles after VIV amplification, base configuration 102
Table 11-33 Lower flex joint angles, staggered configuration 102
Table 11-34 Lower flex joint angles after VIV amplification, staggered configuration 103
Table 11-35 Lower flex joint angles, top 50_150 strakes configuration 103
Table 11-36 Lower flex joint angles after VIV amplification, top 50_150 configuration 103
Table 12-1 Top tension variations base and top 150 strakes configuration 106
Table 12-2 Dominating frequency, VIV amplitude after adjusted top tension, top 50_150 strakes configuration 106
Table 12-3 Max stress after adjusted top tension, top 50_150 strakes configuration 106
Table 12-4 Dominating frequency, base configuration, conlim=0.00005 109
Table 12-5 Stress amplitude, base configuration, conlim=0.00005 109
Table A-1 Dominating response frequency results, base configuration 119
Table A-2 Stress amplitudes, base configuration 119
Table A-3 Fatigue damage, base configuration 119
Table A-4 Dominating response frequency results, staggered configuration 120
Table A-5 Stress amplitudes, staggered configuration 120
Table A-6 Fatigue damage, staggered configuration 120
Table A-7 Dominating response frequency results, bottom strakes configuration 121
Table A-8 Stress amplitudes, bottom strakes configuration 121
Table A-9 Fatigue damage, bottom strakes configuration 121
Table A-10 Dominating response frequency results, middle strakes configuration 122
Table A-11 Stress amplitudes, middle strakes configuration 122
Table A-12 Fatigue damage, middle strakes configuration 122
Table A-13 Dominating response frequencies results, top strakes configuration 123

Table A-14 Stress amplitudes, top strakes configuration 123
Table A-15 Fatigue damage, top strakes configuration 123
Table A-16 Static deflections, base configuration 124
Table A-17 Static deflections, staggered configuration 124
Table A-18 Static deflections, bottom strakes configuration 125
Table A-19 Static deflections, middle strakes configuration 125
Table A-20 Static deflections, top strakes configuration 125
Table A-21 Lower flex joint angles, base configuration 126
Table A-22 Lower flex joint angles after VIV amplification, base configuration 126
Table A-23 Lower flex joint angles, staggered configuration 127
Table A-24 Lower flex joint angles after VIV amplification, staggered configuration 127
Table A-25 Lower flex joint angles, bottom strakes configuration 127
Table A-26 Lower flex joint angles after VIV amplification, bottom strakes configuration 128
Table A-27 Lower flex joint angles, middle strakes configuration 128
Table A-28 Lower flex joint angles after VIV amplification, middle strakes configuration 128
Table A-29 Lower flex joint angles, top strakes configuration 129
Table A-30 Lower flex joint angles after VIV amplification, top strakes configuration 129
Table A-31 Dominating response frequency results, base configuration 1300 m system 130
Table A-32 Stress amplitudes, base configuration 1300 m system 130
Table A-33 Fatigue damage, base configuration 1300 m system 130
Table A-34 Dominating response frequency results, staggered configuration 1300 m system 131
Table A-35 Stress amplitudes, staggered configuration 1300 m system 131
Table A-36 Fatigue damage, staggered configuration 1300 m system 131
Table A-37 Dominating response frequency results, middle strakes config. 1300 m system 132
Table A-38 Stress amplitudes, middle strakes configuration 1300 m system 132
Table A-39 Fatigue damage, middle strakes configuration 1300 m system 132
Table A-40 Dominating response frequency results, top 50_150 strakes config. 1300 m system 133
Table A-41 Stress amplitudes, top 50_150 strakes configuration 1300 m system 133
Table A-42 Fatigue damage, top 50_150 strakes configuration 1300 m system 133
Table A-43 Dominating response frequency results, top strakes configuration 1300 m system 134
Table A-44 Stress amplitudes, top strakes configuration 1300 m system 134
Table A-45 Fatigue damage, top strakes configuration 1300 m system 134
Table A-46 Static deflections, base configuration 1300 m system 135
Table A-47 Static deflections, base configuration 1300 m system 135
Table A-48 Static deflection, middle strakes configuration 1300 m system 136
Table A-49 Static deflection, top 50_150 strakes configuration 1300 m system 136
Table A-50 Static deflection, top strakes configuration 1300 m system 136
Table A-51 Lower flex joint angles, base configuration 1300 m system 137
Table A-52 Lower flex joint angles after VIV amplification, base config. 1300 m system 137
Table A-53 Lower flex joint angles, staggered configuration 1300 m system 137
Table A-54 Lower flex joint angles after VIV amplification, staggered config. 1300 m system 138
Table A-55 Lower flex joint angles, middle strakes configuration 1300 m system 138
Table A-56 Lower flex joint angles after VIV amplification, middle strakes config. 1300 m system 138
Table A-57 Lower flex joint angles, top 50_150 strakes configuration 1300 m system 138

Table A-58 Lower flex joint angles after VIV amplification, top 50_150 strakes configuration 1300 m system 139
Table A-59 Lower flex joint angles, top strakes configuration 1300 m system 139
Table A-60 Lower flex joint angles after VIV amplification, top strakes config. 1300 m system 139

List of equations

Equation 3.1: Navier Stokes equation, x-component, (White, 2003) 8
Equation 4.1: Reynolds number 9
Equation 4.2 Strouhal number 10
Equation 4.3: Equation of oscillation for simple cylinder in incident flow 13
Equation 4.4: Eigenfrequency for simple cylinder in incident flow 14
Equation 5.1: Excitation force in CF direction 17
Equation 5.2: Response frequency method, equation of equilibrium 19
Equation 5.3: Load vector 20
Equation 5.4: Response vector 20
Equation 5.5: Response solution 20
Equation 6.1: Reduced velocity kept under 1 to avoid resonance 21
Equation 6.2: Harmonic lift force 21
Equation 6.3: Equation of motion for riser section 21
Equation 6.4: Steady-state CF solution 21
Equation 6.5: CF response made dimensionless 22
Equation 6.6: Oscillation amplitude at resonance 22
Equation 6.7: Reduced damping 22
Equation 7.1: Drag force 37
Equation 7.2: Drag coefficient Blevins 39
Equation 7.3: Drag coefficient Vandiver 39
Equation 7.4: Drag coefficient Skop et al. 39
Equation 8.1: Effective velocity for simplified VIV analysis 45
Equation 10.1: Buoyancy force of component 70
Equation 10.2: Hydrodynamic diameter of non-circular cross sections 70
Equation 10.3: Density riser segment 72
Equation 10.4: Second area of inertia cylinder 73
Equation 10.5: Angle of fixed cantilever beam subjected to end moment 76
Equation 10.6: Rotational stiffness flex joint 76
Equation 10.7: Flex joint angle 76
Equation 10.8: Bending stiffness beam element representing flex joint 76
Equation 11.1: Lower flex joint angle 89
Equation 12.1: Eigenfrequency for beam subjected to tension force 106
Equation 12.2: Bending stress derivation 108
Equation 12.3: Modal superposition response 108
Equation 12.4: Eigenmode shapes 108
Equation 12.5: Curvature 108

Abbreviations

AKSO	Aker Solutions
API	American Petroleum Institute
BOP	Blow Out Preventer
CF	Cross-flow
CT	Coiled tubing
DAT	Direct Actuating Tensioners
DNV	Det Norske Veritas
DP	Dynamic Positioning
EDP	Emergency Disconnect Package
FEA	Finite Element Analysis
FPS	Floating Production Systems
ID	Inner Diameter
IL	In-line
ISO	International Organization for Standardization
LFJ	Lower Flex Joint
LRP	Lower Riser Package
N/A	Not Applicable
NCS	Norwegian Continental Shelf
OD	Outer Diameter
PSD	Power Spectral Density
RMS	Root Mean Square
TH	Tubing Hanger
TLP	Tension-Leg Platform
TTRD	Through Tubing Rotary Drilling
VIV	Vortex Induced Vibrations
WCP	Well Control Package

WO	Workover
WO/C	Workover and Completion
XMT	Christmas Tree

Non-dimensional parameters

Non-dimensional frequency	$\hat{f}$	$\hat{f} = \frac{D f_{osc}}{U}$
Reduced velocity	U_R	$U_R = \frac{U}{D f_0}$
Reynolds number	Rn	$Rn = \frac{\rho U x}{\mu} = \frac{U x}{\nu}$
Strouhal number	St	$St = \frac{f_v D}{U_\infty}$

1 Introduction

With a growing focus on safety, both for the personnel and on the environment, new operational requirements for all types of offshore equipment operating on the Norwegian Continental Shelf (NCS) are yearly put forward by the Norwegian Government. Organizations like the American Petroleum Institute (API), the International Organization for Standardization (ISO) and Det Norske Veritas (DNV) set standards and Recommended Practices (RPs) that must be followed in order to legally provide offshore equipment for the NCS. Disasters like the Macondo accident in the Gulf of Mexico serves as brutal memories for what is at stake when performing deep water offshore operations. The recent years focus on fatigue damage from wave- and current induced loads in particular has been discussed. For subsea drilling and workover risers this implies that the effect of Vortex Induced Vibrations (VIV) must be studied.

1.1 Motivation

Since the first oil discovery of the Balder field in 1967 (Amdahl, et al., 2005), Norway has gained prosperity and wealth as a result of production of the vast oil resources located on the NCS. Throughout the 1970s, 1980s and 1990s oil production in Norway increased until peak oil was reached in 2000 (Statistisk Sentralbyrå, 2011). With the exception of a slight increase in 2003 and 2004, the oil production on the NCS has declined, as seen in Figure 1.1.

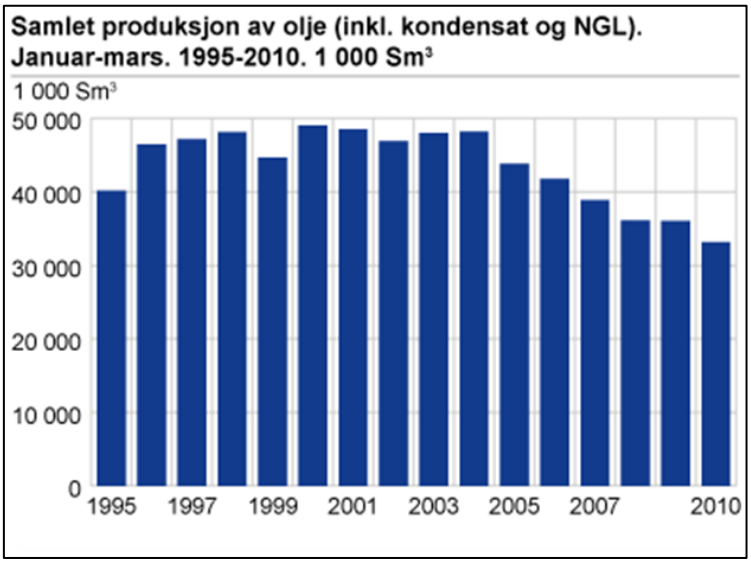

Figure 1.1 Annual production rate of hydrocarbons on the Norwegian Continental Shelf

For the offshore business in Norway 2011 was an important year, as the discoveries of Aldous and Avaldsnes proved to be among the 7th largest fields ever found on the NCS, and the largest find in the world that year (Stangeland, 2011). Even so, the production rate on the NCS is expected to continue its decline in the future. It is therefore important to increase the recovery rate of hydrocarbons in already existing wells. The recovery rate gives the ratio between the amount of hydrocarbons that is successfully pumped and recovered from the reservoir to the surface, to the total amount of hydrocarbons in the reservoir. Advancements in technology have increased today's recovery rate to up to 65%, from a low 16-17% when drilling in the North Sea started in the early 1970s (Amdahl, et al., 2005). Still, as oil field water depths increases, as well as number of new reservoir discoveries go down, combined with a constant desire to increase the recovery rate, the oil

industry finds new economic and technical challenges to overcome. Many of these challenges are linked to workover operations.

Most workover operations today are performed through risers. Depending on the complexity of the operation, different types of risers may be used; however drilling risers, or in-marine risers as they are called when they are used for workover, are the most common. Consequently, problems related to Vortex Induced Vibrations (VIV) may be experienced, particularly for oil fields at large water depths where significant ocean currents may be present.

1.2 Purpose and scope

This Master Thesis is divided into two parts; *Part I: Theory* presents an overview of the physical aspects of VIV. A more detailed study of the phenomenon, and also a presentation of two of the industry standard computer programs used for VIV analyses, is given in the Project Thesis (Knardahl, 2011). In this Master Thesis more focus is given to preventive measures for avoiding VIV, with main emphasis on the use of strakes. Positive and negative effects like drag magnification, as well as a short comparison between strakes and fairings, are discussed.

Part II: The Analysis presents case studies for two different Aker Solutions systems, one for 321 m water depth and one 1300 m water depth. Various different configurations of the systems, as well as various current profiles, have been studied, including:

- VIV analyses for “base configurations”, i.e. no strakes applied
- VIV analyses for variation of external diameter
- VIV analyses for varying strake configurations, i.e. top, middle and bottom of riser covered with strakes

Riser behaviour in VIV conditions for varying external diameter as well as strake effectiveness is reported. Finally possible operational consequences based on the analysis results will be discussed.

Part I: Theory

2 Short on Workover operations

Workover is the field that cover preparation of a new well for production, often called completion, as well as maintenance and stimulation of an already existing well. Aside from making the final installations and tests before production, the main purpose of a workover operation is thus to restore, prolong or enhance the production rate of hydrocarbons.

More specifically, the completion phase of a workover intervention includes:

Installation and Completion

- Christmas tree (XMT) installation
- Well completion, installation of the Tubing Hanger (TH)
- Well testing, pressure testing and flow testing

The well intervention phase typically consists of:

Workover/ Well intervention

- Light well intervention in to tubing
- Heavy well intervention

With water depths now stretching several kilometres down below the sea surface, it is not difficult to understand why well accessibility may prove difficult. Combined with rig or vessel costs of approximately 0.5-1.0 million USD per day and the lost income from unproductive down time during workover, it is inherent to keep the time used for workover operations as low as possible. Today, the most efficient way of conducting workover operations may be divided into three categories depending on what type of intervention is necessary. These are category A, category B and category C workover interventions.

2.1 Category A – Riser less workover (light workover)

Riser less workover uses a wireline (a cable) to transport tools to the submerged equipment on the seabed, see Figure 2.1. As this type of intervention is done without a riser, the operation may be performed without a large offshore rig, which saves costs. Riser less workover is used in less complex operations, and is often called light workover. Typical operations include:

- Perforation
- Installation and pulling of various smaller equipment, for instance plugs.

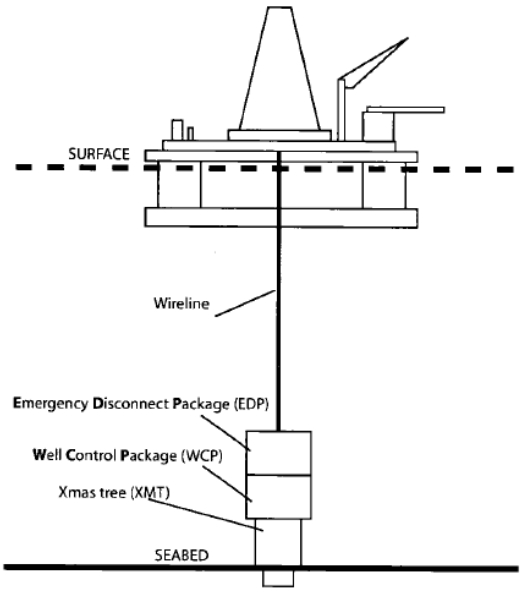

Figure 2.1 Category A workover

2.2 Category B – Riser well intervention

Category B workover intervention applies a workover riser, which means that more complex tasks may be performed. The riser creates a direct link between the surface and seabed, see Figure 2.2, and a variety of tools may be lowered through the riser and down-hole into the well to perform different operations. Category B does however require a drilling rig or a purpose built offshore vessel, which means higher costs. Typical operations are:

- Milling, e.g. to remove blockage
- Colied tubing, e.g. used for cleaning, logging and cementing

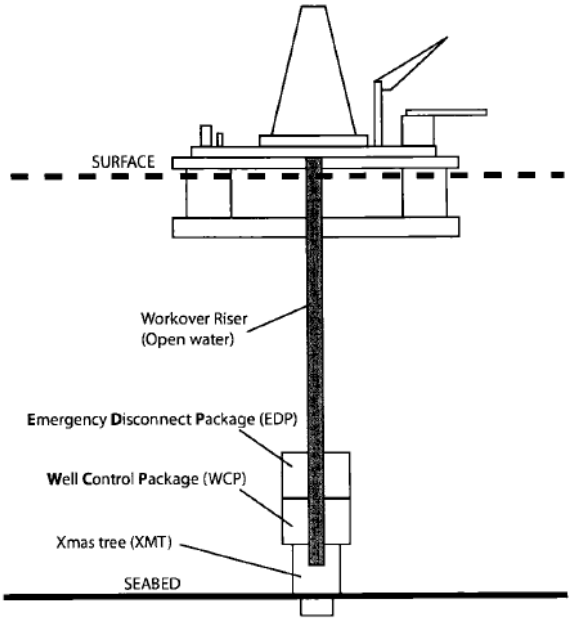

Figure 2.2 Category B workover

2.3 Category C – Workover using a marine riser

Workover with a marine riser, or drilling riser which it is often called, is used for the most complex operations. As this type of workover requires a fully equipped drilling rig, it is the most expensive workover setup. While the Category B assures well control through its Well Control Package (WCP), the Category C applies a Blow Out Preventer (BOP) to control the well. The BOP is standard equipment on a drilling rig, and consists of several powerful cutting and seal valves. The category C workover is often referred to as heavy workover. Typical operations consist of:

- Drilling
- Running and replacement of heavy subsea equipment

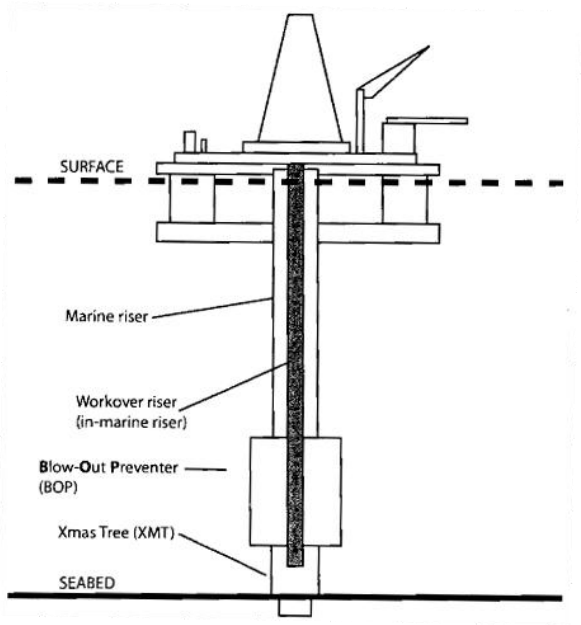

Figure 2.3 Category C workover

3 General notes on Vortex Induced Vibrations

Vortex Induced Vibrations can cause severe oscillations of circular structures subjected to incident flow. This may again lead to fatigue damage and ultimately result in total collapse of the structure. The phenomenon itself is well known both from general engineering situations, and from observations of slender marine offshore structures. In civil engineering the phenomenon can typically occur for long chimney stacks, transmission lines and shrouds supporting suspension bridges. Figure 3.1 below shows a group of three chimney stacks with helical strakes wrapped around the chimney body. This is done to prevent VIV. Helical strakes are also applied to marine risers and pipelines, and are believed to date back as early as the first World War, when a rope was helically wound around submarine periscopes to keep them from vibrating (Lamb, 1991). Strakes will be further discussed later in the report.

Figure 3.1 Helical strakes on chimney stacks to suppress VIV

For marine structures, VIV can typically be a problem for marine risers, umbilicals, anchor lines and free-spanning pipelines. Recent development in deep water exploration and production activities has proved that there still are substantial challenges in VIV evaluation. Large variations in current velocities along the water column are introduced as water depth increases. Furthermore, span-wise varying geometry of deep water risers, both in-marine risers and open-water riser systems, add complexity to the VIV analysis. As a consequence, VIV has proven to be a very difficult physical phenomenon to model analytically. Efforts for providing models and tools for VIV analysis started as early as the 1980s (Larsen & Bech, 1986), however VIV presents characteristics that are still not entirely understood.

3.1 Current VIV analysis programs and models

Several computer programs are today available for VIV evaluation. VIV computer programs may generally be divided into two groups; those which use Computation Fluid Dynamics (CFD) to directly solve the Navier-Stokes equations, and those which use empirical models.

On simpler and smaller 2d-models, computing power of today's computers is sufficiently strong to calculate the velocity and pressure distributions in the fluid, and thus finding the instantaneous forces acting on the circular structure. However, in order to find analytical solutions to the equations,

see Equation 3.1, the discretization of the relevant problem domain, which is the entire riser length for VIV problems, must be particularly fine, both in terms of spatial- and time increments. An extremely large amount of data is thus required for solving the problem, which with current computer power gives inconveniently long computation times. Consequently, solving the equations in the 3D plane for a several hundred meters long riser with varying ODs and local flow velocities is still considered out of reach for today's computers.

Equation 3.1: Navier Stokes equation, x-component, (White, 2003)

$$x: \quad \rho g_x - \frac{\partial p}{\partial x} + \frac{\partial \tau_{xx}}{\partial x} + \frac{\partial \tau_{yx}}{\partial y} + \frac{\partial \tau_{zx}}{\partial z} = \rho\left(\frac{\partial u}{\partial t} + u\frac{\partial u}{\partial x} + v\frac{\partial u}{\partial y} + w\frac{\partial u}{\partial z}\right)$$

Most of the empirical models of today used for VIV assessment apply the assumption that VIV will occur at one or a limited number of discrete frequencies (Larsen, 2011). Based on model tests, lift coefficients for varying oscillating amplitude or non-dimensional frequency can be found. Today Marintek's and NTNU's *VIVANA* and the MIT-developed *Shear7* are the industry standards for VIV evaluation of slender offshore structures. In-house in Aker Solution, both VIVANA and Shear7 are used when VIV is assessed.

4 Fundamental aspects of VIV

Vortex induced vibrations are oscillations at resonance. The motions are caused by time varying forces on the body, acting both in cross-flow (CF) and in-line (IL) direction to the incident flow. In order to provide a basic understanding of VIV, the fluid shedding process as well as the structure response must be studied.

4.1 Reynolds number and Strouhal number

Two parameters are used to describe the flow around a fixed cylinder, namely the Reynolds number and Strouhal number. The Reynolds number gives the ratio between inertial forces and friction forces in the fluid (Myrhaug, 2005) and is defined as

Equation 4.1: Reynolds number

$$Rn = \frac{\rho U x}{\mu} = \frac{U x}{\nu}$$

where

ρ = fluid density

U = flow velocity

x = characteristic length, $x = D$ for a cylinder

μ = dynamic viscosity of fluid

ν = kinematic viscosity of fluid, $\nu = \frac{\mu}{\rho}$

It is convenient to divide the different Reynolds number domains into separate flow regimes. Table 4-1 gives separate flow regimes and corresponding Reynolds number proposed by O.M. Faltinsen (Faltinsen, 1990).

Name	**Reynolds number**
Subcritical flow regime	<2 x 10^5
Critical flow regime	2 x 10^5 < Rn < 5 x 10^5
Supercritical flow regime	5 x 10^5 < Rn < 3 x 10^6
Transcritical flow regime	Rn > 3 x 10^6

Table 4-1 Flow regimes

The Strouhal number is proportional to the shedding frequency of the fluid, and given as

Equation 4.2 Strouhal number

$$St = \frac{Df_v}{U}$$

where

D = cylinder diamater

f_v = vortex shedding frequency

U = flow velocity

In subcritical flow, see Table 4-1, the Strouhal number is stable around $St = 0.2$. Due to limitations in model test set-up, typically carriage speed in towing tests and upper limits for maximum riser diameter, most experimental data are collected from tests in the subcritical flow regime. In real life however, most VIV-relevant conditions take place in higher flow regimes. Still, it is considered conservative to apply experimental data from the sub-critical flow regime to evaluate VIV in real life conditions. One should note however, that this introduces an uncertainty to empirical models.

4.2 Flow around a cylinder

Figure 3.1 shows a simple test set-up where a cylinder with diameter D is subjected to incident flow U.

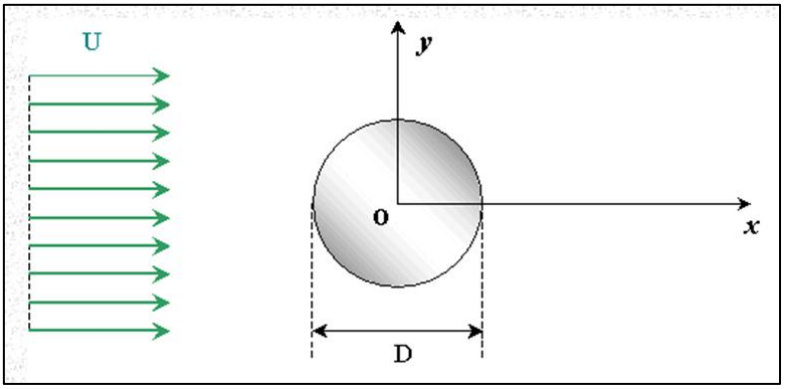

Figure 4.1 Cylinder subjected to incident flow

As the fluid approaches the leading edge of the cylinder, the pressure in the fluid will rise from the fluid pressure in the free flow to the stagnation pressure at the stagnation point on the cylinder. The high pressure near the leading edge of the cylinder will force the flow around the leading edge as the boundary layer on the cylinder develops. The high pressure is however not strong enough drive the flow about the back of the cylinder at sufficiently high Reynolds number. Consequently, the flow separates near the widest section of the cylinder and shed vortices downstream of the cylinder, creating a so-called vortex street. Flow separation starts if there exist a point S on a body surface where $\frac{\partial u}{\partial y} = 0$ and there is backflow aft of this separation point, see Figure 4.2.

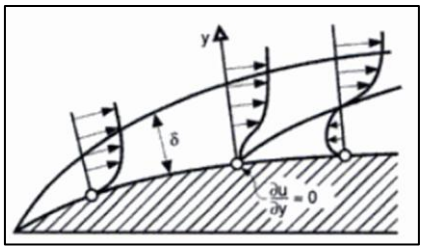

Figure 4.2 2D flow with boundary layer thickness δ, separation illustrated (Faltinsen, 2007)

Depending on the Rn, the shedding process and downstream vortex street will vary. The separate stages of the process for increasing Rn are illustrated below.

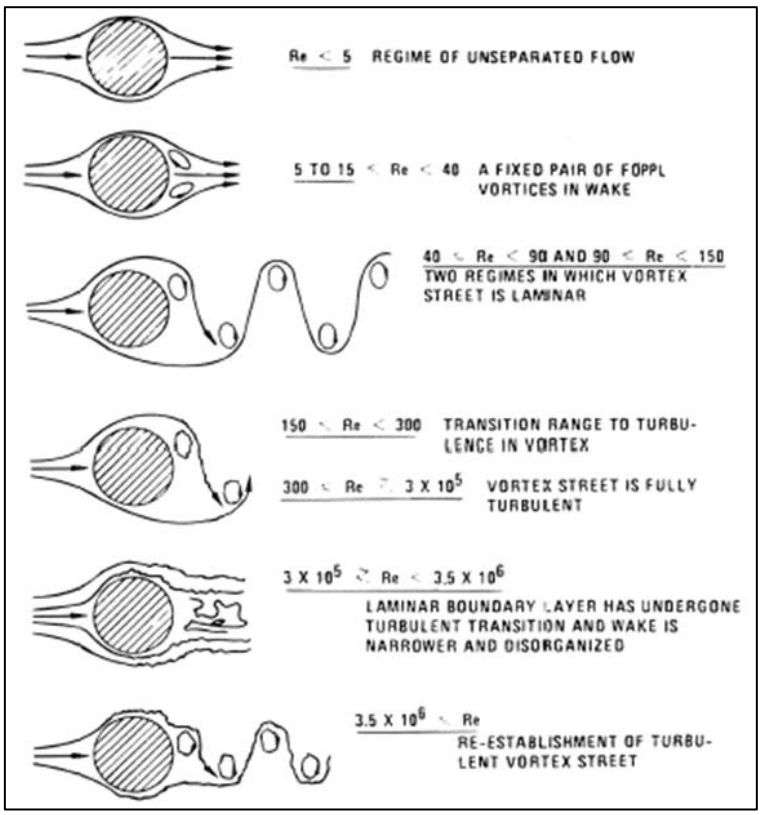

Figure 4.3 Flow regimes and corresponding wake at increasing Rn

From Figure 4.3 we see that flow separation occurs early, already at $5 < Rn < 40$, and a symmetric pair of vortices are formed. For further increasing Reynolds number, $40 < Rn < 150$, the wake becomes unstable, and laminar periodic staggered vortices of opposite signs are created. While the boundary layer on the cylinder remains laminar, the vortices become turbulent in the $150 < Rn < 300$ range. For a further increase in flow velocity, the subcritical flow regime $300 < Rn < 1.5 * 10^5$ is reached. The flow separates close to 80 degrees aft of cylinder leading edge and the vortex shedding is now strong and periodic, creating cyclic forces in both IL and CF direction. Moving into the transitional flow range of $1.5 * 10^5 < Rn < 3.5 * 10^6$, the boundary layer on the cylinder becomes turbulent which effectively delays the separation point to roughly 140 degrees aft of the leading edge. As a consequence the drag force on the cylinder is reduced. The same flow regime is characterised by a disorganized wake caused by bubbles and three-dimensional effects (Blevins,

1994). Entering the supercritical flow regime, regular vortex shedding is established with both a turbulent boundary layer and a turbulent vortex street.

4.3 In-line and cross-flow forces

The alternatively shed vortices induce pressure forces on the cylinder. As each shed vortex will induce a drag force in IL direction, while the sign of the induced pressure in CF direction will be opposite for each shed vortex, IL response will occur at twice the frequency of CF response. Figure 4.4 gives a section of a complete shedding cycle, where the shed vortices and corresponding surface pressures are illustrated (Blevins, 1994).

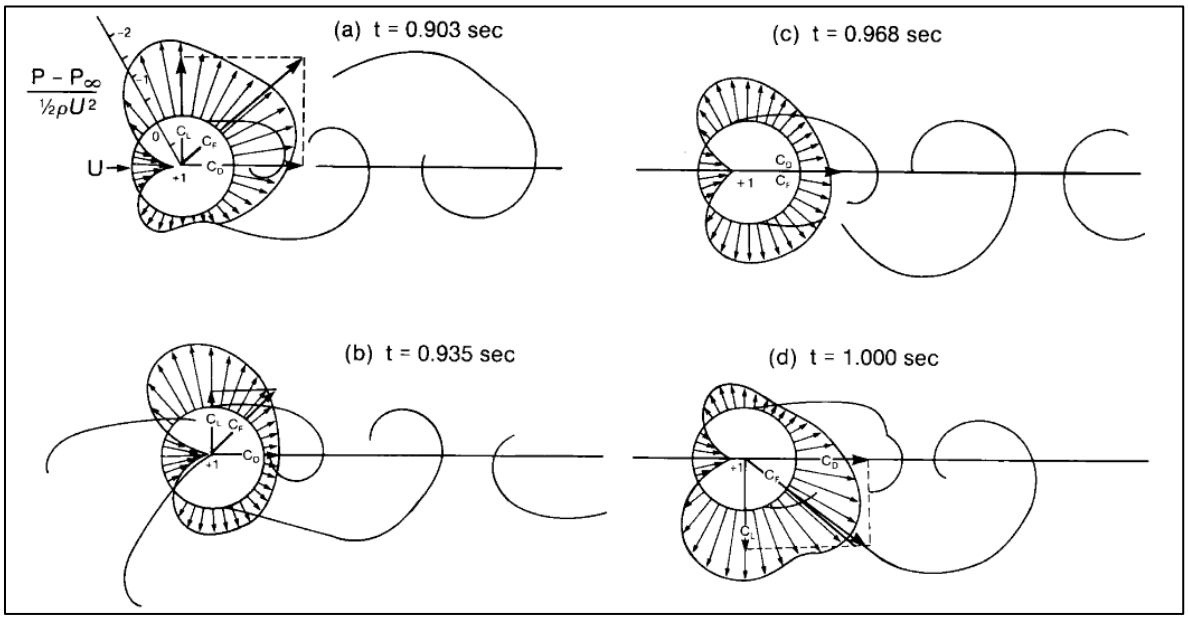

Figure 4.4 Surface pressure from vortex shedding (Blevins, 1994)

Integrated over the cylinder surface, the induced pressures will give excitation forces in IL and CF direction. As mentioned earlier, CFD programs are today capable of evaluating simple 2D-cases as illustrated above. Pressure distributions in the fluid are calculated directly and excitation forces thus found. For larger 3D-models however, empirical models are needed to analyse VIV problems. A critical aspect to evaluating VIV empirically is to be able to calculate correct response frequencies for every excited mode. Influence from added mass, and its influence on response frequency, has proved to be a difficult part of the VIV analysis. This will now be discussed.

4.4 Free oscillation test, added mass and response frequency

For structures in air, the vibrations occur at the structures eigenfrequency. For structures in water however, the picture is somewhat different as added mass plays a significant role in dictating the response frequency. This is easily illustrated by the experiment where a simple cylinder is attached to a spring with stiffness *k* and subjected to a uniform incident flow *U* (Larsen, 2011), see Figure 4.5.

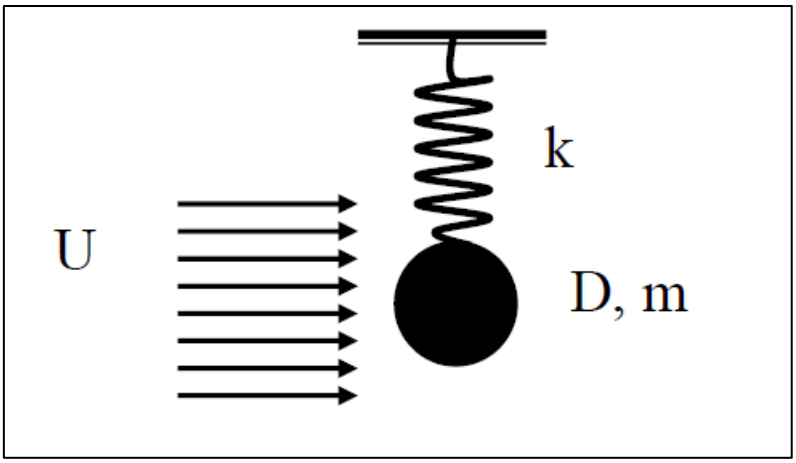

Figure 4.5 Simple experiment of cylinder in incident flow

The corresponding equation of oscillation for evaluating the eigenfrequency of the system is given by Equation 4.3:

Equation 4.3: Equation of oscillation for simple cylinder in incident flow

$$(m + m_{a0})\ddot{y}(t) + ky(t) = 0$$

where

m = mass of cylinder

m_{a0} = added mass

k = spring stiffness

$y(t)$= CF displacement of cylinder

The response $y(t)$ may be set to be

$$y(t) = Asin(\omega_0 t)$$

where

A = amplitude of excitation

ω_0 = still water eigenfrequency

Differentiating the response $y(t)$ with respect to time gives

$$\dot{y}(t) = \omega_0 A\cos(\omega_0 t) \Rightarrow \ddot{y}(t) = -\omega_0^2 A\sin(\omega_o t)$$

Inserted into Equation 4.3 this gives the still water eigenfrequency of the cylinder:

Equation 4.4: Eigenfrequency for simple cylinder in incident flow

$$-\omega_0^2(m+m_{a0})+k=0 \Rightarrow \omega_0=\sqrt{\frac{k}{(m+m_{a0})}} \Rightarrow f_0=\frac{1}{2\pi}\sqrt{\frac{k}{(m+m_{a0})}}$$

The calculated eigenfrequency in Equation 4.4 applies for still water oscillations of the cylinder, which means that $\mathbf{m_{a0}}$ in the same equation denotes the still water added mass. For an oscillating cylinder the added mass is not a constant quantity; it will vary as a function of both oscillating amplitude and response frequency. This means that for a given frequency and response amplitude, a specific added mass different from the still water added mass will be valid for the cylinder.

Figure 4.6 shows the added mass coefficient versus reduced velocity distribution found by Vikestad (Vikestad, 1998). Note that negative added mass is given for reduced velocity $U_R \geq 8$. The reason for this behaviour is that added mass is defined as the component of the hydrodynamic force which is in phase with the CF acceleration of the cylinder; negative added mass is thus possible. Finding the added mass may be done in two ways. One way is to measure the force at one end of the cylinder. The force in phase with the acceleration may be found through Fourier decomposition. If the force from the physical mass of the cylinder, i.e. not the hydrodynamic part, is subtracted, the hydrodynamic mass of the cylinder is found, which is added mass. The other way of finding added mass is to assume that the oscillations occur at resonance. The cylinder mass and stiffness is known, and the frequency of the oscillations is measured. According to Equation 4.4 there is only one unknown left, namely the added mass. Vikestad (Vikestad, 1998) found that the calculated added mass from the first way was equal to the added mass calculated using method number two. This proves that VIV indeed is vibration at resonance.

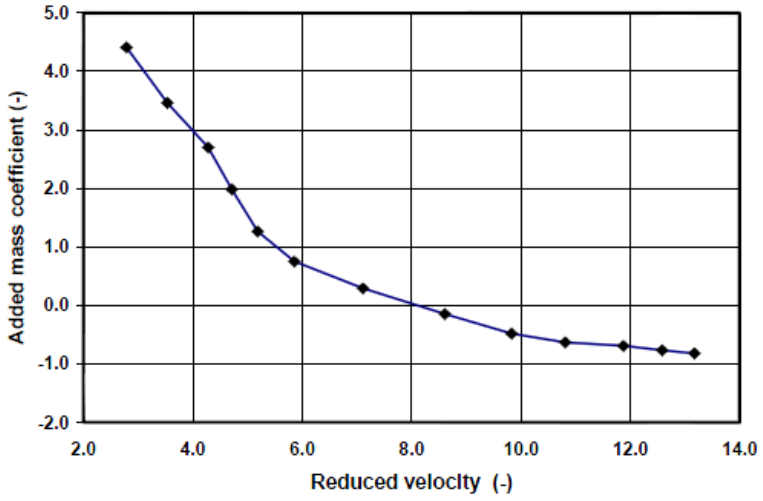

Figure 4.6 Added mass coefficient vs. Reduced velocity

For simple cylinders subjected to incident flow, the vortex shedding process can to a large extent be influenced by the response of the cylinder. The phenomenon is called “Lock-in” and refers to the situation where the vortex shedding frequency f_v becomes controlled by the oscillation frequency f_{osc} (Larsen, 2011). Depending on the mass of the cylinder, added mass may have large influence on the oscillating frequency, which means that the oscillation frequency may be different from the still water eigenfrequency of the cylinder. In practice this means that the response frequency of the

cylinder will become a compromise between the vortex shedding frequency f_v and the eigenfrequency f_o of the cylinder in still water.

Varying added mass, varying OD and thus varying Strouhal number along the riser length are some of the challenges that must be accounted for by empirical models for VIV evaluation. The following will present a brief summary of the program used for analyses in this master thesis; VIVANA.

5 VIVANA

VIVANA is a semi-empirical program used for VIV analysis of slender offshore structures. The initial static analysis is based on the finite element method, while the dynamic part of the analysis uses the frequency method.

5.1 Energy balance, C_L, added mass and Strouhal number in VIVANA

For a slender structure in VIV conditions, there will be a net global balance between energy transported in to the system, and energy dissipated from the system. VIVANA handles this by identifying excitation zones and damping zones, see Figure 5.1.

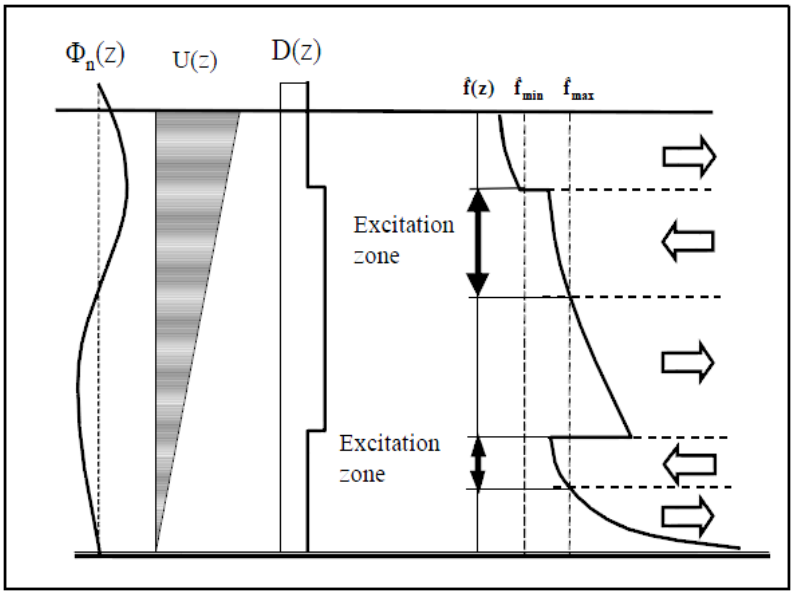

Figure 5.1 Energy balance illustrated (Larsen, et al., 2009)

The excitation force is found from built in or user-defined lift coefficient curves in VIVANA. The curves are based on experimental data. Note that excitation force in CF direction, $F_{E,CF}$ is also called lift force F_L in the literature.

Equation 5.1: Excitation force in CF direction

$$F_{E,CF} = \frac{1}{2}\rho C_{E,CF} U^2 D * dl$$

where

ρ = fluid density

$C_{E,CF}$ = cross-flow excitation coefficient, also called lift coefficient

U = fluid velocity

D = riser diameter

dl = span-wise increment

The excitation force given in Equation 5.1 is defined as positive if it acts in phase with the CF velocity of the riser, making negative lift force possible. This is also illustrated in Figure 5.2 where lift coefficient versus non-dimensional amplitude is given. The physical explanation behind a negative C_L is that for sufficiently large response amplitudes energy is transported from the riser to the fluid, thus inducing a damping force on the system.

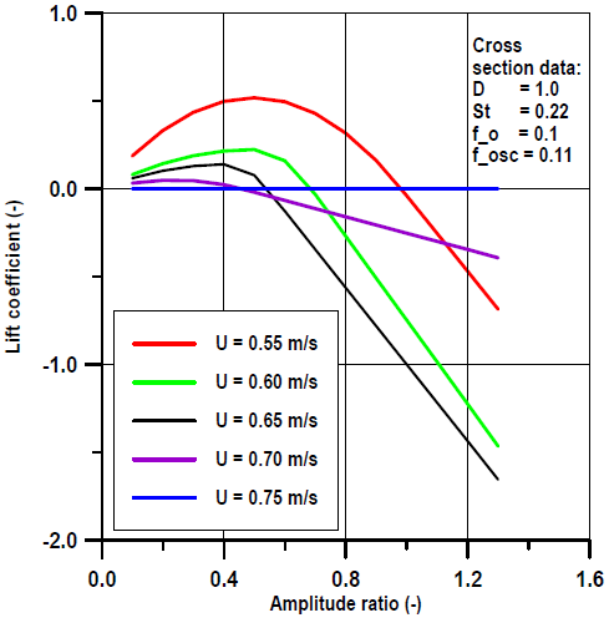

Figure 5.2 C_L versus A/D from VIVANA (Larsen, et al., 2009)

Similarly as for the lift coefficient, Strouhal number and added mass curves based on experimental data are applied in VIVANA. The user is free to define the curves as he/she likes, or use the built-in distributions.

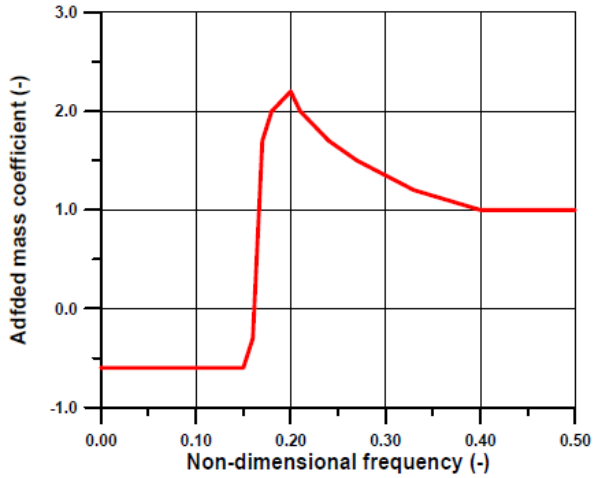

Figure 5.3 Added mass versus non-dimensional frequency (Larsen, et al., 2009)

As explained earlier, both the added mass and Strouhal number are important parameters in determining the response frequency of the riser. Reliable and correct empirical data from experiments and test are therefore essential.

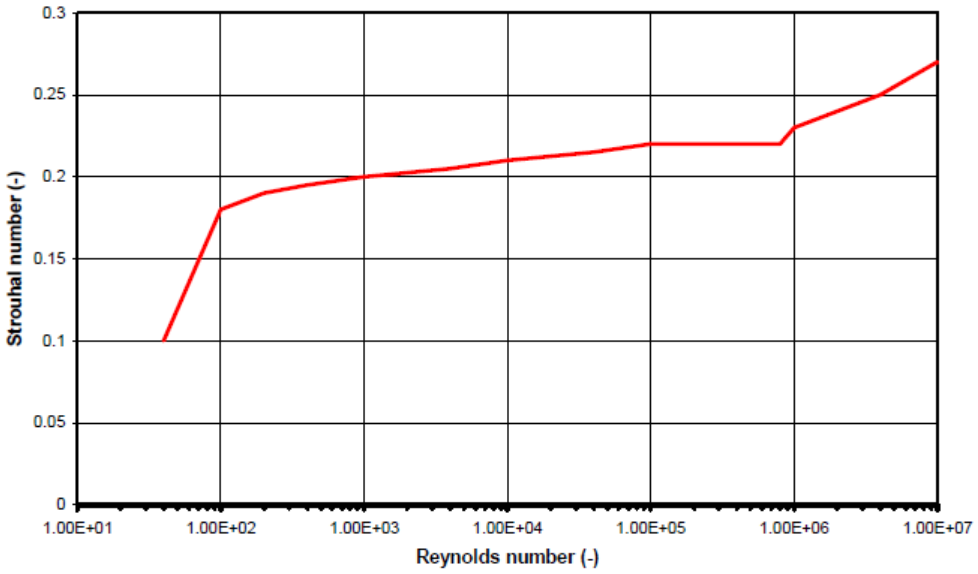

Figure 5.4 Strouhal number versus Reynolds number (Larsen, et al., 2009)

5.2 Analysis method

VIVANA performs 6 steps to provide a full VIV analysis of a given problem (Larsen, et al., 2009):

1 Static Analysis

A static analysis is performed in RIFLEX. Static deflection of the riser from current loads are calculated

2 Eigenvalue Analysis

Eigenvectors and eigenfrequencies for the riser in still water are found.

3 Identification of dominating frequency and other possible response frequencies

As the added mass for the riser will vary in VIV conditions compared to still water conditions, an iteration process is performed for each eigenfrequency found in step 2. All modified eigenfrequencies that give a zone along the riser with non-dimensional frequency in the 0.125-0.3 range are chosen as possible response frequency. The dominating frequency is found from a given energy criterion.

4 Response calculation at dominating response frequency

VIVANA applies the response frequency method to calculate response. The equation of equilibrium is given as

Equation 5.2: Response frequency method, equation of equilibrium

$$\boldsymbol{M\ddot{r} + C\dot{r} + Kr = R}$$

where

$\boldsymbol{M}$ = mass matrix, including structural and hydrodynamic mass

$\boldsymbol{C}$ = damping matrix, including structural and hydrodynamic damping

$\boldsymbol{K}$ = stiffness matrix

The load vector may written as

Equation 5.3: Load vector

$$\boldsymbol{R} = \boldsymbol{X}e^{i\omega t}$$

In Equation 5.3 $\boldsymbol{X}$ is a complex vector, and ω is the load frequency. Similarly, the response vector is written as

Equation 5.4: Response vector

$$\boldsymbol{r} = \boldsymbol{x}e^{i\omega t}$$

where $\boldsymbol{x}$ is a complex vector and ω is the response frequency.

The solution to Equation 5.2 may formally be given as

Equation 5.5: Response solution

$$\boldsymbol{x} = \boldsymbol{H}(\omega)\boldsymbol{X}$$

where $\boldsymbol{H}(\omega)$ is the transfer function matrix.

5 Identifying response frequencies different that the dominating frequency

Variations in riser diameter and current velocity along the span of the riser may give local response frequencies different than the dominating frequency. VIVANA performs a similar analysis to that explained above for the different response frequencies. Excitation zones already taken by more dominating response frequencies are subtracted from new zones, thus avoiding that different response frequencies cover the same excitation zone.

6 Fatigue analysis and post-processing

The final step is a fatigue analysis, where fatigue lives for the different riser sections are calculated.

6 Preventing VIV

VIV can in theory be avoided through several different measures. Changes in the structural properties of riser can be done, but as will be shown, alterations to the outer geometry of riser are easier in practice.

6.1 Changes to riser structural properties

As mentioned in chapter 4, VIV are oscillations at resonance. Thus, avoiding resonance would be an efficient way of avoiding the phenomenon. This means that the reduced velocity U_R is kept lower than 1 (Blevins, 1994), see Equation 6.1.

Equation 6.1: Reduced velocity kept under 1 to avoid resonance

$$U_R = \frac{U}{Df_n} < 1$$

Increasing the stiffness of the structure will according to Equation 4.4 increase the eigenfrequency f_n of the structure, thus reducing the reduced velocity. For longer riser sections, however, this will in practice not be possible as higher mode eigenfrequencies will be excited.

Oscillations at resonance can be significantly decreased if the reduced damping of the structure is sufficiently high.

Assuming a harmonic time varying lift force acting on the riser section

Equation 6.2: Harmonic lift force

$$F_L = \frac{1}{2}\rho U^2 C_L D * sin(\omega_s t)$$

Equation of motion thus becomes

Equation 6.3: Equation of motion for riser section

$$m\ddot{y} + 2m\zeta\omega_0\dot{y} + ky = F_L = \frac{1}{2}\rho U^2 C_L D * sin(\omega_s t)$$

where

y = CF displacement

m = mass per unit length, added mass included

ζ = structural damping factor

k = spring stiffness

ω_0 = eigenfrequency

Assuming the steady-state solution is given as

Equation 6.4: Steady-state CF solution

$$y(t) = A_y \sin(\omega_s t + \varphi)$$

Inserting Equation 6.4 into Equation 6.3 and differentiating gives the solution

Equation 6.5: CF response made dimensionless

$$\frac{y}{D} = \frac{\frac{1}{2}\rho U^2 C_L \sin(\omega_s t + \varphi)}{k\sqrt{\left[1 - \left(\frac{\omega_s}{\omega_0}\right)^2\right]^2 + \left(\frac{2\zeta\omega_s}{\omega_0}\right)^2}}$$

The largest amplitudes occurs when the shedding frequency ω_s approaches the eigenfrequency ω_0 of the cylinder, $\omega_s = \omega_0$. Inserting Equation 6.4 into Equation 6.5 gives resonant amplitude

Equation 6.6: Oscillation amplitude at resonance

$$\left.\frac{A_y}{D}\right|_{\omega_s=\omega_0} = \frac{\rho U^2 C_L}{4k\zeta} = \frac{C_L}{4\pi S^2 \delta_r}$$

The right hand side of Equation 6.6 applies the Strouhal number relationship and the natural frequency relationship given in Equation 4.4. $\boldsymbol{\delta_r}$ in Equation 6.6 denotes the reduced damping, given as

Equation 6.7: Reduced damping

$$\delta_r = \frac{2m(2\pi\zeta)}{\rho D^2}$$

Blevins (Blevins, 1994) has found that a reduced damping δ_r larger than 64 reduces peak resonate amplitudes to less than 0.01*D. However, for most marine structures the reduced damping is smaller than one (Larsen, 2011).

As can be seen from the above discussion, avoiding VIV through modifying the marine structure and its properties has proved to be difficult. Therefore VIV suppression devices have been used to increase the hydrodynamic damping and disrupt the vortex shedding process to reduce VIV oscillations.

6.2 VIV suppression devices

Applying suppression devices to prevent VIV was first done on land based structures, i.e. structures subjected to wind, see Figure 3.1. The specific use of strakes to supress VIV in wind has been used since the early 1960s (Allen, et al., 2008). For marine structures, efforts for developing VIV suppression devices in water started later, around the late 1970s.

6.2.1 Radial water jet suppression

Initially a variety of different VIV suppression devices were studied and many different devices have been proposed over the last three decades. Skaugset investigated the use of radial water jets in a helical pattern along the riser span (Lie & Larsen, u.d.). The jets disrupted the vortex shedding process, thus reducing the CF and IL forces on the riser.

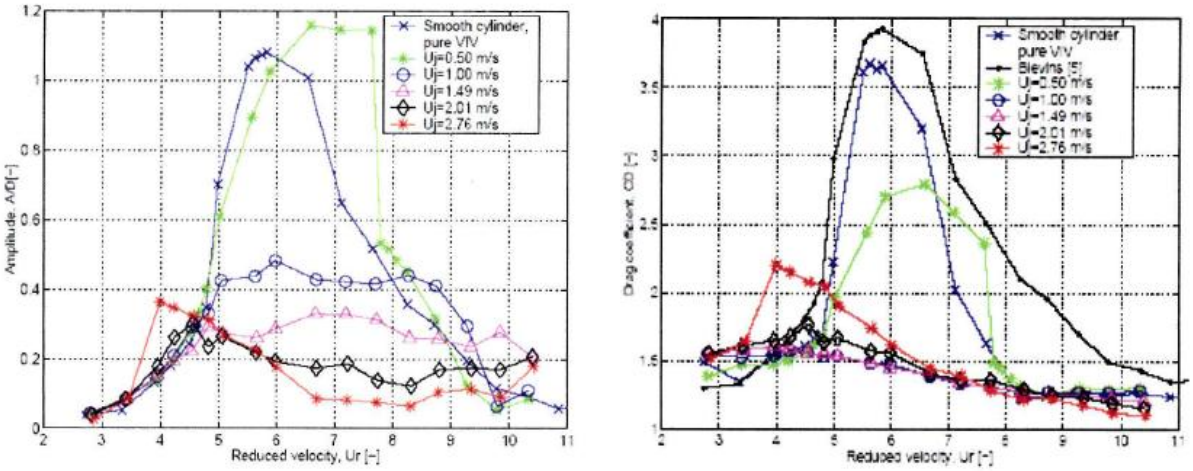

Figure 6.1 Response amplitude and drag coefficients from experiments with radial water jets (Lie & Larsen, u.d.)

Figure 6.1 presents some of the results found by Skaugset (Lie & Larsen, u.d.). As can be seen from the plots, the radial water jets successfully reduce both oscillation amplitude and drag coefficient compared to a smooth cylinder. Limitation to this form of VIV suppression lies in riser length, as distributing water to power the water jets will be difficult for long riser sections.

6.2.2 Other VIV suppression devices

As mentioned above, several proposals have been made for VIV suppression devices. Figure 6.2 illustrates some of the contributions to suppression devices (Blevins, 1994):

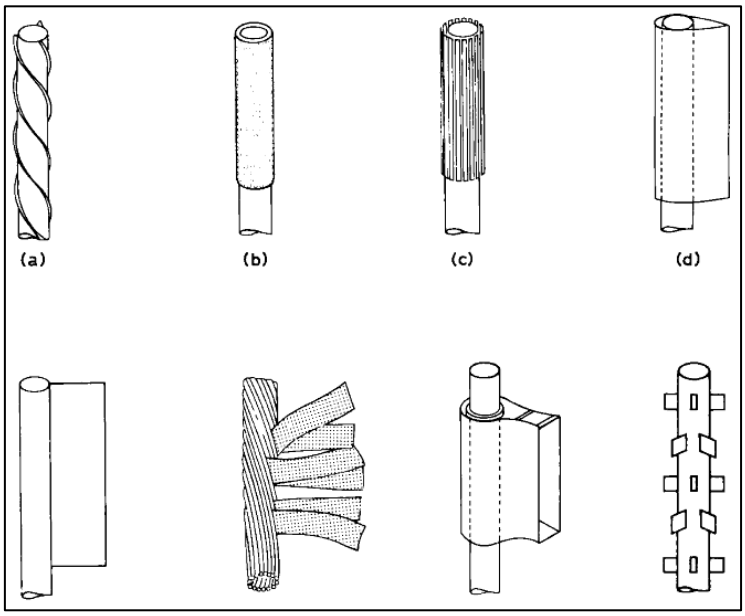

Figure 6.2 Various devices for VIV suppression

a) Helical strakes

This is perhaps the most common way of suppressing VIV, and, as mentioned in chapter 1, is used in a range of different applications. Critical parameters for strake efficiency are height of strake, number of strake and pitch of strake. A more detailed description of strakes will follow later.

b) Perforated shroud

A perforated shroud may be fitted outside the cylinder section to suppress VIV. Blevins (Blevins, 1994) states the following parameters for maximum suppression efficiency:

- Shroud outside diameter: 1.25D
- Per cent open area: 30-40%
- Hole geometry: 0.125D

c) Axial slats

- Slat shroud outside diameter: 1.29D
- Slat width: 0.09D
- Per cent open area: 40%
- Number of slats around circumference: 25-30

d) Streamlined fairings

Along with helical strakes, streamlining of riser sections is today regarded as an efficient way of suppressing VIV. Fairings has been used on a numerous of deep water Gulf of Mexico risers with success (Allen, et al., 2008). Critical parameters are chord length and thickness of fairing.

e) Splitter

The splitter length is 4-5 times the riser diameter to be effective.

f) Ribbon or hair cable

Ribbons or hair cables may be used to prevent organized vortex formation in the wake of the cylinder section, and thus preventing VIV. Figure 6.3 show incident flow on a bare cylinder. The wake clearly shows organized shed vortices. Figure 6.4 shows the same cylinder in the same flow, but fitted with ribbons. Shed vortices in the wake are significantly reduced.

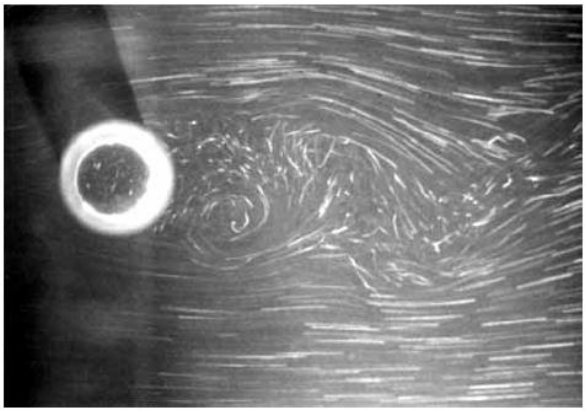

Figure 6.3 Regular cylinder with no ribbons attached

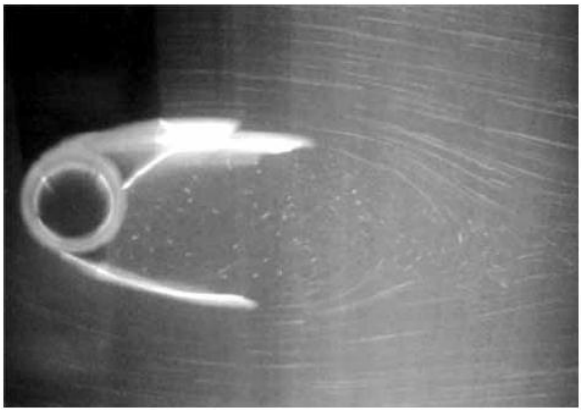

Figure 6.4 Cylinder with ribbons attached to trailing edge

This type of suppression device has many advantages over other devices like helical strakes. The advantages include ease of fabrication, simple design, easy handling and low maintenance (Kumar, et al., 2007). Blevins (Blevins, 1994) gives the following parameters:

- Ribbon width: 1-2D
- Ribbon length: 6-10D
- Ribbon thickness: 0.05D

g) Guide vane

The guide vanes work in a similar way as the streamlined fairing, namely by reducing flow separation around the cylinder. Design of a typical guide vane includes:

- Plate length of roughly 1D
- Lateral separation between the trailing edges of 0.9D.

h) Spoiler plates

Spoiler plates have proved to disrupt the vortex formation and shedding, and thus reducing vortex induced oscillations. Experiments have found a reduced excitation of up to 70% by use of spoilers (Kumar, et al., 2007). A trade-off however, is increased drag. Suggested spoiler geometry and configuration:

- Plate size: squares, D/3 on each side
- Number of plates: 4 in a circumferential ring
- Distance between plates: 2/3 D axial distance

6.3 Strakes

6.3.1 Short background

As previously mentioned, the use of strakes to prevent VIV is not a new idea. While early use of strakes to prevent VIV predominately was found on land based structures, submarines in the First World War used helically wound ropes on the telescopes to prevent oscillations (Lamb, 1991). In the offshore industry however, active use of strakes to suppress VIV was not applied until the late 1970s.

Figure 6.5 Helical strakes. Photo courtesy of VIV Solutions

6.3.2 Function

Helical strakes are used to “control” the vortex shedding process, that is, disrupt the span wise correlation of vortex shedding on the cylinder.

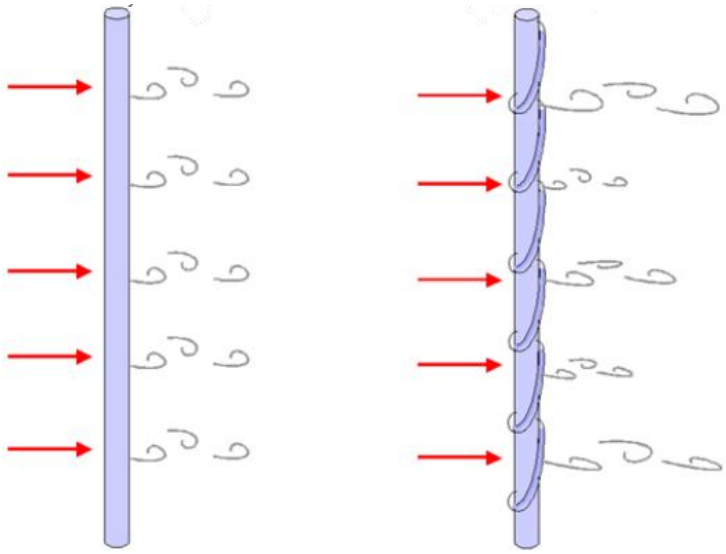

Figure 6.6 Helical strakes controlling the vortex shedding

Figure 6.6 shows a simple sketch of how helical strakes disrupt the vortex shedding process. The riser to the left is bare. Under ideal conditions where influence from riser response has no effect on the shedding process, the vortex shedding will show strong correlation along the riser axis. Consequently, the time varying pressures as illustrated in Figure 4.4 will act on a significant area of the riser, resulting in CF and IL forces.

On the riser to the right, the sharp edges on the strakes force the flow to separate at the strake instead of on the cylinder surface (Lamb, 1991). This means that even though vortices indeed are shed, the geometry of the strakes disrupt the axial correlation of the vortices. This is seen in Figure 6.6 as the strength and location of the shed vortices are varying in the span wise direction. Thus, the global lift-and drag forces are reduced.

6.3.3 Configuration

Several different strake geometries have been tested to find the most efficient configuration. From tests in wind tunnels a geometry with three starts, pitch of 5D and fin height equal to 0.1D was found to be most efficient for VIV suppression in wind. See Figure 6.7 for strake geometry description.

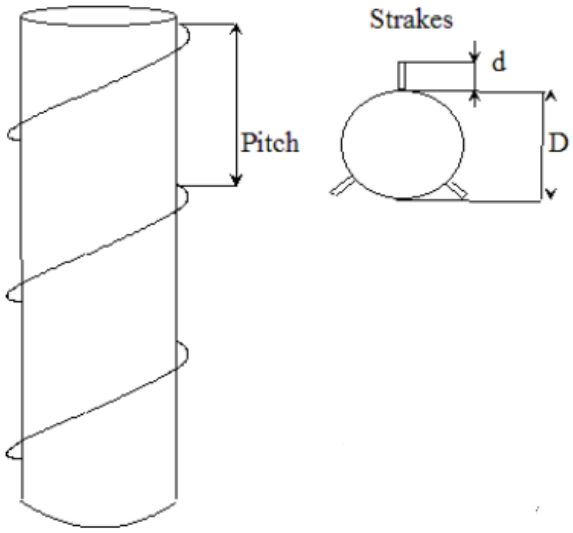

Figure 6.7 Helical strakes parameters illustrated (DNV, 2010)

In water a configuration of triple-start strakes, strake height d=0.25D and pitch equal to 17.5D was found to be more efficient than the previous models from wind tunnel tests. Most helical strakes used for VIV suppression in the offshore industry today have this configuration, or similar strake height with slightly different pitch, usually in the 15-20D range (Allen, et al., 2008).

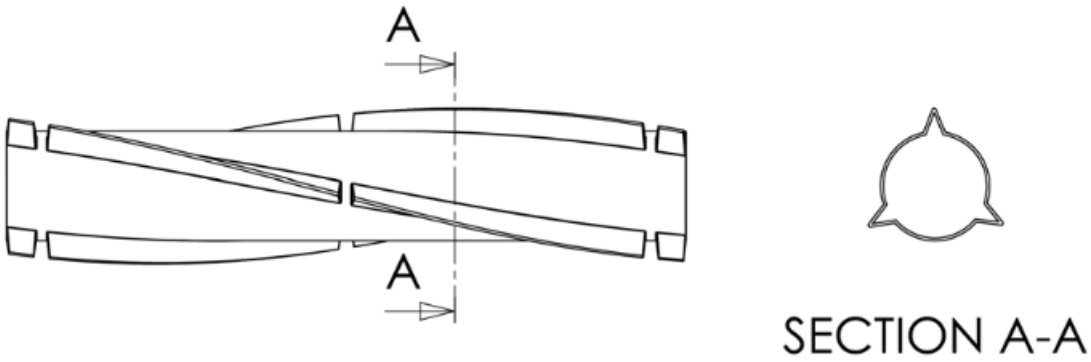

Figure 6.8 Typical helical strake configuration with three starts (Allen, et al., 2008)

6.3.4 Coverage density

A very important aspect when applying helical strakes for VIV suppression is the percentage of strake coverage, also called the *coverage density*. Allen et al. (Allen, et al., 2008) reports that while the

suppression of VIV will be efficient locally for the riser segment covered with strakes, the bare riser sections will still experience significant displacements. Furthermore, Vandiver et al. (Vandiver, et al., 2006) discovered that for a riser with a 40% coverage density at the bottom end, a stress concentration was found in the interface between the straked section and bare section. An explanation may be that traveling waves generated by the vortex induced vibrations were reflected, and thus causing a stress concentration, when meeting the change in mass per length of the straked region.

Larsen et al. (Larsen, et al., 2005) found in a case study using VIVANA that a too small coverage density is possible. Given two helical strake configurations where both configurations are bare close to the water surface, the configuration with the higher coverage density will give better fatigue results. This is of particular importance if the current profile is uniform or close to uniform through the water column.

Figure 6.9 shows the three different strake configurations used in the case study conducted by Larsen et al. (Larsen, et al., 2005). As can be seen, the water depth is 600 meters, and for configuration 1 and 3 the riser segments close to the water surface are bare. Configuration 1 does however have a coverage density of nearly twice that of configuration 3.

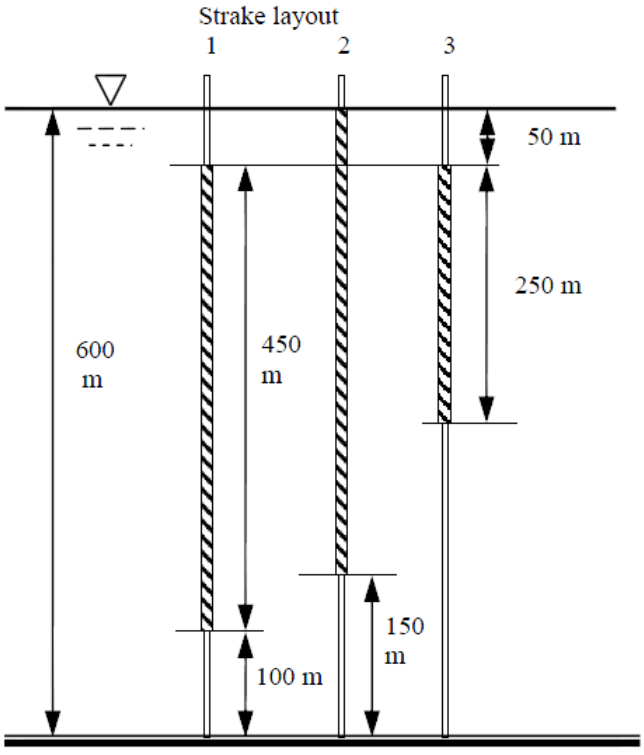

Figure 6.9 Strake configurations used for case study (Larsen, et al., 2005)

Figure 6.10 shows calculated fatigue damage for a uniform current velocity of U=0.5 m/s. As can be seen there is a significant difference between configuration 1 (red line) and configuration 3 (purple line).

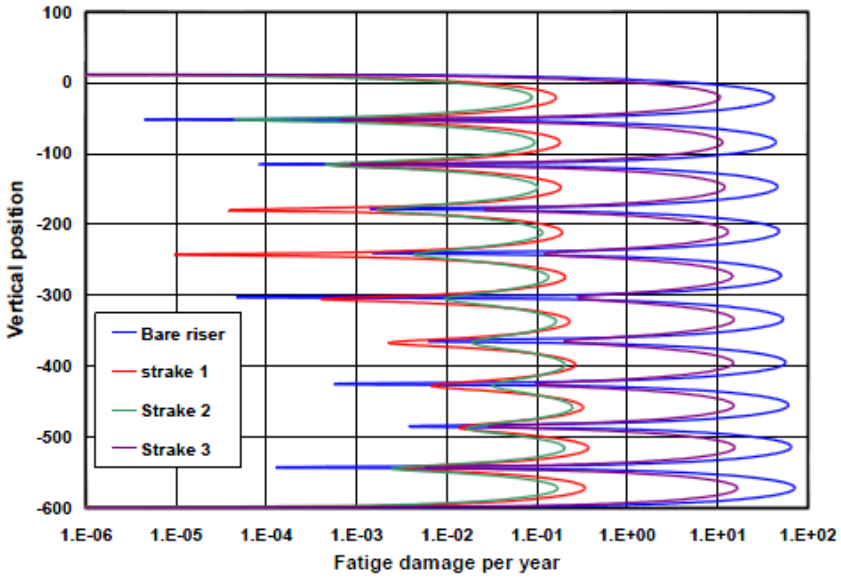

Figure 6.10 Resulting fatigue damage for uniformly current flow U=0.5 m/

While all three strake configurations will give lower fatigue damage than for a bare riser, the smaller coverage density of strake layout 3 only provides a fatigue reduction of less than one decade compared to the bare riser. For strake layout 1 and 2 fatigue reductions of 2 decades are found.

6.3.5 Pros and cons

Applying fairings to deep water risers have both in practice and through analyses proved to reduce and even eliminate VIV. Both case studies performed with VIV analysis software like VIVANA, and experimental work show a, often dramatic, decrease in CF displacements. Furthermore, helical strakes have proved to change and reduce the response frequency of the induced oscillations. Both of these are important aspects in reducing fatigue damage of the riser.

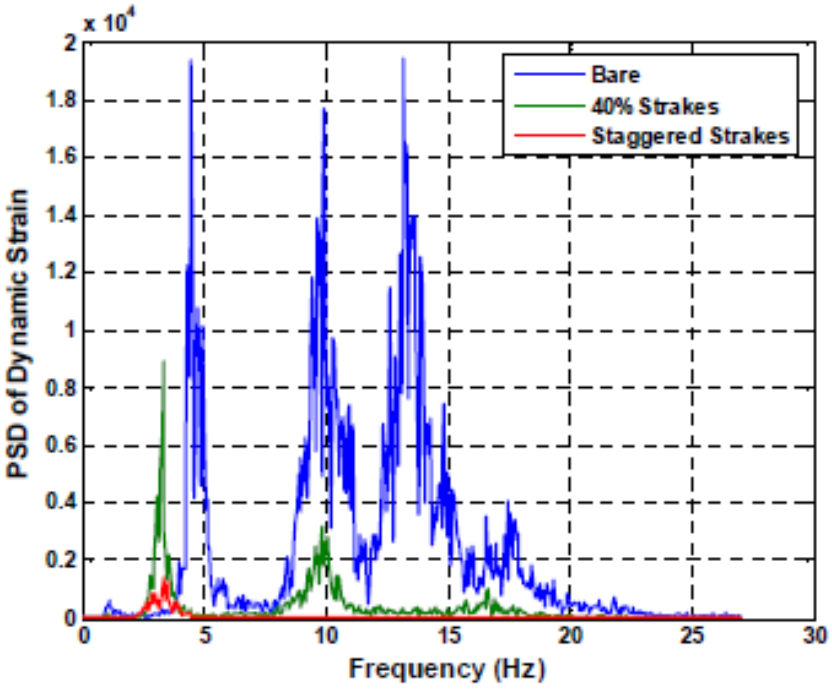

Figure 6.11 PSD distribution for bare riser, 40% coverage density and 70% staggered density (Vandiver, et al., 2006)

Figure 6.11 above shows the Power Spectral Density (PSD) for three different strake configurations of a 100 meter long riser in sheared current (Vandiver, et al., 2006). The bare riser in blue line shows three clear energy peaks, corresponding to response at the first, second and third harmonic frequency. Note that the first harmonic response frequency is set to be equal to the shedding frequency given from the Strouhal relationship in Equation 4.2. While the first, second and third harmonic is found for frequencies roughly equal to 4.48Hz, 10Hz and 13.5Hz respectively, the bare riser also shows significant energy up to 25Hz. This implies that bare riser response may be expected for modes higher than the third harmonic.

The green line represents response for a riser where the bottom 40% is covered with strakes. Response at first and second harmonic may be observed, with a small energy peak at the third harmonic. The frequency content is however limited to 20Hz, with no significant energy above a frequency of 12Hz, which implies that the number of excited modes will be less than for the bare riser.

Lastly, the red line illustrates a 70% staggered strake coverage, which means that 70% of the riser is covered with strakes distributed along the riser length in five separate sections. The frequency content in this configuration is limited to 6Hz, with the first harmonic occurring at roughly 3Hz.

The reduction in response frequency from use of strakes seen above has a positive effect on the fatigue life. The higher the response frequency, the more strain cycles the riser will experience per unit time, which again will lower fatigue life.

As mentioned above, helical strakes can also significantly reduce the amplitude of the oscillations cause by vortex induced vibrations. Figure 6.12 shows the measured non-dimensional CF amplitude of a horizontal riser with roughly one half of riser length covered with strakes.

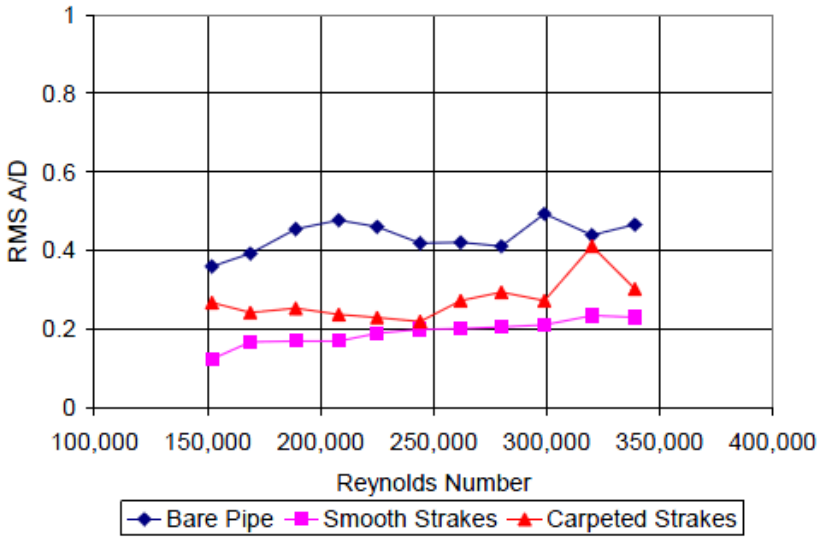

Figure 6.12 RMS non-dimensional CF amplitude versus Reynolds number, outer end (Allen, et al., 2008)

The outer half of the riser has strakes, and the riser is rotating in a test rig to simulate sheared current. This implies that the section of the riser that experiences the highest current velocities is covered with strakes.

The amplitudes, which in Figure 6.12 are measured close to the outer end of the riser, show a significant drop in magnitude for the straked section compared to the bare. This trend is valid across the Reynolds number range.

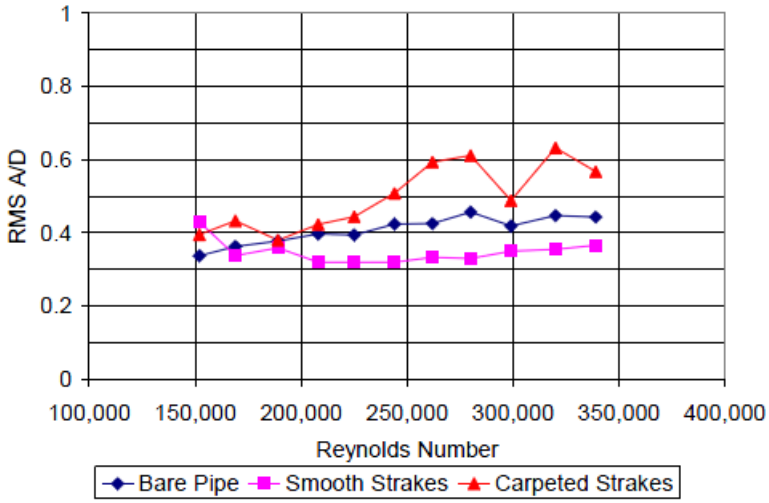

Figure 6.13 RMS non-dimensional CF amplitude vs. Reynolds number, inner end (9)

Figure 6.13 shows the same results measured at inner end of the riser, thus where the riser is bare for all configurations. At low Rn the induced amplitudes are higher for the case where the top half of the riser is equipped with strakes compared to a completely bare riser. However, as the Rn increases, the vortex induced amplitudes for the riser with straked top half are smaller than those of the bare riser, indicating that strakes have a positive effect on suppressing VIV also on the bottom bare half of the riser.

Figure 6.12 and specifically Figure 6.13 give hints to one of the limitations to helical strakes. The red graph in both figures gives the amplitudes for carpeted strakes. The carpet is used to simulate marine growth, which is an important aspect for permanently installed risers, or risers that are designed to operate over a substantial period of time. In both figures, the carpeted strakes provide poorer results than smooth strakes. Note that for amplitudes measured at the inner end of the riser, Figure 6.13, the amplitudes indeed are *higher* for the carpeted strake than for a conventional bare riser. Allen et al. have conducted experiments that show 30% on average, and even as high as 50% worse results for carpeted strakes (Allen, et al., 2008). This serves as a warning for usage of helical strakes in areas with large amounts of marine growth.

Allen et al. (Allen, et al., 2008) conducted similar tests as described above with a fairing equipped riser, see Figure 6.14, and found that this configuration gave better results than those of the helical strakes.

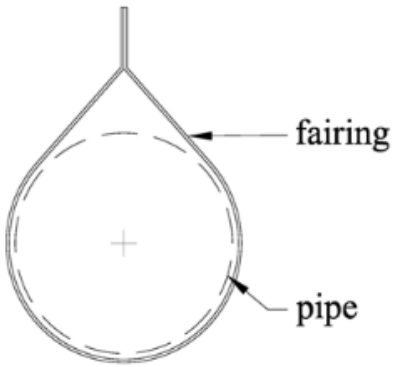

Figure 6.14 Fairing geometry (Allen, et al., 2008)

Both compared to smooth strakes and carpeted strakes, the fairings provide significantly better results. Furthermore, fairing's ability to guide the fluid flow around the structure without early separation will reduce both static drag forces, as well as VIV induced dynamic drag forces on the riser.

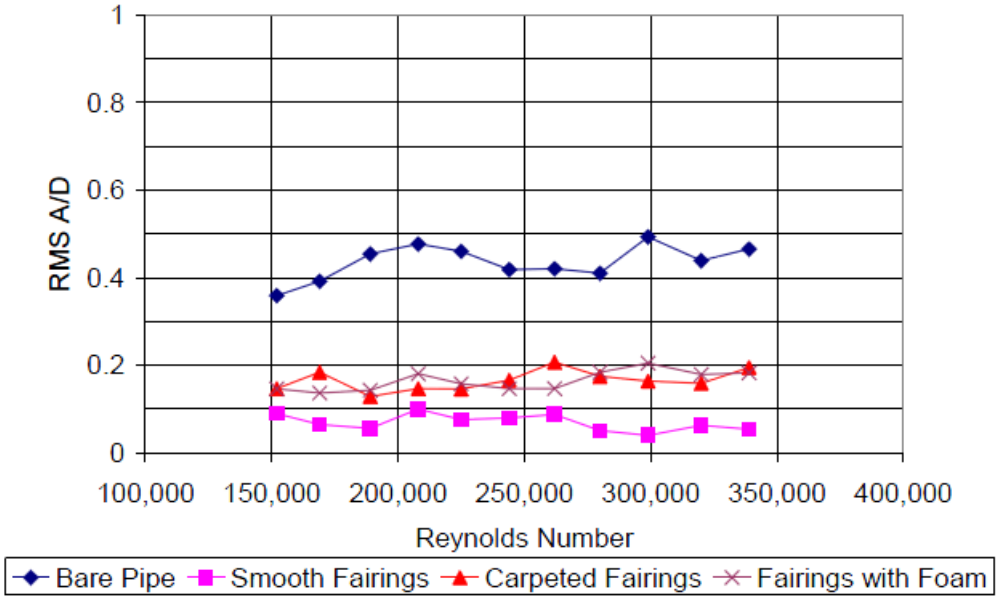

Figure 6.15 RMS non-dimensional CF amplitude vs. Reynolds number with fairings, outer end (Allen, et al., 2008)

Figure 6.15 shows the resulting non-dimensional CF amplitudes of the riser section fitted with fairings. Note that even the carpeted fairings provide more or less the same VIV suppression as the smooth strakes as given in Figure 6.12.

From the discussion above one can draw the conclusion that from a theoretical point of view, smooth helical strakes will provide a good measure for suppressing VIV. However, for areas where marine growth is particularly high, the ability of strakes to suppress VIV is greatly reduced. In fact, helical strakes covered with marine growth may give worse response amplitudes than a bare riser for particular cases. Experiments (Allen, et al., 2008) show that fairings provide better results for VIV suppression. Fairings will reduce the drag coefficient of the static riser, and provide better VIV suppression than a riser equipped with smooth strakes. Furthermore, fairings also perform better when subjected to marine growth. However, in practice aspects like installation and maintenance

costs must be considered. Helical strakes work for all current directions, making them suitable for areas where the current direction may vary over time. For fairings to perform equally, the fairing must be free to weathervane around the riser axis.

Figure 6.16 Fairing installation on drilling riser. Photo courtesy of VIV Solutions

Figure 6.16 shows how fairings may be retrofitted to a drilling riser (VIV Solutions, 2010). Notice the short length of the tail fairing, making the overall chord length small. As can be seen, the fairing is free to weathervane around the riser axis through a patented system. This adds complexity; both during installation and operation, which again adds costs.

6.3.6 Strakes in VIVANA

Riser sections with strakes are in VIVANA modelled by modifying drag coefficients, added mass coefficients and excitation coefficients for the relevant section. Both the drag- and excitation coefficients will show large modifications from a bare to a straked riser, while added mass will only show a slight change (Larsen, 2012).

Both added mass and drag coefficient modification are defined in the INPMOD-module of the program, while the excitation coefficients are defined in the VIVANA module, see VIVANA User's Manual (Yttervik, et al., 2011).

Currently there is no default lift coefficient model for strakes in VIVANA, as the excitation coefficients will depend on strake design which often will vary from case to case. Consequently, user defined input for excitation coefficients of a straked riser section is required, typically found from experimental tests of that particular strake design. Lift coefficient data for a strake design may be presented in the VIVANA module by defining discrete points along curves that define the excitation force coefficient as a function of amplitude for a set of non-dimensional frequencies, as illustrated in Figure 6.17. In the same figure, the different colour curves gives the excitation coefficients for different non-dimensional frequency.

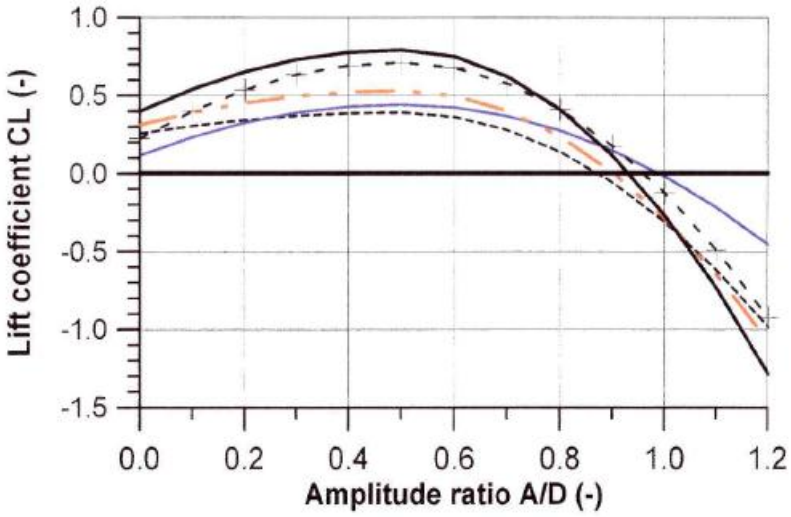

Figure 6.17 CF Excitation force coefficients bare riser

Values for the excitation coefficients used in the present analyses are gathered from recent model tests executed at the Department of Marine Technology, and have been modified compared to excitation coefficients previously used for modelling of straked riser sections (Larsen, 2012).

```
' Strakes15D AIMS
' iprono cprpid
   4   STK15D     14
' fhtyp2    npoint
  0.33         8
'  ad       cl
  0         0
  0.100    -0.390
  0.200    -1
  0.300    -1.85
  0.390    -2.94
  0.490    -4.25
  0.600    -5.80
  0.700    -7.58
'
```

Figure 6.18 Strake excitation coefficient distribution for $\hat{f} = 0.33$

Figure 6.18 shows the excitation coefficient for the non-dimensional frequency $\hat{f} = 0.33$ as defined in the VIVANA module. Note that for all non-dimensional amplitudes denoted *ad* in the table, the corresponding excitation coefficient is negative, which means damping rather than excitation are taking place for all amplitudes at non-dimensional frequency $\hat{f} = 0.33$.

7 Drag forces

The forces parallel to the incident flow acting on a riser are called drag forces. As seen from Figure 4.4 in section 4.3, IL motions during VIV are caused by a time varying drag force acting parallel to the incident flow. These dynamic forces are the result of a non-symmetrical vortex shedding process. However, in addition to the time-varying forces a time-averaged static drag force will give a static response to a riser. Furthermore, CF oscillations from VIV will increase the "efficient" hydrodynamic diameter of the riser section and thus give larger drag forces and static response. In order to calculate this increase in drag from VIV, it is common to separate between drag forces acting on the riser as if the riser was fixed, and add the contribution from amplified drag from VIV.

7.1 Static drag force on a fixed circular cylinder

As for the time-varying drag force discussed earlier, the static drag force on a fixed cylinder is primarily caused by flow separation on the top and bottom side of a cylinder. This will induce a pressure difference between the leading and trailing edge, which integrated over the surface, gives a drag force. Friction forces acting tangentially to the cylinder surface will also add to the total drag force, but compared to the pressure force caused by flow separation, the viscous part is small.

The part of the drag force caused by a pressure difference from the leading and trailing is primarily a function the wake width. The width of the wake will again be a function of fluid separation; more specifically where on the cylinder surface separation occurs. For laminar boundary layer flow, fluid separation will start at approximately $\pm 80°$ measured from the leading edge. For an increased flow velocity and moving through the supercritical and transcritical flow regime, the boundary layer becomes fully turbulent. This induces later separation, and flow separation occurs at angels roughly equal to $\pm 120°$. The result is a narrower wake and reduced drag force. There are other ways of forcing the boundary layer to become turbulent than simply increasing flow velocity. Increased surface roughness will give a turbulent boundary layer earlier than a smooth surface, and may therefore decrease drag. The most famous example is the dimples on a golf ball.

The drag force may be expressed in a similar fashion as the excitation force given in Equation 5.1.

Equation 7.1: Drag force

$$F_D = \frac{1}{2}\rho U^2 C_d D * dl$$

where

ρ = fluid density

U= fluid velocity

C_d = drag coefficient

D = cylinder diameter

dl = span-wise increment

As can be seen from Equation 7.1, the total drag force is a function of both the drag coefficient C_d and the cylinder diameter D. Below is a drag coefficient plot for a circular cylinder subjected to

incident flow of varying flow velocity. The plot shows how a rough cylinder will experience a turbulent boundary layer earlier than the smooth cylinder, and therefore shows the associated drop in drag from a narrower wake, earlier.

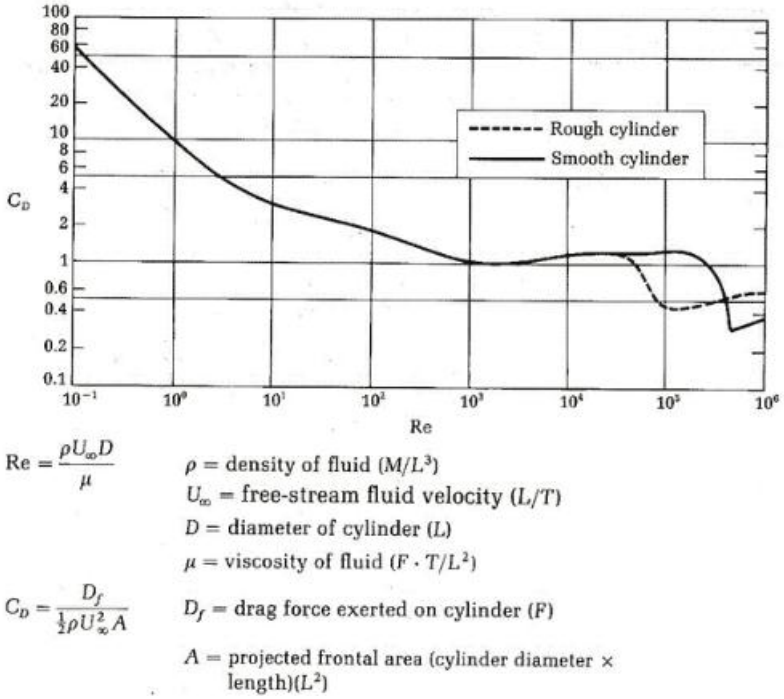

Figure 7.1 Drag coefficient for circular cylinder, smooth and rough surface (Schlichting & Gertsen, 2000)

The increased cylinder diameter from suppression devices like strakes, will clearly create a larger drag force on the riser section which means a larger static deflection. However, as will be discussed next, the benefits from strakes will not only reduce the fatigue damage from dynamic response, it will also reduce the VIV drag amplification, and thus the static response.

7.2 Drag amplification from VIV

As mentioned above, vortex induced vibrations will increase the hydrodynamic diameter of the riser. This means that the effective diameter the incident flow "sees" is increased, resulting in a larger projected area and thus larger drag force. For long riser sections, this drag increase may result in a dramatic increase in static response.

Drag coefficient for risers in VIV conditions are found empirically, and several drag coefficient proposals have been introduced. Equation 7.2, Equation 7.3 and Equation 7.4 are examples of proposed drag coefficients by Blevins, Vandiver and Skop et al. respectively (Blevins, 1994).

Equation 7.2: Drag coefficient Blevins

$$\frac{C_d\left(\frac{A}{D}\right)}{C_d(A=0)} = 1 + 2.1 * \left(\frac{A}{D}\right)$$

where

$C_d(A=0)$ = drag coefficient at zero amplitude, i.e. for the fixed cylinder as given in Figure 7.1

A = VIV amplitude

D = cylinder diameter

Equation 7.3: Drag coefficient Vandiver

$$\frac{C_d\left(\frac{A}{D}\right)}{C_d(A=0)} = 1 + 1.043 * \left(\frac{2 * A_{rms}}{D}\right)^{0.65}$$

where

A_{rms} = Root Mean Square, square root of the time average of the square of the amplitude

Equation 7.4: Drag coefficient Skop et al.

$$\frac{C_d\left(\frac{A}{D}\right)}{C_d(A=0)} = 1 + 1.16\left\{\left[\left(\frac{1+2A}{D}\right) * \frac{f_n}{f_s}\right] - 1\right\}^{0.65}$$

where

f_n = eigenfrequency

f_s = vortex shedding frequency

Both MIT's Shear7 (Vandiver & Li, 2005) and Marintek's and NTNU's VIVANA use Vandiver's model for VIV drag amplification, given in Equation 7.3.

Larsen et al. (Larsen, et al., 2005) conducted case studies where different strake configurations and current profiles were evaluated, see Figure 6.9. For a linearly shared current in 600 meter water

depth, and maximum current velocity of $U_{max} = 0.5\ m/s$, the following static displacements were found, see Figure 7.2.

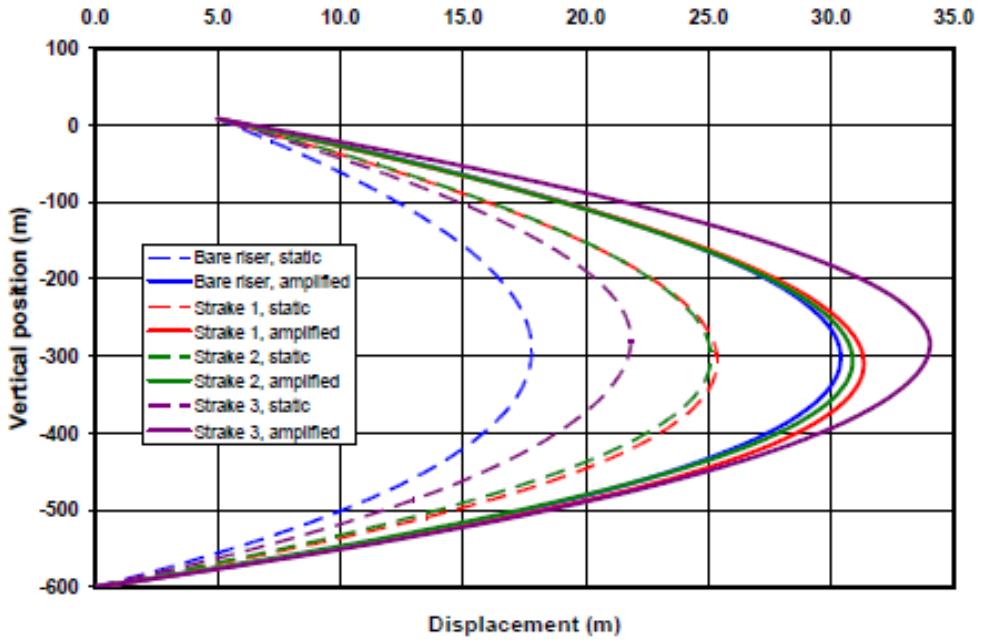

Figure 7.2 Static displacement of drilling riser in varying current distributions (15)

In the Figure 7.2 above strake configuration number 1, see Figure 6.9, marked with red lines represent the strake layout with highest coverage density. This can be seen from the static displacement of the riser section when no VIV amplitudes are present, i.e. $A = 0$, illustrated by the striped red line. Compared to the striped blue line which illustrates the static displacement for $A = 0$ for the bare riser, there is a clear increase in drag from the added strakes. From the discussion above this is expected. Note however, that the increase in static displacement from no VIV to the amplified drag from VIV is greatly reduced for the riser with strakes. The total average drag will still be larger than that of the bare riser, but the increase from no VIV to VIV amplified drag is greatly reduced when strakes are applied. The reason for this is the reduced VIV amplitudes of a straked riser, which will reduce the amplified drag as seen in Equation 7.3.

7.3 Drag amplification consequences

As discussed above, drag forces will create a static deflection of the riser. For large water depths where ocean currents can reach high velocities, the static riser response may be significant. Consequently, the possibility of damaging the riser stack-up increases. With the emphasis on riser integrity and well control after the Macondo accident, clear design guidelines to maximum allowable flex joint angles are presented in the standards.

Figure 7.3 shows an excerpt of the drilling riser design guidelines as given in ISO 13624-1 (ISO, 2009). The rows marked in yellow gives the mean and maximum allowable flex joint angles for drilling and non-drilling operations. Non-drilling operation typically includes completion and workover operations.

Design parameter	Riser connected		Riser disconnected
	Drilling	Non-drilling	
Mean upper flex/ball jt. angle [a]	1° to 1,5°	N/A	N/A
Max. upper flex/ball jt. angle [a]	5,0°	90 % available (or contact with moonpool structure)	90 % available (or contact with moonpool structure)
Mean lower flex jt. angle [b]	2,0°	N/A	N/A
Max. lower flex jt. angle [b]	5,0°	90 % available	N/A
Stress criteria: [c,d]			
– Method "A" - allowable stress [e]	0,40 σ_y [f]	0,67 σ_y [f]	0,67 σ_y [f]
– Method "B" - allowable stress [e]	0,67 σ_y [f]	0,67 σ_y [f]	0,67 σ_y [f]
– Sign. dyn. stress range [e]			
@ SAF $\leqslant$ 1,5 [g]	69 MPa (10 ksi)	N/A	N/A
@ SAF > 1,5 [g]	$15/F_{SA}$	N/A	N/A
Minimum top tension [h]	T_{min}	T_{min}	N/A
Dynamic tension limit [i]	F_{DTL}	F_{DTL}	N/A
Maximum tension setting	90 % F_{DTL}	90 % F_{DTL}	N/A

NOTE 1 The flex/ball joint angles are differential global angles around the flex or ball joints and, because the wellhead tilt and riser angle (or vessel pitch/roll and riser angle) can be in different planes, they are not easily determined by independent bullseye levels both above and below the flex/ball joint. It is necessary to keep the flex/ball joint angles as small as practicable to avoid wear in the riser system components. The value of 2° in Table 2 is specified to include routine situations with low risk of significant wear, which could not continue with a more restrictive angle. For many drilling operations, mean differential angles are maintained at less than 1°.

NOTE 2 The rate of wear at flex/ball joints between two pieces of metal is dependent on four parameters:

— contact force;
— relative velocity;
— material parameters;
— properties of the surrounding fluid.

For a drillstring in a riser system, the relative velocity is dictated by operations, either rotation rate or running/pulling speed; the material properties are usually specified (steel); and the surrounding fluid is the drilling fluid returns (more of an abrasive than a lubricant). The only parameter subject to control is the contact force.

The contact force is of concern where the drillstring is forced to conform to the bore of the riser system (primarily near the flex/ball joints). The force is amplified when the annulus between the drillstring and the riser bore is small (smaller ID risers, larger OD drillpipe), and when the drill-string tension at the point of contact is high (drill-string is less flexible). Examples of high wear cases include

a) wells deep below the mud line: high tension in the drillstring at the lower flex/ball joint;
b) use of large diameter drillpipe (168 mm [6-5/8 in], for example): smaller annulus, together with higher tension due to a heavier drillstring.

An example of a low wear case is a shallow well drilled with small diameter drillstring. The tool joints are usually responsible for much of the wear.

Figure 7.3 Excerpt of Marine drilling risers Design Guidelines, ISO 13624-1 (ISO, 2009)

As can be seen, a mean lower flex joint (LFJ) angle of 2° should not be exceeded during drilling, while the maximum allowed LFJ angle during drilling is 5°. For non-drilling operations such as completion and workover, the LFJ angle should not exceed 90% of available angle. ISO 13628-7 states the following values (ISO, 2006) for workover operations performed through a drilling riser, also called in-marine workover operations, see Figure 7.4.

As can be seen from Figure 7.4, the maximum allowable flex joint angle for running and retrieval, normal workover operations and retrieval of stuck tubing shall not be more than $\pm 1°$, $\pm 3°$ and $\pm 2°$ respectively. According to ISO 13624-1 (ISO, 2009) the maximum allowable flex joint angle is typically 10°.

Load condition	Minimum values of the maximum drilling riser angle ball/flex joint angle degrees
Running and retrieval [a]	± 1,0
Normal operation	± 3,0
Overpull to retrieve stuck tubing	± 2,0

[a] The angle shall allow for passage of tubing hanger, tubing hanger running tool and landing string.

Figure 7.4 Flex joint angles for workover operations according to ISO 13628-7 (ISO, 2006)

The values given above are valid for operational conditions. In case of an emergency where an emergency disconnect is necessary, the LFJ angle should be less than 2 degrees to ensure that the release of the riser from the BOP stack is executed without problems. Thus, for large static riser deflections a change in platform position may be required to ensure a small LFJ angle and successful emergency disconnect.

8 Methodology

This chapter states the main problem of the analysis part of the thesis, as well as presents some of the industry standards and recommended practices that discuss the phenomenon of VIV.

8.1 Standards

This section gives a short presentation of some of the standards and regulation which today set guide lines for VIV assessment of marine risers in the offshore industry. As mentioned in the Introduction, strict rules and regulations for any type of equipment assigned to work on the Norwegian Continental Shelf are put forward by the Petroleum Safety Authority. The Petroleum Safety Authority is the part of the Norwegian Government that has legislative authority on matters concerning the offshore industry and activity on the NCS. Typically the Petroleum Safety Authority will refer to certain standards and recommended practices from organisations and foundations such as API, ISO and DNV that must be used and followed under design and construction of the equipment. As engineering challenges linked to VIV may occur for a variety of different offshore structures and equipment, assessment of VIV is described in a number of standards and RPs. Ranging from VIV in tubular sections of fixed structures like XMTs, to VIV evaluation of several kilometre long production lines, standards and recommended practices should cover all aspects of safe design in the relevant case. In the following however, only standards and RPs applicable for marine risers and workover systems are presented.

8.1.1 ISO 13628

The International Organization for Standardization (ISO) is a non-governmental, international standard-setting foundation composed of representatives from various national standard organizations. For the petroleum and natural gas industries, the standard ISO 13728 “Design and operation of subsea production systems” sets requirements and rules that must be followed. Part 7 of this standard “Completion/workover riser systems” forms the benchmark for system and functional requirements, design and analysis as well as testing of workover riser systems.

Chapter 6 in ISO 13628-7 handles design requirements of the system, and section 6.3.4.4 lists the points that shall be considered with respect to fatigue load analysis of the relevant system. Point c) in the list specifically points out that Vortex Induced Vibrations shall be analysed and considered when cyclic load effects are evaluated (ISO, 2006).

In Appendix B of the same standard, the procedures of a global riser analysis are described. In section B.3.1 point f) the standard points out that VIV should be assessed and an evaluation for the need of monitoring and inspecting if the riser is susceptible to VIV should be executed. If so, increased top tension and/or suppression devices are given as possible measures for VIV avoidance. The last paragraph of section B.3.4 in Appendix B gives a short sentence about the effects of VIV on hydrodynamic coefficients. In particular VIV’s effect on increased drag is mentioned in the standard.

Appendix C in ISO 13628-7 gives assessment procedures for fatigue damage. Section C.5.3 explains that VIV may be an important factor when fatigue damage is evaluated. Where VIV is likely to represent a design problem, refined assessment methods preferably supplemented by tests are required. As a last note, Appendix C in ISO 13628-7 mentions the following: “Many aspects of vortex-induced vibrations causing fatigue damage in C/WO risers are not understood. However, assessment

should be performed to investigate the possible susceptibility for vortex-induced vibrations" (ISO, 2006).

8.1.2 DNV-RP-C205

Det Norske Veritas (DNV) is an autonomous and independent foundation that writes standards and recommended practices for a number of different industries. DNV's main objectives are "safeguarding life, property and the environment, at sea or onshore" (DNV, 2010).

DNV-RP-C205 "Environmental Conditions and Environmental Loads" lists and explains analysis methodology for all environmental loads on offshore structures. Chaphter 9 handles Vortex Induced Oscillations solely, which includes vortex induced vibrations in *any* fluid, including water and wind. A brief theoretical introduction is given where parameters like Strouhal number, Reynolds number and reduced velocity are explained. Lock-in where the response frequency "locks on" and becomes controlled by the eigenfrequeny is described, however the standard states that for flexible risers that respond for multiple modes, pronounced lock-in does not occur. Added mass and hydrodynamic damping is discussed, and the same experiments used as basis for the added mass- and damping models in VIVANA, see VIVANA Theory Manual (Larsen, et al., 2009), are given as examples. The same equations for drag coefficients (Blevins, 1994) given in section 7.2 in this report are also listed in DNV-RP-C205.

For VIV analysis and assessment the standard divides the current computational models into three:

- Response based models
- Force based models
- Flow based models

VIVANA falls into the response based model category, and reference is made to DNV-RP-F204 (DNV, 2010) for recommended practice of response based models.

8.1.3 DNV-RP-F204

The standard DNV-RP-F204 "Riser Fatigue" gives recommended practices for analysis and evaluation of fatigue loads on marine risers. Chapter 4 in DNV-RP-F204 handles VIV fatigue damage and VIV analysis. When use of semi-empirical VIV software, the standard stresses the importance of sensitivity studies linked to user controlled input parameters, as these play a significant part for the end result of the VIV analysis. According to the standard the applied user controlled parameters should be "realistic and justifiable" (DNV, 2010).

The standard proposes a simplified method for VIV assessment. The method is loosely based on the procedure that VIVANA uses for VIV evaluation, namely by defining an excitation zone, or length as is used in the simplified model, where energy is transferred into the riser system:

1. Determine eigenfrequencies and eigenmodes in CF and IL direction from a numerical FEM analysis.
2. An effective velocity U_{eff} is found from Equation 8.1 once the hydrodynamic diameter is determined. The excitation length L_{exc} is taken to be the part of the riser where the velocity is larger than 2/3 of the maximum velocity, see Figure 8.1.

Equation 8.1: Effective velocity for simplified VIV analysis

$$U_{eff} = \frac{1}{L_{exc}} \int_{L_{exc}} U(z)dz$$

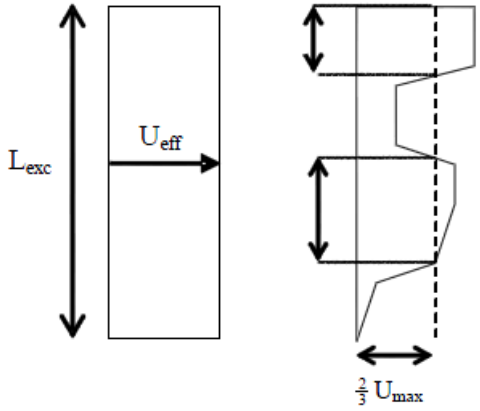

Figure 8.1 Uniform velocity profile where the excitation zone is indicated (DNV, 2010)

3. The shedding frequency f_s is defined from the Strouhal relationship, St=0.17 to 0.25
4. All eigenmodes with an eigenfreqency within a band around the shedding frequency are assumed to be excited, see below:

$$f^{CF} \in [(1-\Delta)f_s, (1+\Delta)f_s]$$
$$f^{IL} \in [(1-\Delta)2f_s, (1+\Delta)2f_s]$$

   The factor 2 for IL frequencies indicate that IL response appears at twice the frequency of CF response, as explained in section 4.3.

5. From the excitation length found in step 2, the rms response amplitudes of CF amplitudes may be found from Figure 8.2.

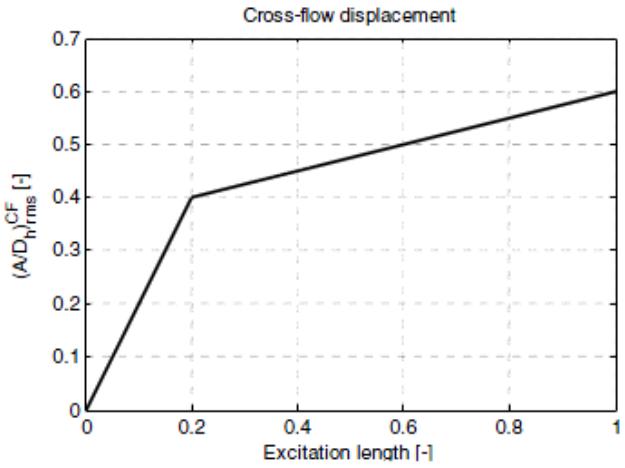

Figure 8.2 (A/D) for as function of excitation length for CF response

For suppression of VIV the standard explains that several modifications to the riser properties may be done, including change of riser tension, diameter and structural damping. The standard refers to the suppression devices given by Blevins (Blevins, 1994) and described in section 6.2.2 of this thesis report. A modification of the procedure given above is also given for simplified analysis of risers with

strakes. The modification is valid for two specific strake designs. The strakes have triple start helical configuration, and the following properties (DNV, 2010):

- Pitch of 17.5 D and strake height of 0.25 D
- Pitch of 5 D and strake height of 0.14 D.

A modified excitation length, point 2 above, is found by only considering the part of the riser where the riser is bare. This implies that the effective velocity is set to zero at straked parts of the riser. In point 5 where the rms CF response is calculated, the reduction factor $(1-\alpha^2)$, where α is the strake coverage fraction, is valid and will further reduce the response. α is only valid for the two strake configuration given above.

There are several simplifications to the procedure described above compared to a full analysis in VIVANA. One of the most important ones is the assumption that riser response appears at or close to the shedding frequency given from the Strouhal relationship. Furthermore, added mass variation for the oscillating riser is not accounted for.

When a general strake design is applied to a riser and VIV analyses are executed, the standard requires that the effectiveness of the relevant strake configuration must be quantified, and the following should be considered by third-party verification (DNV, 2010):

- Model test results with and without strakes
- Effect of hydrodynamic scaling
- Range of current velocities and associated efficiency
- Durability and impact assessments
- Effect of marine growth
- Effect of surface finish

8.1.4 API RP 2RD

The American Petroleum Institute is a national trade association that aims to represent all aspects of America's oil and natural gas industry. For more than 75 years the association has led the development of petroleum and petrochemical equipment and operating standards (api.org, 2011).

API RP 2RD "Design of Risers for Floating Production Systems (FPSs) and Tension-Leg Platforms (TLPs)" gives guidelines and requirements for design consideration, design loads, analytical considerations as well as use of materials for FPSs and TLPs.

In chapter 6 "Analytical Considerations", section 6.3.5 discusses hydrodynamic considerations in riser analysis (API, 1998). A separate section, section 6.3.5.7 is given to vortex suppression devices. Wake fairing, helical strakes and alternate buoyancy joints are mentioned and discussed as possible measures for preventing VIV.

Section 6.6.3 of the standard gives an algorithm of how a VIV analysis should be performed. The procedure is fairly similar to that given in DNV-RP-F204, however no model is presented for determining riser response. The user is free to choose the model: "If VIV is possible, the VIV responses are determined from an appropriate model" (API, 1998).

8.1.5 Concluding remarks on the presented standards

With the exception of the algorithm for the simplified VIV analysis presented in DNV-RP-F204 “Riser Fatigue”, no detailed description of recommended procedure for a full VIV analysis is given in the standards. The formulations in the standards are often vague, as is exemplified by the quote taken from API RP 2RD “If VIV is possible, the VIV responses are determined from an appropriate model” (API, 1998).

The DNV standard DNV-RP-F204 “Riser Fatigue” is somewhat more precise in its formulations linked to validation of user-defined inputs to the semi-empirical models, typically lift coefficient distributions and added mass distributions. For appliance of strakes, third party verification of the strakes effectiveness must be performed.

For the presented analysis, all input parameters given in VIVANA are validated by current and updated model tests at the Department of Marine Technology and in collaboration with SINTEF (Larsen, 2012). The requirements stated above in DNV standard DNV-RP-F204 “Riser Fatigue” are therefore fulfilled.

8.2 Literature review

VIV is a well-known phenomenon in the engineering industry, and may occur in any circular structures subjected to fluid currents. Several books and scientific papers on VIV have been published through the last decades, and a variety of computer programs have been proposed for VIV analysis.

Blevin’s book “Flow Induced Vibration” (Blevins, 1994) is a particularly important book on the matter, and has been used as reference in a number of standards (DNV, 2010) and scientific papers (Lie & Larsen, u.d.).

The majority of the scientific papers used as references in this thesis report are publications from the Offshore Technology Conference (OTC) or the Conference on Offshore Mechanics and Arctic Engineering (OMAE). Both conferences are considered among the world’s foremost events for development of offshore resources in fields of drilling, exploration, production and environmental production.

The computer program VIVANA used in this master thesis is considered, along with the MIT developed *Shear7*, as the industry standard for VIV analysis. VIVANA has undergone several iterations since its first version, and is the result of more than a decade of experimental VIV research at MARINTEK/NTNU. The Bearman/Chaplin benchmark case proved VIVANA’s strong capabilities in VIV prediction, when a number of computer codes were invited to a study where laboratory measurements were compared with blind predictions by the codes. VIVANA gave the best predictions for a number of different parameters in the study (Larsen, 2011).

8.3 Scope of case study

As is discussed above, several of the standards and RPs used in the offshore industry touches on the matter of VIV. While the standards underline that there still are aspects of VIV that still are not clearly understood, most require complete VIV analyses of new riser systems for the systems to be in accordance with the standards.

In the analysis two Aker Solutions workover systems have been chosen as base platforms for a thorough investigation of VIV on medium and deep water depths using the computer program VIVANA. Both systems are Category C systems, see section 2.3, which means that the workover operations are performed through a drilling riser, so called in-marine workover operations. No VIV analyses have been conducted on the Category B open water workover risers, see section 2.2, as the geometry of this type of riser will introduce uncertainties to the analysis. The open water riser applies a number of umbilicals clamped to main riser tube thus giving a non-circular cross section. It was therefore concluded that a VIV analysis of the category B open water riser would give too many sources for error, and was thus excluded (Larsen, 2012).

The standards propose several measures that may prevent VIV, including the use of strakes and span wise variation of OD along the riser length. Still, no details regarding coverage density or placement of strakes are given in the presented standards; sensitivity analyses must be performed. Based on some of the experiments, (Larsen, et al., 2005) and (Allen, et al., 2008), given in the literature review of the report, a coverage density of roughly 50% is used for the presented analyses. While a coverage densities from 40% up to 75% are seen in the mentioned experiments, (Larsen, et al., 2005) and (Allen, et al., 2008), 50% was chosen for the reduced static riser deflection of the lower coverage densities.

The analysis considers the effects of applying strakes to sections of the riser, and important parameters like static riser deflection from added drag from VIV, dominating VIV frequencies and amplitudes are studied. Furthermore, varying outer diameter of riser joints is investigated. Finally, operational consequences from VIV' effect on flex joint angles are addressed.

A detailed description of the analysis procedure as performed in the presented case study is given in chapter 10.

Part II: The analysis

9 The systems and current models

Two Aker Solutions systems have been used as basis for the current VIV analyses. Both systems will be installed on oil fields located far north off the Norwegian coast, one west of Bodø in the Norwegian Sea, and one northwest of Hammerfest in the Barents Sea. The water depths at the two fields are 1300 meters and 321 meters respectively.

An initial analysis for both systems with no strakes is performed. Critical results as initial riser deflection, added deflection from VIV as well as active VIV response frequencies and resulting fatigue damage is reported for several different current profiles.

A VIV assessment for alternate bare and buoyancy joints is also performed for both systems. Vortex induced vibrations may be reduced by having a staggered buoyancy and bare joint configuration, as the outer diameter of a bare joints is significantly smaller than for a buoyant joint (API, 1998). This will give varying span wise shedding frequency, which in theory may result in smaller VIV oscillations and thus lower fatigue damage.

Finally case study analyses are performed for varying locations of strakes on the two systems. Thus, for the 321 m water depth system, the configurations are:

- Base configuration, no strakes
- Staggered configuration, buoyant and bare joints in alternate order along 160 m of the riser
- Bottom 150 m of the riser length covered with strakes
- Middle 160 m of the riser length covered with strakes
- Top 145 m of the riser length covered with strakes

Analyses of the 1300 m water depth system consist of the following configurations:

- Base configuration, no strakes
- Staggered configuration, buoyant and bare joints in alternate order along 1234 m of the riser
- The bottom strake configuration is replaced by a configuration where the top 150 m of the riser is bare, i.e. no strakes, while the next 650 m of the riser is straked
- Middle 650 m of the riser length is straked
- Top 650 m of the riser length is straked

The analyses are performed using actual measured current profiles from the two locations, current profiles based on measurements from other locations on the NCS as well as more “theoretical current models”.

All analyses executed for the 1300 m water depth system are done in drilling mode, which means that there is no XMT in the stack-up. For the 321 m water depth, analyses are made in completion mode, which means that the stack-up includes a XMT.

9.1 System description 321 m water depth

As can be seen in Figure 9.1, the 321 m water depth system in completion mode applies a fairly standard stack-up configuration with Christmas Tree (XMT) attached to the wellhead. Then a Blow Out Preventer (BOP) is fixed to the XMT for well control and emergency measures. On top the BOP, a Lower Marine Riser Package is situated, which in turn is fixed to the Lower Flex Joint (LFJ). The LFJ provides a softer transition from the LMRP with high bending stiffness, to the first of three bare riser joints which have significantly less bending stiffness. Note that in Figure 9.1 the length of the lower flex joint has been included in the LMRP length. To reduce the required top tension, roughly 50% of the riser length consists of buoyancy joints, which are basic riser joints covered in low density, buoyant material.

Following the 7 buoyancy joints are two bare joints, which again is fastened to a pup joint. From there a spacer joint is linked to the telescopic joint for heave compensation. Note that no Pipe-in-Pipe (PIP) effects have been considered in the analyses, this will be further discussed later. The Upper Flex Joint (UFJ) provides transition to the diverter, and absorbs some of the bending moments from drift-off or other weather induced motions.

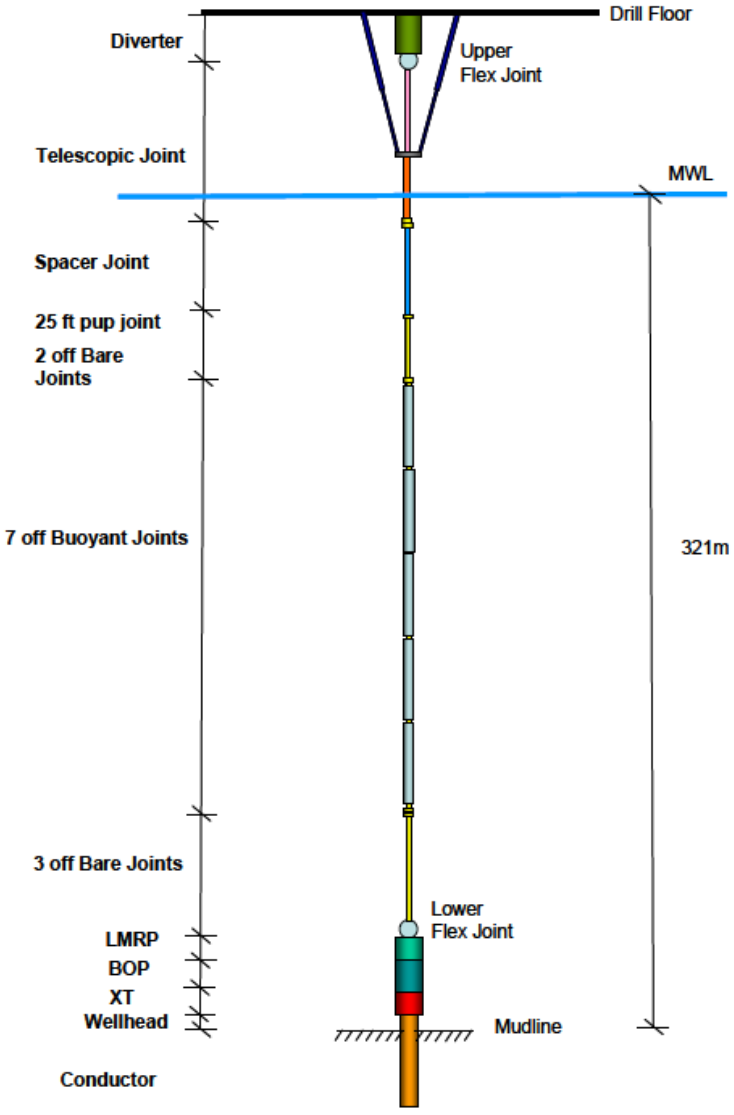

Figure 9.1 System overview 321 m water depth

Table 9-1 gives the total stack-up data for the 321 m water depth.

component	length [m]	quantity	Total length [m]	OD [m]	OD buoyancy [m]	ID [m]	Mass [kg]
Diverter	6,18	1	6,18	1,575	-	1,511	3410
UFJ	1,525	1	1,525	0,612	-	0,495	5210
Telescopic joint	31,24	1	31,24	0,66	-	0,483	40131
Spacer joint	12,87	1	12,87	0,556	-	0,495	10520
Pup joint	7,63	1	7,63	0,556	-	0,495	6230
Riser bare	22,86	2	45,72	0,533	-	0,495	13910
Riser buoyant	22,86	7	160	0,533	1,397	0,495	13910
Riser bare + adaptor	23,76	3	71,28	0,533	-	0,495	13910
LFJ	1,525	1	1,525	0,612	-	0,495	5210
LMRP	3	1	3	0,737	-	0,476	85409
BOP	9	1	9	0,737	-	0,476	194591
XMT	3,2	1	3,2	0,737	-	0,476	55000
WH	3,2	1	3,2	1	-	0,452	60000

Table 9-1 Stack-up data 321 m water depth

Both flex joints are assumed to have linear rotational stiffness. Values for rotational stiffness are given below.

component	Rotational stiffness [kNm/deg]	Maximum rotation [deg]	Mass [kg]
Upper flex joint	13	9	5210
Lower flex joint	46	10	5210

Table 9-2 Flex joint data 321 m water depth

The stiffness of the upper flex joint for both 321 m and 1300 m water depth is the same at 13kNm/degree, while the stiffness of the lower flex joint is half that of the 1300 m water depth system, as will be discussed later.

9.1.1 Staggered configuration, 321 m system

While it would have been possible to add alternate buoyant and bare joints for the majority of the riser length, only the middle 160 m of the riser has staggered joints in this analysis. Previous in-house global wave analyses at Aker Solutions revealed problems with substantial drag forces on the riser fitted with a larger buoyancy section than that given in Figure 9.1. Consequently, the buoyancy joints close to the surface where wave action is largest were removed and replaced by bare joints to decrease drag. This analysis builds on the modified AKSO setup, which implies that a further half of the buoyancy joints have been removed and replaced by bare joints in a staggered configuration, see Figure 9.2.

	Depth [m]
Stagger start	-230.595
Stagger stop	-70.595
Total length staggered segment	160

Table 9-3 Staggered configuration data 321 m water depth

Table 9-3 above gives the start and stop of the staggered section of the riser. Note that Figure 9.2 is not to scale; refer to the table above for details.

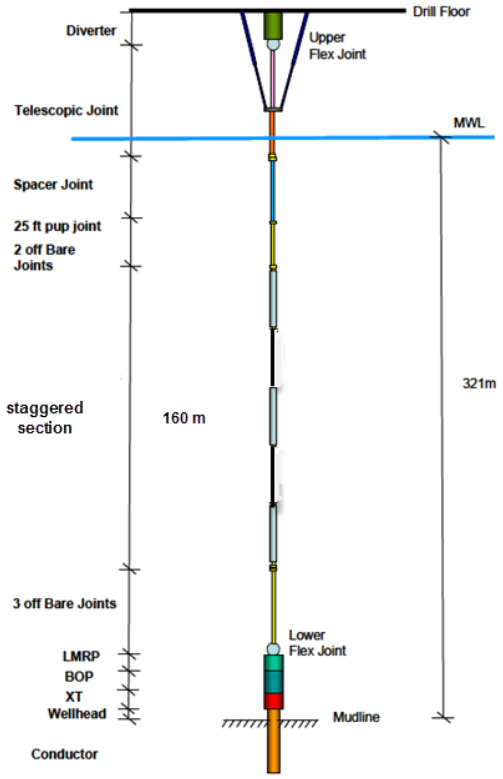

Figure 9.2 Staggered buoyant and bare joint configuration 321 m water depth

9.1.2 Bottom strakes configuration, 321 m system

For the bottom strake configuration, 151.28 m of the lower riser length is covered with strakes. This implies that the straked section will have two different outer diameters, namely that of the bare joints and that of the buoyant joints, see Table 9-1 for details. Note also that only the riser section itself is straked, no strakes are applied to WH, XMT, BOP or LMRP, see Figure 9.3. The stapled black line marks the straked section of the riser. The figure is not to scale, refer to the table below for details.

Water depth for bottom strakes segment start and stop is given in Table 9-3 below.

	Depth [m]
Strake start	-301.875
Strake stop	-150.595
Total length straked segment	151.28

Table 9-4 Bottom strakes configuration data 321 m water depth

No other changes to the stack-up inputs other than the addition of strakes, as is described in section 10.5, have been given.

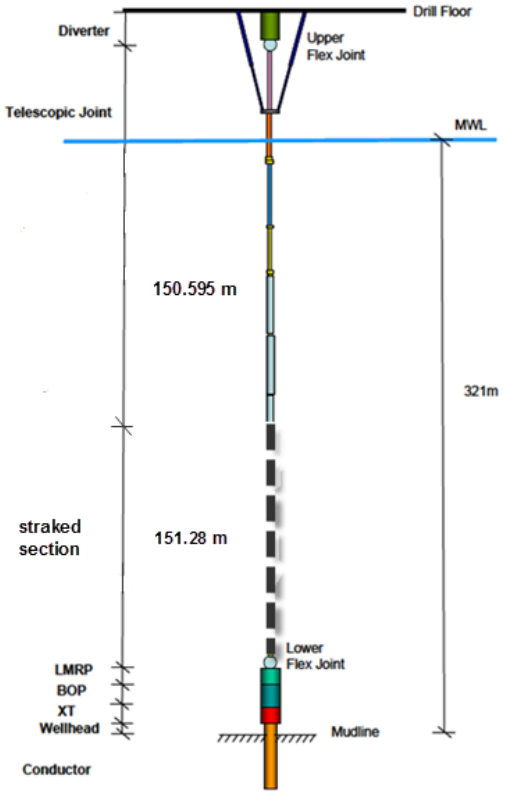

Figure 9.3 Bottom strake configuration 321 m water depth

9.1.3 Middle strakes configuration, 321 m system

For the middle strakes configuration the entire buoyancy field of the riser as it is given in Figure 9.4 is covered with strakes. The figure is not to scale. Water depth for straked section start and stop is given below.

	Depth [m]
Strake start	-230.595
Strake stop	-70.595
Total length straked segment	160

Table 9-5 Middle strakes configuration data 321 m water depth

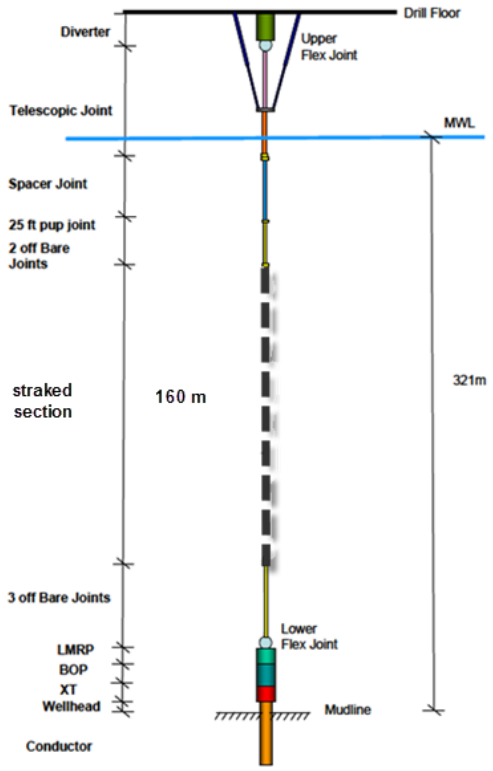

Figure 9.4 Middle strakes configuration 321 m water depth

9.1.4 Top strakes configuration, 321 m system

Half of the buoyancy field, along with 2 bare joints, the pup joint and the spacer joint are covered with strakes for the top strakes configuration, see Figure 9.5.

	Depth [m]
Strake start	-4.375
Strake stop	-150.595
Total length straked segment	146.22

Table 9-6 Top strakes configuration data 321 m water depth

As can be seen from the Table 9-6 above, the top strakes configuration is the configuration with the lowest coverage length at 146.22 m.

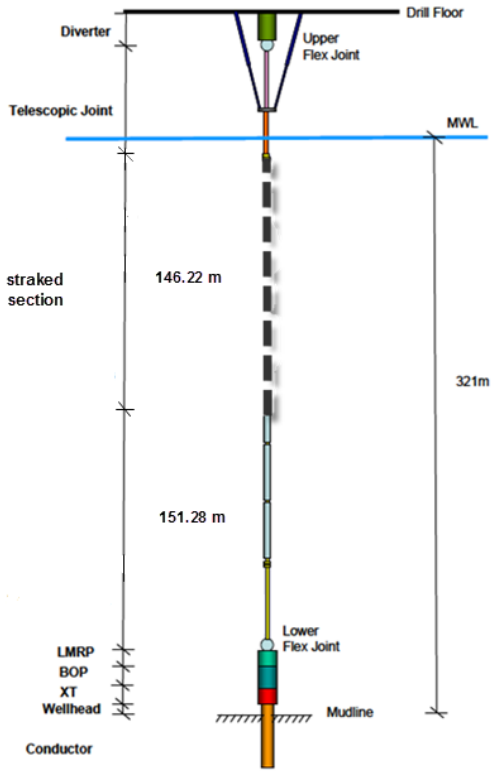

Figure 9.5 Top strakes configuration 321 m water depth

9.2 System description 1300 m water depth

Figure 9.6 illustrates the 1300 m system. The main difference from the 321 m system is the lack of XMT in the stack-up, as well as a significant increase in applied buoyancy joints. While roughly 50% of the riser length had buoyancy joints in the 321 m system, around 95% of the 1300 m riser length is covered with buoyant elements.

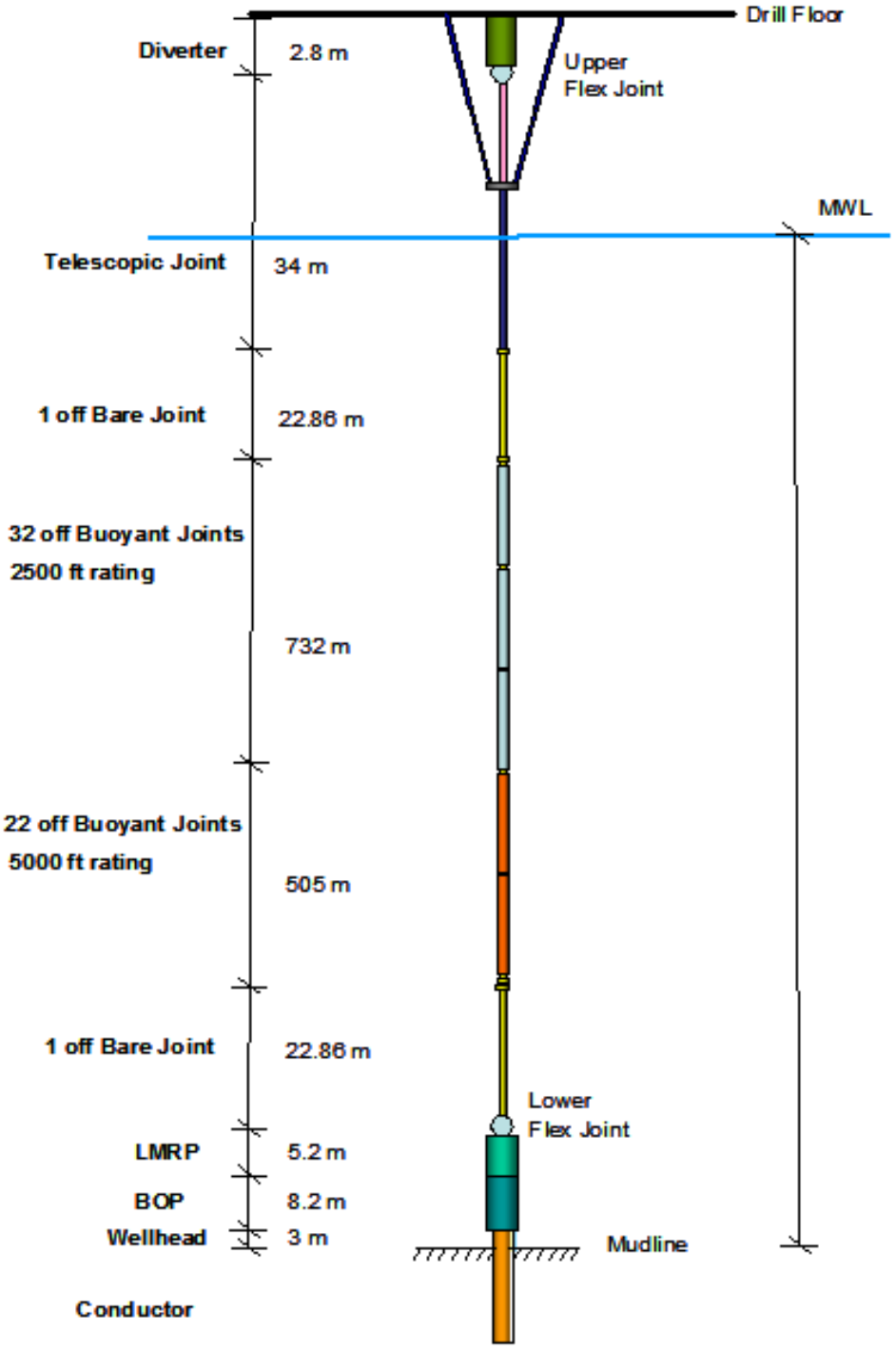

Figure 9.6 System overview 1300 m water depth

The stack-up data for 1300 m water depth used as input for the analyses is given in Table 9-7 below.

component	length [m]	quantity	Total length [m]	OD [m]	OD buoyancy [m]	ID [m]	Mass [kg]
Diverter	2,8	1	2,80	1,575	-	1,511	3410
UFJ	1,525	1	1,53	0,612	-	0,492	5210
Telescopic joint	34	1	34,00	0,66	-	0,492	40131
Riser bare	22,86	1	22,86	0,533	-	0,492	13910
Riser buoyant 2500ft	22,86	32	731,52	0,533	1,397	0,492	13910
Riser buoyant 5000ft	22,86	22	502,92	0,533	1,397	0,492	13910
Riser bare + adaptor	23,86	1	23,86	0,533	-	0,492	13910
LFJ	1,525	1	1,53	0,612	-	0,492	5210
LMRP	3,675	1	5,2	0,737	-	0,476	162000
BOP	8,2	1	8,2	0,737	-	0,476	224000
WH	3	1	3	1	-	0,452	60000

Table 9-7 Stack-up data 1300 meter water depth

Flex joint data is given Table 9-8 below. The upper-and lower flex joints are both assumed to have linear rotational stiffness. Implementation of flex joints in the model will be discussed later.

component	Rotational stiffness [kNm/deg]	Maximum rotation [deg]	Mass [kg]
Upper flex joint	13	9	5210
Lower flex joint	92	10	5210

Table 9-8 Flex joint data 1300 m water depth

9.2.2 Staggered configuration, 1300 m system

The staggered configuration applies staggered buoyant and bare joints for the entire length of the buoyancy field of the base system, which implies that a total riser length of 1234.44 m is staggered.

	Depth [m]
Stagger start	-25.3
Stagger stop	-1259.74
Total length staggered segment	1234.44

Table 9-9 Staggered configuration data 1300 m water system

Figure 9.7 illustrates the staggered configuration for the 1300 m water depth system. Note that the figure is not to scale.

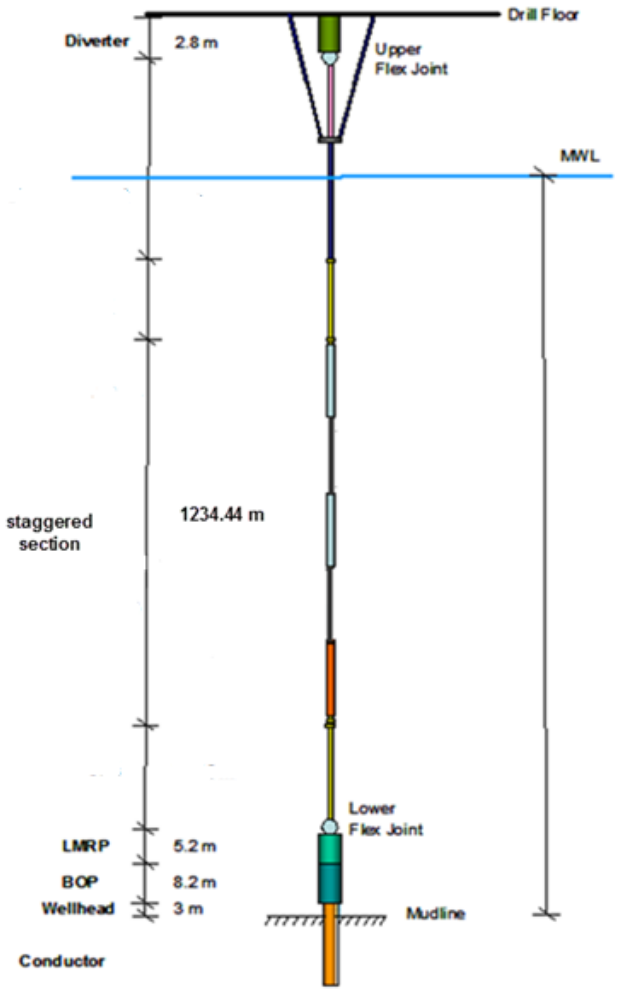

Figure 9.7 Staggered buoyant and bare joint configuration 1300 m water depth

9.2.3 Middle strakes configuration, 1300 m system

A total length of 650 m of the middle section of the riser is straked in the presented configuration. This implies that roughly 52% of the buoyancy field as given in the base configuration in section 9.1 will have strakes, see Table 9-10 for details.

	Depth [m]
Strake start	-325.0
Strake stop	-975.0
Total length straked segment	650.0

Table 9-10 Middle strakes configuration data 1300 m water depth

Figure 9.8 shows the middle strakes configuration, the black, stapled line represents strakes. The figure is not to scale, and reference is made to the table above for strake coverage details.

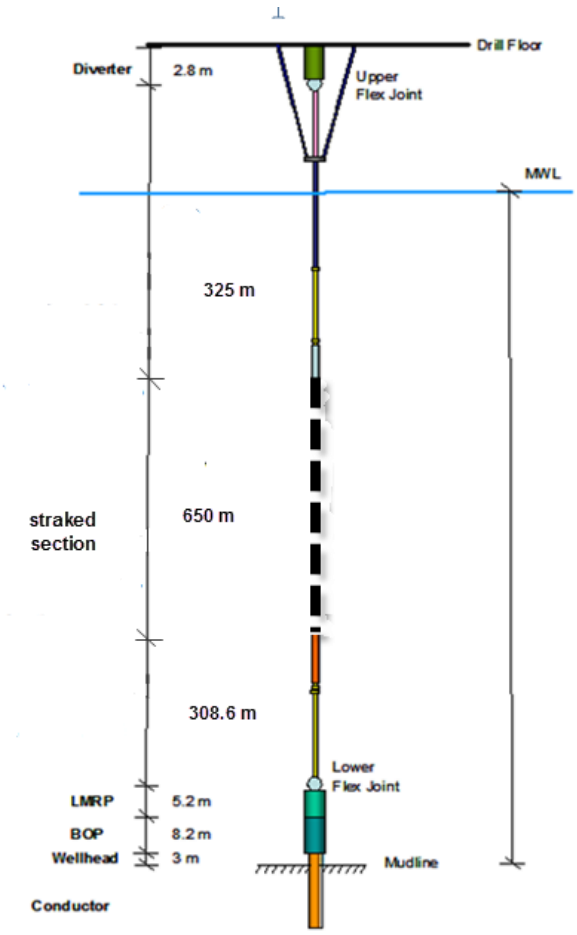

Figure 9.8 Middle strakes configuration 1300 m water depth

9.2.4 Top 150 m bare, next 650 m straked configuration

To reduce the added drag from increased wave action and wave induced fluid velocities close to the surface, a case study where the top 150 m of the riser is free from strakes is analysed. Note that, as discussed earlier, no influence from waves has been considered in the present analyses. See Table 9-11 for details.

	Depth [m]
Strake start	-150.0
Strake stop	-800.0
Total length straked segment	650.0

Table 9-11 Top 150 m bare, next 650 m straked 1300 m water depth

The black stapled line in Figure 9.9 represents the 650 m long straked section of the riser. Again, the figure is not to scale, strakes details are given in the table above.

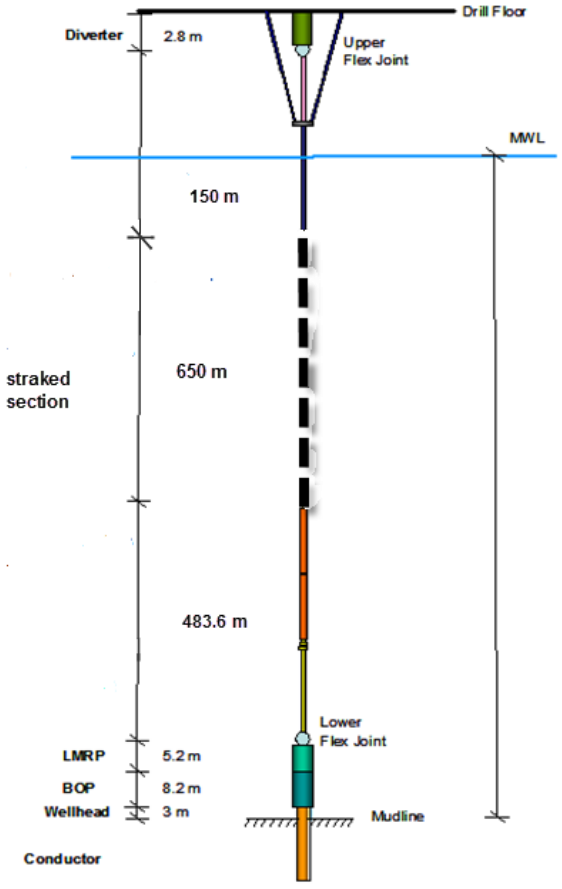

Figure 9.9 Top 150 m bare, next 650 m straked config. 1300 m water depth

Note: for the remainder of the report, this configuration is named Top 50_150 strakes configuration.

9.2.5 Top strakes configuration, 1300 m system

The final setup for the 1300 m water depth system includes a 652.44 m straked length of the top section of the riser, see Figure 9.10. As mentioned earlier, the figure is not to scale and Table 9-12 should be used for details. The straked section length was increased by 2.44 m from the previous configurations to include the entire length of the top bare joint, confirm Table 9-7.

	Depth [m]
Strake start	-4.44
Strake stop	-656.88.0
Total length straked segment	652.44

Table 9-12 Top strakes configuration data 1300 m depth

As can be seen from the figure below, the straked section includes both bare joints and buoyant joints. As a consequence the straked section will have two different diameters; 0.533 m for the bare joints and 1.397 m for the buoyant joints.

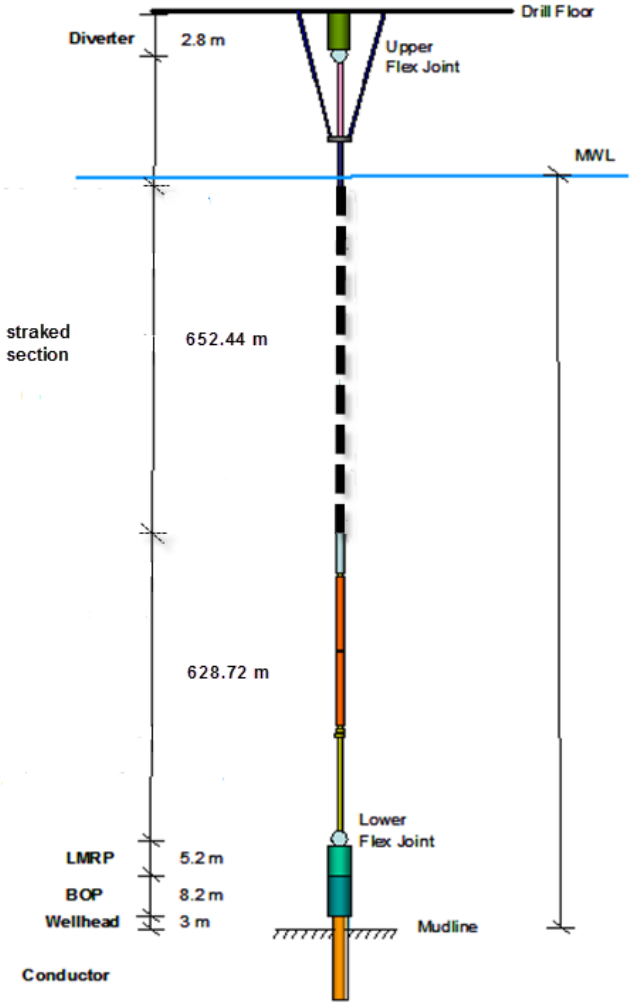

Figure 9.10 Top strakes configuration 1300 m water depth

9.3 Current models for 321 m water depth

The 4 different current profiles for the 321 m water depth are:

1) 2/3 current distribution

This current distribution has a constant current velocity for the first 1/3 of the water column, where it changes to a linearly sheared distribution for the remaining 2/3 of the water depth, hence why it is called 2/3 current in the thesis. Table 9-13 gives the water depth and corresponding current velocity.

Depth [m]	Current velocity [m/s]
0	0.5
-107	0.5
-321	0

Table 9-13 2/3 current data

Figure 9.11 illustrates the current distribution from VIVANA.

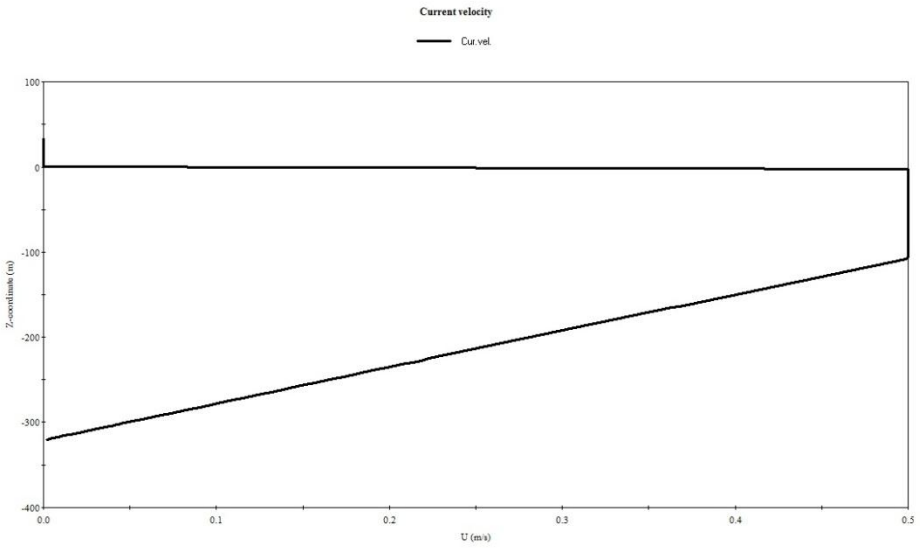

Figure 9.11 2/3 current for 321 m water depth

2) Linearly sheared current distribution

The linearly sheared current decreases from a fixed current velocity at the surface to zero current velocity at the sea bed with a constant gradient. Table 9-14 gives the current distribution data.

Depth [m]	Current velocity [m/s]
0	0.5
-321	0

Table 9-14 Sheared current data

Only two coordinates are required as input to VIVANA as linear interpolation is applied in the remaining interval, as can be seen in Figure 9.12.

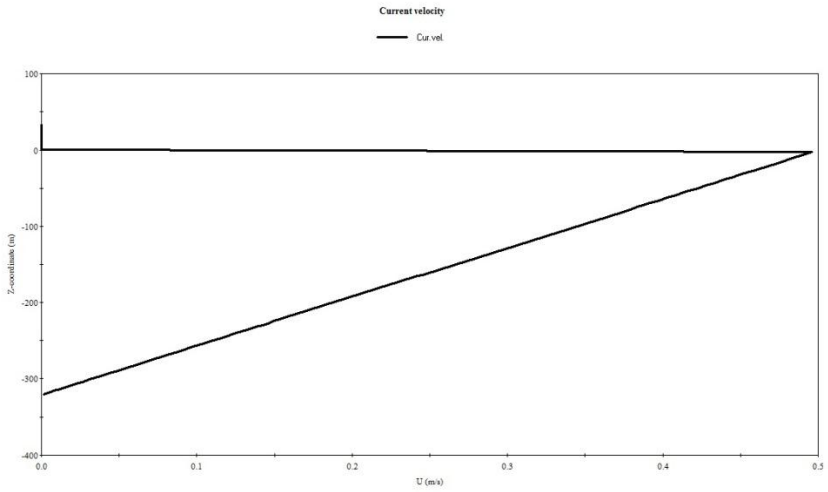

Figure 9.12 Sheared current for 321 m water depth

3) Uniform current distribution

For the 321 m water depth analyses were also run using a uniform current distribution. This model has a constant current velocity through the water column, and is therefore of a more theoretical nature as uniform current distributions rarely occurs in real life.

Depth [m]	Current velocity [m/s]
0	0.5
-321	0.5

Table 9-15 Uniform current data

Figure 9.13 illustrates the uniform current distribution from VIVANA.

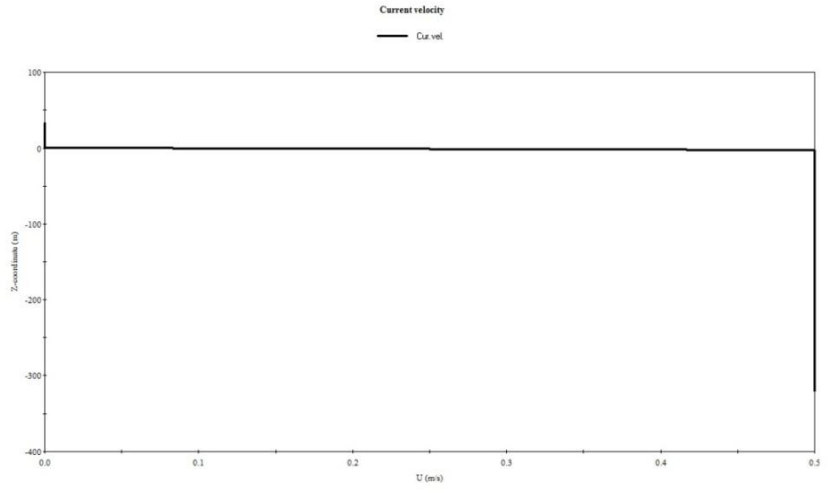

Figure 9.13 Uniform current distribution for 321 m water depth

4) Measured current distribution

The measured current profile is taken from actual current measurements from the relevant oil field.

Depth [m]	Current velocity [m/s]
0	0.56
-1.5	0.56
-54	0.41
-134	0.38
-214	0.36
-294	0.34
-321	0.34

Table 9-16 Measured current data

Figure 9.14 illustrates the measured current distribution from VIVANA.

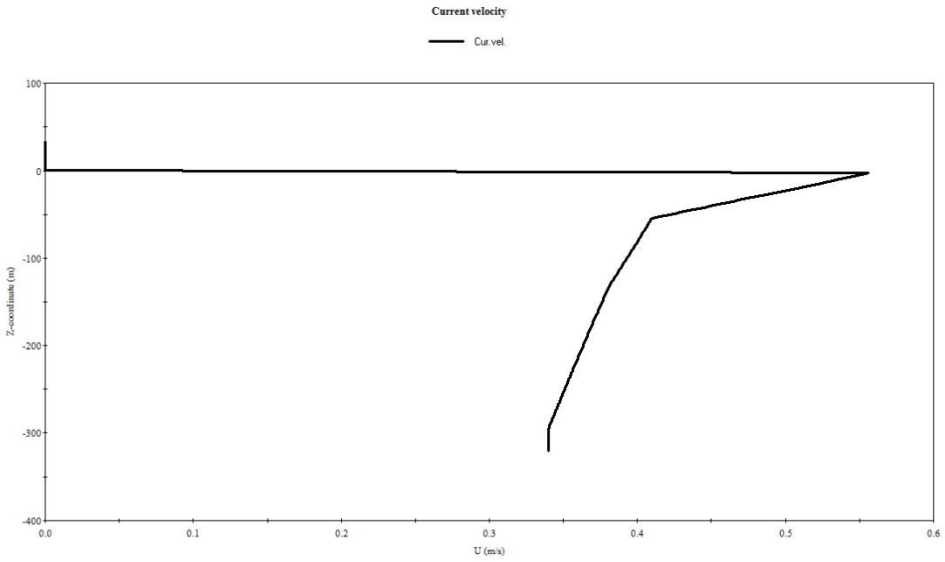

Figure 9.14 Measured current distribution for 321 m water depth

9.4 Current models for 1300 m water depth

For the 1300 m water depth the uniform current model has been replaced by a model taken from the Ormen Lange field (Rustad, 2007) on the Norwegian Continental Shelf (NCS). Thus, the four current distributions used in VIV analyses of the 1300 m water depth system are:

1) 2/3 current distribution

This is the same distribution used in 321 m water depth, however the current velocity at surface has been increased to 1.0 m/s. Current data is given in Table 9-17.

Depth [m]	Current velocity [m/s]
0	1.0
-433	1.0
-1300	0

Table 9-17 2/3 current data

Taken from VIVANA, Figure 9.15 illustrates the 2/3 current distribution used for analysis of the 1300 m water depth system.

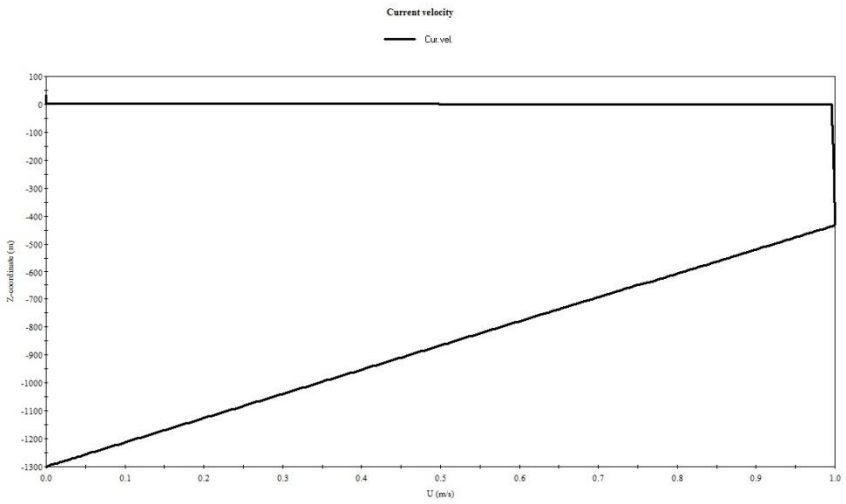

Figure 9.15 2/3 current distribution for 1300 m water depth

2) Linearly sheared current

Compared to the 321 m water system, the current velocity at the surface has been increased to 1.0 m/s, see Table 9-18.

Depth [m]	Current velocity [m/s]
0	1.0
-1300	0

Table 9-18 Sheared current data

Figure 9.16 illustrates the sheared current model, and is taken from VIVANA.

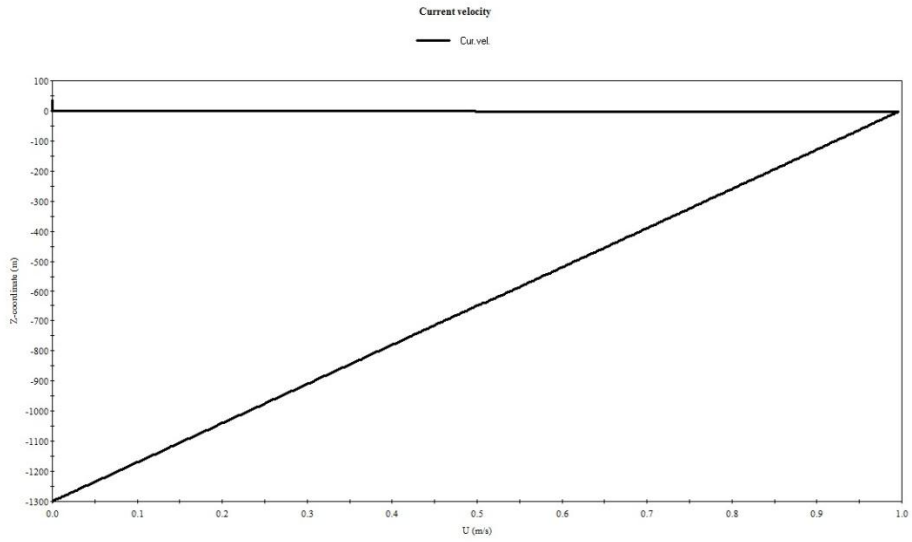

Figure 9.16 Sheared current distribution for 1300 m water depth

3) Measured current distribution

As for the 321 m water depth, VIV analyses are run with actual current data from the relevant location of the 1300 m water depth system.

Depth [m]	Current velocity [m/s]
0	1.44
-200	0.97
-400	0.67
-600	0.54
-800	0.54
-1000	0.50
-1297	0.41

Table 9-19 Measured current data

As can be seen, the measured current data has particularly high current velocities close to the surface. This is also illustrated in Figure 9.17 taken from VIVANA.

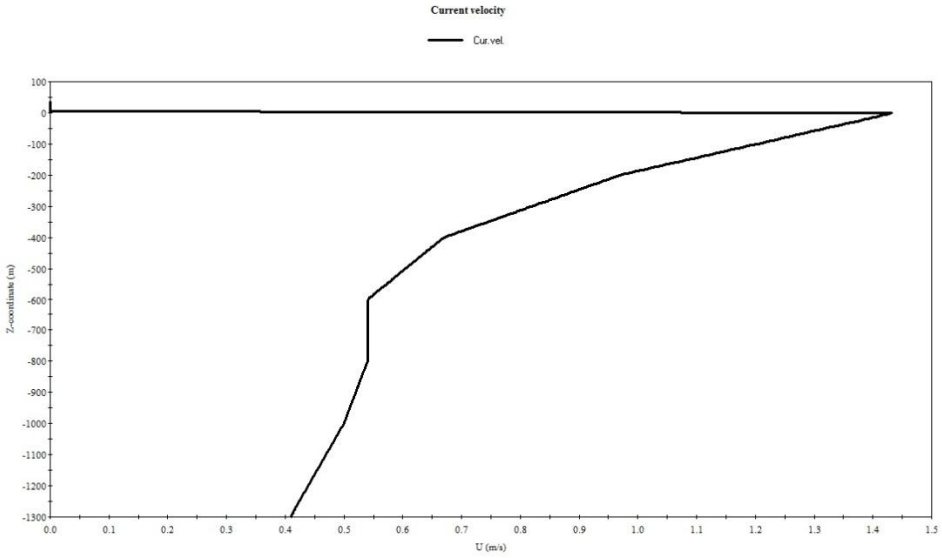

Figure 9.17 Measured current distribution for 1300 m water depth

4) Extended Ormen Lange 2 current distribution

The 4th current distribution used in the analyses is taken from the Ormen Lange field (Rustad, 2007). The distribution was originally given for a water depth of 850 m with a return period of 1 year. The current model has been extended to 1300 m water depth for the present analysis. Current data for the extended Ormen Lange 2 model is given in Table 9-20. As can be seen, a constant velocity of 0.55 m/s is assumed from a water depth of 850 m and down to the sea bed.

Depth [m]	Current velocity [m/s]
0	1.15
-50	1.15
-100	1.15
-200	1.10
-300	1.05
-400	1.0
-500	0.95
-600	0.75
-750	0.55
-850	0.55
-1297	0.55

Table 9-20 Ormen Lange 2 data

The extended Ormen Lange 2 model is illustrated in Figure 9.17.

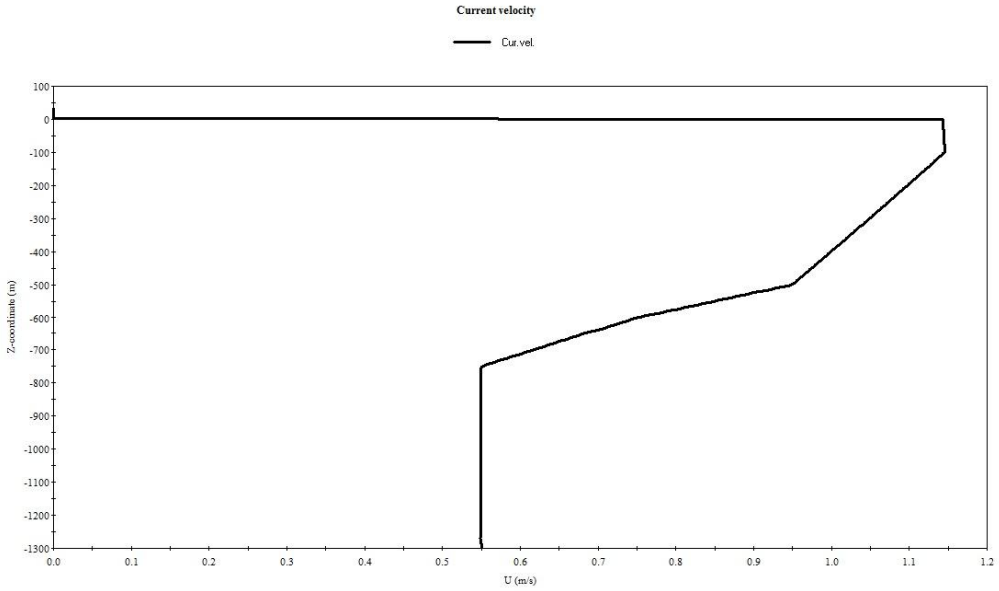

Table 9-21 Extended Ormen Lange 2 current distribution for 1300 m water depth

10 Modelling and input to RIFLEX and VIVANA

Modelling of a complete riser stack-up and rig subjected to wind, -wave-and current forces is not straightforward. Only in the interaction between the rig and riser, challenges like Pip-in-Pipe (PIP) interaction and dynamic riser tension forces are met. For riser analyses, varying outer diameters through the riser length, clamped umbilicals giving non-circular cross-sections and pressure-and temperature variations give further challenges. While today's computer software have come a long way in understanding and calculating rig- and riser behaviour, combined wave and VIV riser analysis is still not regarded as possible, at least not with confident and reliable results.

10.1 Boundary conditions and simplifications

All systems in the present study use simplified boundary conditions, and several physical effects have not been accounted for. These effects include

1. **PIP effects on riser tensioners:**

   Tensioner systems on modern drill rigs use pulling Direct Actuating Tensioner (DAT) cylinders which are attached to the marine riser. This way the cylinders will extend or retract depending on the rig motions, minimizing the variations in the riser top tension. Some tension variation will however always be present. Correct modelling of DATs would require pipe-in-pipe interaction. This has not been implemented in the current analyses. However, as the rig is assumed to be motionless in the analyses, this simplification is assumed to be reliable.

2. **PIP effects on riser stiffness:**

   Modern marine risers consist of several pipes in a bundle. The main contributors of riser stiffness, both axial- and bending stiffness, are the main riser tube and the landing string. However, auxiliary lines containing hydraulic and electrical communication will add to the total stiffness of the main marine riser. For the present analyses, only the stiffness calculated from Table 9-7 and Table 9-1 are applied. However, the contributions from auxiliary lines on bending- and axial stiffness will be small, and are therefore considered negligible.

   Note that recent versions of RIFLEX have proved to model and calculate PIP effects with good results (Larsen, 2012).

3. **Soil and well bay insert stiffness:**

   The soil in the area where the oil well is located will be a factor of the global boundary conditions of the system. The soil stiffness may vary from area to area, as well as depth below the sea bed. In order to properly model the behaviour of the soil, thorough geotechnical surveys of the well area should be made. Based on these surveys, the well bay insert stiffness and wellhead stiffness may be modelled using a combination of linear and rotational springs. The springs are designed to behave in accordance with the soil stiffness.

   All analyses in this master thesis are calculated using a fixed connection between the wellhead and the seabed. This is done under the assumption that the soil stiffness in the relevant areas will be significantly higher than the bending and axial stiffness of other components in the analyses, thus justifying a fixed connection.

4. Non-linear flex joint stiffness:

The stiffness of the flex joints used in the AKSO systems behave non-linearly. However, as discussed in chapter 10.6, the flex joints in the present analyses are modelled as beam sections with bending stiffness corresponding to the defined rotational stiffness of the flex joints. As a consequence, non-linear flex joint stiffness is not applied in the present study.

5. Non-circular cross sections:

In the present study, all components of the riser stack-up are modelled as circular cylinders. The non-circular components like the BOP, XMT and LMRP are modelled with an increased hydrodynamic diameter to account for added drag associated with sharper corners and flow separation of non-circular cross sections.

The hydrodynamic diameters of non-circular cross sections are calculated using the buoyancy force of the component. The buoyancy force is found by the difference in weight of the component in air and in water.

Equation 10.1: Buoyancy force of component

$$B = (Weight\ in\ air - Weight\ in\ water) * g$$

Equation 10.2: Hydrodynamic diameter of non-circular cross sections

$$D_H = \sqrt{\frac{4B}{\rho_w g L} + {D_i}^2}$$

where

D_H = hydrodynamic diameter

B = buoyancy force

ρ_w = density of water

L = length of component

D_i = inner diameter as given Table 9-7 and Table 9-1

g = gravitational constant

6. **Umbilical proximity:**

During workover operations, additional umbilicals in the proximity of the marine riser may be required. These umbilicals will typically provide communication between the rig and components close to the sea floor, for instance the BOP. An upstream umbilical of sufficient size and proximity to the main riser will shed vortices that may interact with the shedding process of the main marine riser. This can again affect the VIV induced forces on the riser. In the presented analyses however, only the main marine riser is evaluated.

7. **Added drag from clamps and other fittings**

The outer cross section of the marine riser will not be of perfectly uniform circular shape. Sections of the riser where the bare pipe is exposed, and no riser-guards are applied, clamps and fittings for the auxiliary lines will be exposed. This may influence the hydrodynamic behaviour, and in particular the drag, of this section. In all analyses presented, the cross sections of all riser segments are assumed to be perfectly circular. As a consequence, the only geometrical variation along the riser span will be that of the diameter. As the majority of the riser lengths are either fitted with circular buoyancy elements or riser guards, this simplification is assumed to be reliable. However, for 321 m water depth system where roughly 30% of the riser length consists of bare riser joints, the assumption above may be questionable.

Based on the simplifications given above, the boundary conditions for all systems analysed are given in Figure 10.1. As can be seen, all systems analysed are fixed in both translation and rotation at the seabed-wellhead interface. Top-side, the riser is free to move in vertical direction, i.e. z-direction, while all other translational and rotational degrees of freedom are fixed.

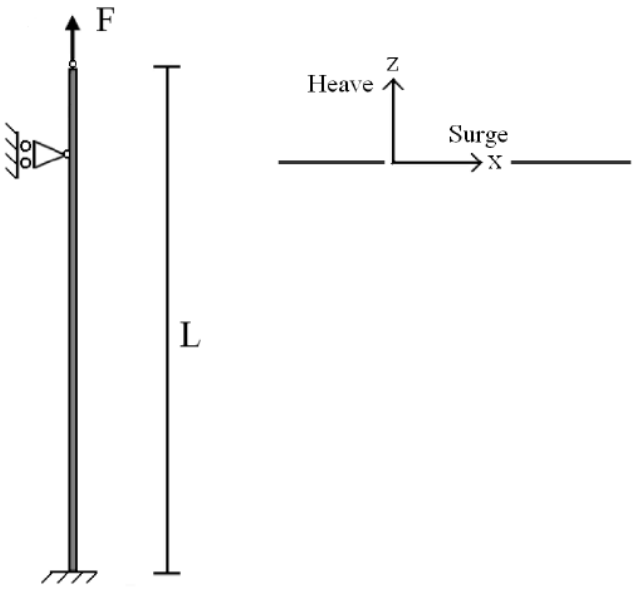

Figure 10.1 Boundary conditions used for all systems

As will be discussed later, the applied top tension varies for each system configuration. The details around implementation of flex joints in the models are also described later in the report.

10.2 Structure of RIFLEX AND VIVANA

A VIV analysis in VIVANA is conducted through three steps. Initially a model of the system must be defined in the RIFLEX module IMPMOD. A static analysis of the system under induced wave and/or current loads is then executed in the RIFLRX module STAMOD. Finally, the module VIVANA is run to perform the actual VIV analysis. For further explanation and description of RIFLEX and VIVANA, reference is made to the RIFLEX and VIVANA User's Manual, (Yttervik, et al., 2011) and (Yttervik, et al., 2009).

10.3 INPMOD

INPMOD is the module in RIFLEX that defines the model, both in terms of geometry and structural characteristics. Riser cross section lengths, diameters and other parameters are given, including material properties. All sections are in VIVANA and RIFLEX analysed as circular cylinders (Yttervik, et al., 2011), and the user may choose from a variety of different component types to model the different riser sections, see RIFLEX User's Manual (Yttervik, et al., 2011) for a detailed description.

The analyses only use two component types. The component type CRS1 is used for specifying wellhead, BOP, LMRP and flex joints characteristics, while CRS0 is used for definition of riser joints.

Based on the stack-up data given in Table 9-7 and Table 9-1, the required parameters used for riser definition in IMPMOD may be calculated. The following assumptions and equations are applied when calculating "backwards" from the stack-up data in Table 9-7 and Table 9-1:

Constants:

- **Young's modulus *E* = 210MPa**
- **Shear modulus *G* = 80MPa**
- **Torsional stiffness is assumed constant equal to $\mathbf{1.0 * 10^{11}}$ Nm^2/radian**
- **Relative structural damping is 1%**
- $\boldsymbol{\rho_{water} = 1025 \frac{kg}{m^3}}$
- $\boldsymbol{\rho_{steel} = 7850 \frac{kg}{m^3}}$
- $\boldsymbol{\rho_{fluid} = 1500 \frac{kg}{m^3}}$

As can be seen in Table 10-1 below, the CRS0 component inputs require specification of segment density. Where possible, Equation 10.3 is used to calculate the relevant density. Otherwise, the density of steel is used as input.

Equation 10.3: Density riser segment

$$\rho_{segment} = \frac{weight\ in\ air\ of\ segment}{volume\ of\ segment}$$

CRS1 component inputs require definition of axial and bending stiffness, as well as torsional stiffness. The torsional stiffness is assumed constant as given above, and axial stiffness can be calculated from cross-section area and Young's modulus. The second area of inertia is used for finding bending stiffness, see Equation 10.4

Equation 10.4: Second area of inertia cylinder

$$I_x = I_y = \frac{\pi}{64} * (d_{outer}^4 - d_{inner}^4)$$

Using the 321 m water depth system as example, Table 10-1 through Table 10-4 through give the resulting input for CRS0 and CRS1 component types.

CRS0 components are given in Table 10-1 below:

icmpty	component	length [m]	quantity	Total length [m]	OD [m]	OD buoyancy [m]	ID [m]	thickness [m]	Volume [m^3]	Weight in air [kg]	Weight in water [kg]	Density [Mg/m^3]
11	Diverter	6,18	1	6,18	1,575	-	1,511	0,032	0,959	7525,3	6542,70	7,85
10	Telescopic joint	31,24	1	31,24	0,66	-	0,483	0,0885	4,964	40131	35043,03	8,08
9	Spacer joint	12,87	1	12,87	0,556	-	0,495	0,0305	0,648	10520	9152	16,23
8	Pup joint	7,63	1	7,63	0,556	-	0,495	0,0305	0,384	6230	5420	16,22
7	Riser bare	22,86	2	45,72	0,533	-	0,495	0,019	0,701	13910	12102	19,83
6	Riser buoyant	22,86	7	160	0,533	1,397	0,495	0,019	0,701	13910	-1403	19,84
5	Riser bare + adaptor	23,76	3	71,28	0,533	-	0,495	0,019	0,729	13910	12102	19,08

Table 10-1 CRS0 riser components, 321 m water depth

CRS1 components are given in Table 10-2 below:

icmpty	component	length [m]	quantity	Total length [m]	OD [m]	OD buoyancy [m]	ID [m]	hydrodynamic diameter [m]	thickness [m]	Volume [m^3]	Weight in air [kg]	Weight in water [kg]	Density [Mg/m^3]
4	LMRP	3	1	3	0,737	-	0,476	2,204	0,1305	0,746	85409	74220	114496,2
3	BOP	9	1	9	0,737	-	0,476	1,935	0,1305	2,238	194591	169099	86953,9
2	XMT	2,4	1	2,4	0,737	-	0,476	1,982	0,1305	0,597	55000	47850	92163,8
1	WH	3,2	1	3,2	1	-	0,452	2,021	0,274	2,000	60000	50000	30003,0

Table 10-2 CRS1 riser components, 321 m water depth

Additional required input for CRS1 components is given in Table 10-3 below:

icmpty	component	Mass per unit length [Mg/m]	Second area of inertia [m^4]	Area [m^2]	Area external [m^2]	Area internal [m^2]	Young's modulus [N/m^2]	Shear modulus [N/m^2]	Bending stiffness [kNm^2]	Axial stiffness [kN]	Torsion stiffness [kNm^2/radian]
4	LMRP	28,470	0,01196	0,2487	0,4266	0,1780	2,1E+11	8,00E+10	2,51E+06	8,959E+07	1,00E+08
3	BOP	21,621	0,01196	0,2487	0,4266	0,1780	2,1E+11	8,00E+10	2,51E+06	8,959E+07	1,00E+08
2	XMT	22,917	0,01196	0,2487	0,4266	0,1780	2,1E+11	8,00E+10	2,51E+06	8,959E+07	1,00E+08
1	WH	18,750	0,04704	0,6249	0,7854	0,1605	2,1E+11	8,00E+10	9,88E+06	1,649E+08	1,00E+08

Table 10-3 Additional input for CRS1 riser components, 321 m water depth

Flex joint definitions are also given as CRS1 components. Below are the flex joint characteristics for the 321 m water depth system. Further discussion on flex joint implementation is given in section 10.6.

icmpty	component	length [m]	quantity	Total length [m]	Rotational stiffness [kNm/deg]	Mass [kg]	Mass per unit length [Mg/m]	Area external [m^2]	Area internal [m^2]	Young's modulus [N/m^2]	Shear modulus [N/m^2]	Bending stiffness [kNm^2]	Axial stiffness [kN]	Torsion stiffness [kNm^2/radian]
44	LFJ 46kNm/deg	1,525	1	1,525	46	5210	3416,39	0,294	0,192	2,1E+11	8,00E+10	4,02E+03	2,14E+07	1,00E+08
55	UFJ 13kNm/deg	1,525	1	1,525	13	5210	3416,39	0,294	0,192	2,1E+11	8,00E+10	1,14E+03	2,14E+07	1,00E+08

Table 10-4 Flex joint data as given in INPMOD

Drag coefficients for bare and straked components (Larsen, et al., 2005) are given in the Table 10-5 below.

Component	Drag coefficient Cd
Bare	1.0
Straked	1.35

Table 10-5 Drag coefficient for bare and straked components

Added mass coefficients for bare and straked components (Larsen, et al., 2005) are given in Table 10-6.

Component	Added mass coefficient Cd
Bare	1.0
Straked	1.02

Table 10-6 Added mass coefficient for bare and straked components

In addition to defining the geometrical and structural properties of the riser stack-up, current distributions induced on the system are given in INPMOD.

10.4 STAMOD

After the riser stack-up has been defined in IMPMOD, RIFLEX runs the module STAMOD to calculate the static configuration of the riser system when subjected to current forces.

A tension force at the riser top end is applied for each riser system. The magnitude of the force will vary from system to system, and is determined based on the resulting axial force at or near the wellhead datum. A positive axial force (tension force) of magnitude equal to roughly 400kN is wanted (Larsen, 2012) at or near the wellhead datum, and the top tension is varied and found accordingly. Table 10-7 gives the resulting top tension for the various configurations of the 321 m water depth system.

321 m water depth	
Configuration	**Top tension [kN]**
Base	5500
Staggered	5950
Bottom strakes	5400
Middle strakes	5450
Top strakes	5450

Table 10-7 Top tension 321 m water depth

A 400kN overpull at the wellhead datum gave the following top tensions for the 1300 m water depth configurations, see Table 10-8.

1300 m water depth	
Configuration	**Top tension [kN]**
Base	6080
Staggered	9950
Mid strakes	6080
Top 50_150 strakes	6050
Top strakes	6050

Table 10-8 Top tension 1300 m water depth

10.5 VIVANA

For the bare riser, default values are used for Strouhal number, added mass and damping. The excitation frequency bandwidth has however been increased from [0.125,0.2] as is default, to [0.120,0.31]. The excitation coefficients for the corresponding increase in bandwith are also different from default. The changes are made based on recent model test results executed at the Department of Marine Technology (Larsen, 2012), and will become default values for future VIVANA versions.

For sections of the riser that have strakes, modifications have been made to the excitation frequency bandwidth, excitation coefficient distribution and added mass coefficient distribution. The excitation bandwidth has been further increased to [0.0625,0.33] for straked sections. As discussed in 6.3.6, a new distribution for excitation coefficients of straked sections has been applied, and a fixed added mass value $m_a = 2.0$ is set for all non-dimensional frequencies. The values are based on recent model test results at the Department of Marine Technology (Larsen, 2012).

All analyses apply the Fixed Point method in the response frequency iteration process. The user may choose between two iteration methods, Fixed point and Newton-Raphson. Fixed point has been chosen as it has given consistent good results, all analyses have converged within the required number of iterations. For the 1300 m water depth system, a maximum number of 8 iterations were observed in the response frequency iteration process.

The concept of time sharing is applied for all VIVANA calculations in the thesis, as opposed to space sharing which is the second concept used for VIV prediction in VIVANA. Time shearing means that a number of frequencies will compete to be the dominating one. One discrete frequency will be the dominating one for a period of time, after which a second, different frequency will take over as the dominating frequency for a new period of time. For a more detailed description of the concepts of time- and space sharing, reference is made to Project Thesis (Knardahl, 2011).

Time sharing has proven to predict VIV well, however new research are evaluating the need for a combination of space- and time sharing to improve VIV predictions even further (Larsen, et al., 2012).

For fatigue calculations, the analyses apply the same SN-curve as used in a recent comparison study of model tests and VIVANA analyses executed at the Department of Marine Technology (Larsen, 2012).

10.6 Flex joint implementation

The RIFLEX and VIVANA versions used in the current analyses are development versions, and have not yet been published for commercial use. The reason for using this version was the implementation of flex joint as a separate component input in INPMOD. Used between lines, the component has zero length and can typically model ball joints, hinges and universal joints with a specified rotational stiffness. However, results from early analyses where the FLEX components was applied in INPMOD revealed un-physical fatigue results. Therefore the flex joints are modelled as beam elements with a bending stiffness "corresponding to" the relevant rotational stiffness of the flex joint.

The angle of a fixed cantilever beam subjected to a moment at one end must equal the angle of the flex joint subjected to the same moment:

$$\theta_{beam} = \theta_{flex\ joint}$$

The angle of a fixed cantilever beam is given as

Equation 10.5: Angle of fixed cantilever beam subjected to end moment

$$\theta_{beam} = \frac{M * l_{beam}}{EI}\ ;\ \theta_{beam} = [rad]$$

where l_{beam} = length of beam element

The rotational stiffness of the flex joint is given as

Equation 10.6: Rotational stiffness flex joint

$$k_{flex\ joint} = \left[\frac{M}{deg}\right] \Rightarrow\ k_{flex\ joint} = \frac{180\ deg}{\pi\ rad} * \left[\frac{M}{deg}\right] = \frac{180}{\pi} * \left[\frac{M}{rad}\right]$$

Now, from dimensional analysis we get

Equation 10.7: Flex joint angle

$$k_{flex\ joint} = \left[\frac{M}{\theta_{flex\ joint}}\right] \Rightarrow\ \theta_{flex\ joint} = \left[\frac{M}{k_{flex\ joint}}\right]$$

Thus, by claiming $\theta_{beam} = \theta_{flex\ joint}$, we find the bending stiffness of the beam to be

Equation 10.8: Bending stiffness beam element representing flex joint

$$\frac{M * l_{beam}}{EI} = \frac{M}{k_{flex\ joint}} \Rightarrow EI = l_{beam} * k_{flex\ joint}$$

Note that the derivation above does not include the geometric stiffness contribution to the element. However, as the element length of the beam representing the flex joint is small, the geometric stiffness contribution is considered negligible.

icmpty	component	Rotational Stiffness [kNm/deg]	Length [m]	Mass [kg]	Bending stiffness [kNm^2]	Axial stiffness [kN]	Calculated Axial stiffness [kN]
55	Upper flex joint, 321 m water depth	13	1.525	5210	1.136E+06	2.5E+06	2.14E+07
55	Upper flex Joint, 1300 m water depth	13	1.525	5210	1,136E+03	3.0E+06	2.14E+07
44	Lower flex joint, 321 m water depth	46	1.525	5210	4.019E+03	5.0E+06	2.14E+07
44	Lower flex joint, 1300 m water depth	92	1.525	5210	8.038E+03	5.5E+06	2.14E+07

Table 10-9 Flex joint data

Table 10-9 above gives flex joint data for medium and deep water depth. Note that the axial stiffness for all flex joints is not a calculated value, but an estimation based on previous in-house RIFLEX analyses in Aker Solutions. Compared to the calculated value for axial stiffness, the estimated values are of order 10 lower.

11 Results

The following will present the results from the analyses, including dominating frequencies, maximum stresses and fatigue results. Drag amplification from VIV, as well as resulting flex joint angles are also presented. As discussed previously, a total of 4 current profiles have been evaluated for 5 configurations on each water depth, a total of 40 analyses. The amount of data collected from each analysis proved to be too much to present in a result chapter. Therefore only the main findings of the base, staggered and best performing strakes configuration are given in this chapter. A total overview of the results for each configuration for both the 321 m and 1300 m water depth may be found in Appendix A.

11.1 321 m water depth VIV results

11.1.1 Dominating frequency, duration and VIV amplitudes

The dominating frequencies, durations and corresponding length of excitation zones, as well as VIV amplitudes for the base configuration are given in Table 11-1.

Current profile	Dominating frequency no.	Frequency [Hz]	Duration [%]	Length of excitation zone [m]	VIV amplitude [m]
2/3-current	1	0.0583	83.67	182.332	0.656
Linearly sheared	1	0.0597	54.43	95.384	0.215
Measured current	1	0.0514	81.19	174.525	1.019
Uniform	1	0.0673	86.71	177.525	1.029

Table 11-1 Dominating frequencies, durations and VIV amplitudes for base configuration, 321 m water depth

The same results for the staggered configuration are given in Table 11-2 below.

Current profile	Dominating frequency no.	Frequency [Hz]	Duration [%]	Length of excitation zone [m]	VIV amplitude [m]
2/3-current	1	0.0707	60.59	124.794	0.609
Linearly Sheared	2	0.1574	54.43	92.202	0.133
Measured current	1	0.0727	51.98	94.565	0.487
Uniform	1	0.0666	68.12	108.965	0.983

Table 11-2 Dominating frequencies, durations and VIV amplitudes for staggered configuration, 321 m water depth

As can be seen, with the exception of the linearly sheared current profile, the dominating frequency number is no. 1 for both configurations. For all current profiles, the duration and excitation length of the staggered configuration is shorter than for the base case. Furthermore, the amplitudes of mode 1 of the staggered configuration are smaller than for the base case.

Dominating frequencies, durations and VIV amplitudes for the top strakes configuration are given in Table 11-3 below.

Current profile	Dominating frequency no.	Frequency [Hz]	Duration [%]	Length of excitation zone [m]	VIV amplitude [m]
2/3-current	1	0.0528	92.61	195.896	0.0814
Linearly Sheared	2	0.1309	50.45	69.344	less than 0.533E-2
Measured current	1	0.0512	87.54	206.529	0.204
Uniform	1	0.0580	85.94	240.620	0.176

Table 11-3 Dominating frequencies, durations and VIV amplitudes for top strakes configuration, 321 m water depth

While the VIV amplitudes of the top strakes configuration actually were higher than that of the middle strakes configuration, see Appendix A, this was the only configuration that effectively managed to suppress VIV entirely for one of the current profiles. VIVANA sets a lower limit for the minimum amplitude for VIV to occur. This limit is equal to $0.533 * 10^{-2}$. As can be seen above, the calculated VIV amplitude for the dominating frequency in linearly sheared current is smaller than the limit, thus implying no VIV.

Compared to the base and staggered configuration, the VIV amplitudes of the top strakes configuration are significantly smaller. This result is also reflected in the calculated maximum stresses, as will be discussed next.

11.1.2 Stress amplitudes

Stress amplitudes for the base case configuration are given Table 11-4.

Current profile	Frequency no.	Frequency [Hz]	Max stress amplitude [MPa]
2/3-current	1	0.0583	11.213
Linearly sheared	1	0.0597	3.536
Measured current	1	0.0514	16.829
Uniform	1	0.0673	17.264

Table 11-4 Stress amplitudes, base configuration

As can be seen from the table above the maximum stress amplitudes of the base configuration occur for the same frequency number as the dominating frequency given in Table 11-1. Below, Figure 11.1 illustrates the stress amplitudes for the base configuration subjected to the measured current profile. The spike in Figure 11.1 is found to be exactly at the wellhead and XMT interface, and the same trend of maximum stress in the WH/XMT interface was found for all current profiles.

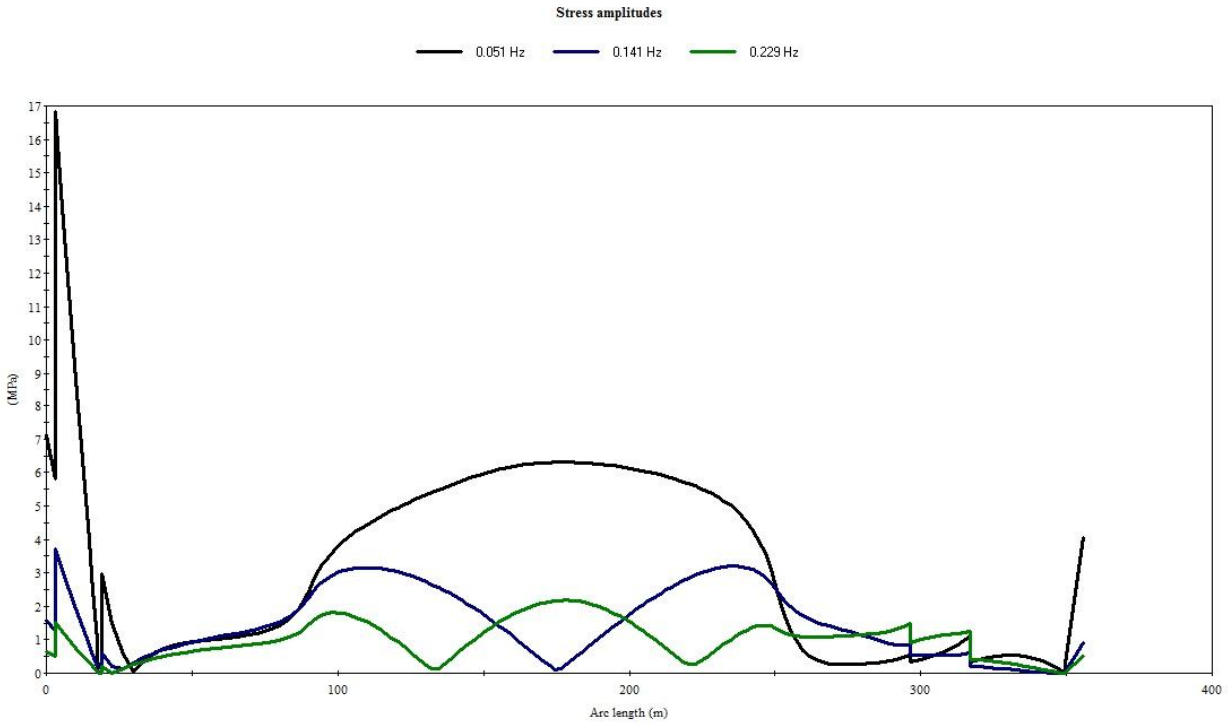

Figure 11.1 Stress amplitudes for measured current, base configuration

Table 11-5 gives the stress amplitudes for the staggered configuration. As can be seen the calculated stresses are lower for this configuration compared to the base case for every current profile except the linearly sheared profile.

Current profile	Frequency no.	Frequency [Hz]	Max stress amplitude [MPa]
2/3-current	1	0.0707	10.499
Linearly sheared	2	0.1574	4.382
Measured current	2	0.155	8.528
Uniform	1	0.0666	14.240

Table 11-5 Stress amplitudes, staggered configuration

As for the base configuration, the maximum stress for the staggered configuration subjected to the measured current profile is found to be at wellhead/XMT interface, as seen in Figure 11.2.

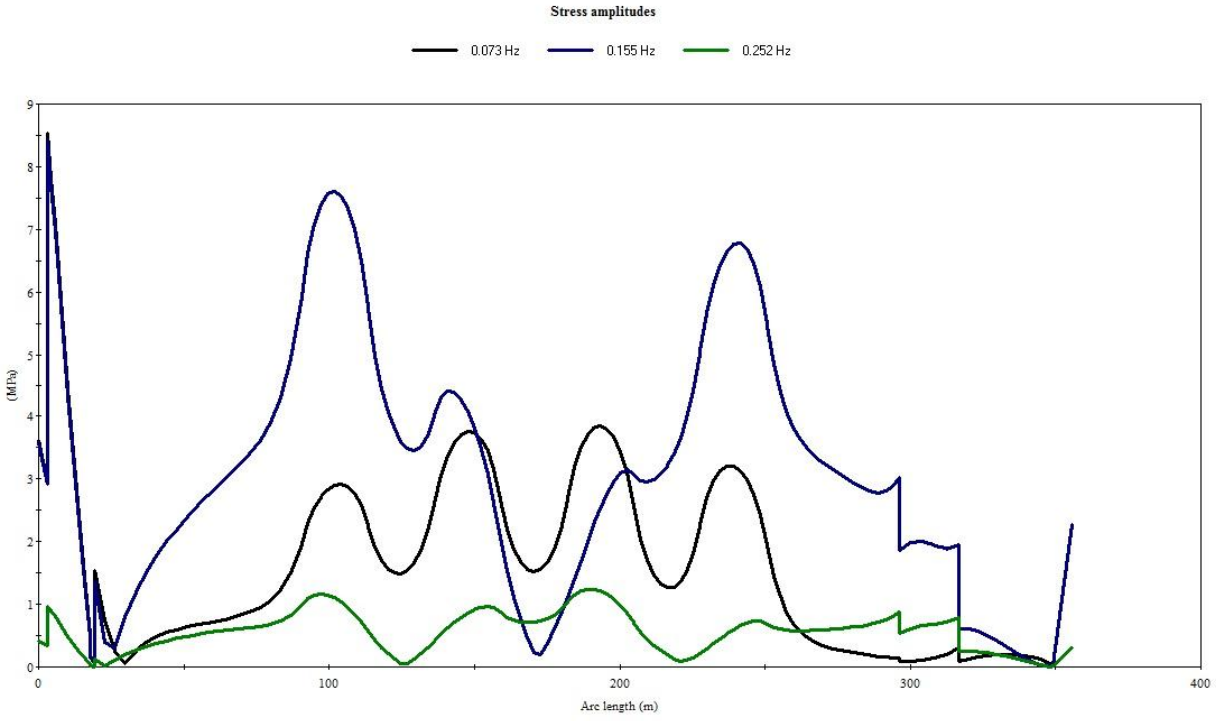

Figure 11.2 Stress amplitudes for measured current, staggered configuration

As mentioned earlier, the low VIV amplitudes of the top strakes configuration gave low maximum stresses as seen in Table 11-6.

Current profile	Frequency no.	Frequency [Hz]	Max stress amplitude [MPa]
2/3-current	1	0.0528	1.332
Linearly sheared	2	0.1309	N/A
Measured current	1	0.0512	3.420
Uniform	1	0.0580	2.771

Table 11-6 Stress amplitudes, top strakes configuration

Maximum stress for the linearly sheared current profile was not calculated, as no VIV occurs for this current profile. Using the base configuration as a comparison, the maximum experienced stresses in the system decreases drastically when strakes are applied to the top end of the riser. Figure 11.3 illustrates the location of maximum stress for the top strakes configuration in measured current. As for the base and staggered configuration, the spike is found at the WH/XMT interface.

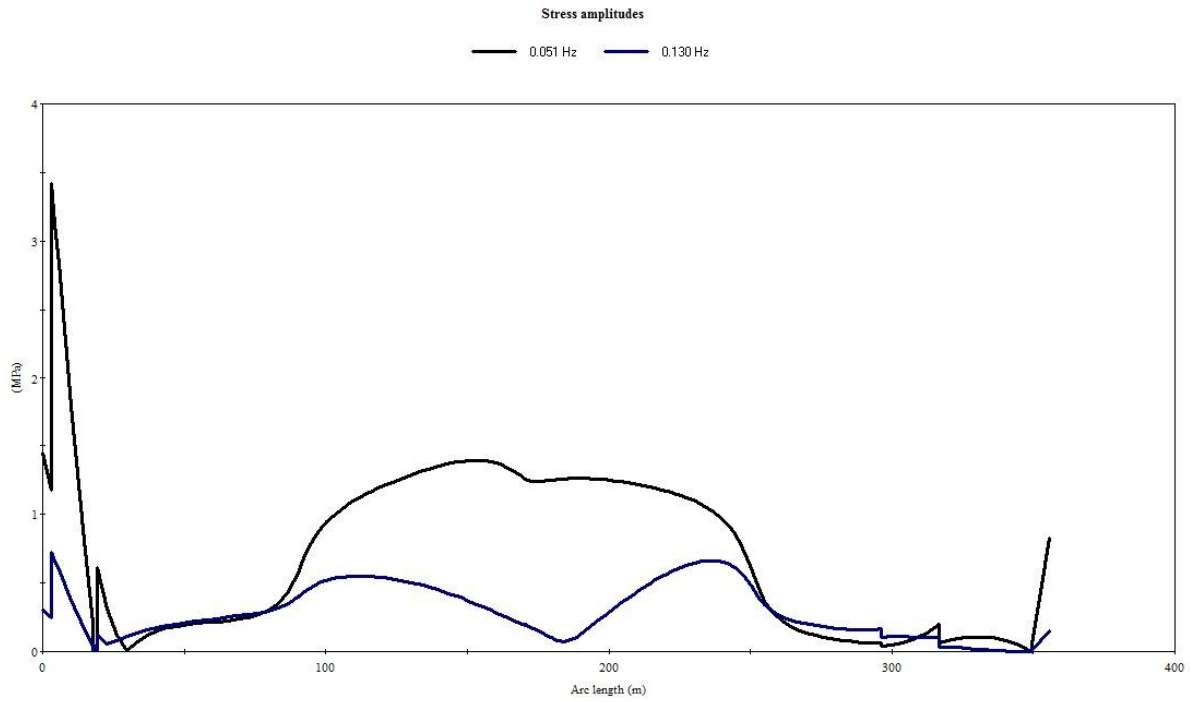

Figure 11.3 Stress amplitudes for measured current, top strakes configuration

11.1.3 Fatigue damage

Little investigation and background study has been done for applying correct SN-curve in the presented analysis, as the scope of the thesis does not emphasise this. The applied SN-curves are the same as used in a recent VIV study at the department of Marine Technology (Larsen, 2012).

The calculated fatigue damage for the base configuration is given in Table 11-7 below. For all current profiles the max accumulated damage is located at the exact point of the WH/XMT interface.

current profile	fatigue damage	fatigue life years	location
2/3-current	5,43E-02	18,40	WH/XMT interface
Linearly sheared	2,34E-03	427,83	WH/XMT interface
Measured current	1,57E-01	6,36	WH/XMT interface
Uniform	2,15E-01	4,65	WH/XMT interface

Table 11-7 Fatigue damage, base configuration

Figure 11.4 illustrates the accumulated fatigue damage for base configuration in measured current. The spike in the graph is located at the WH/XMT interface, and is associated with a large difference in bending stiffness of the two components, see Table 10-2.

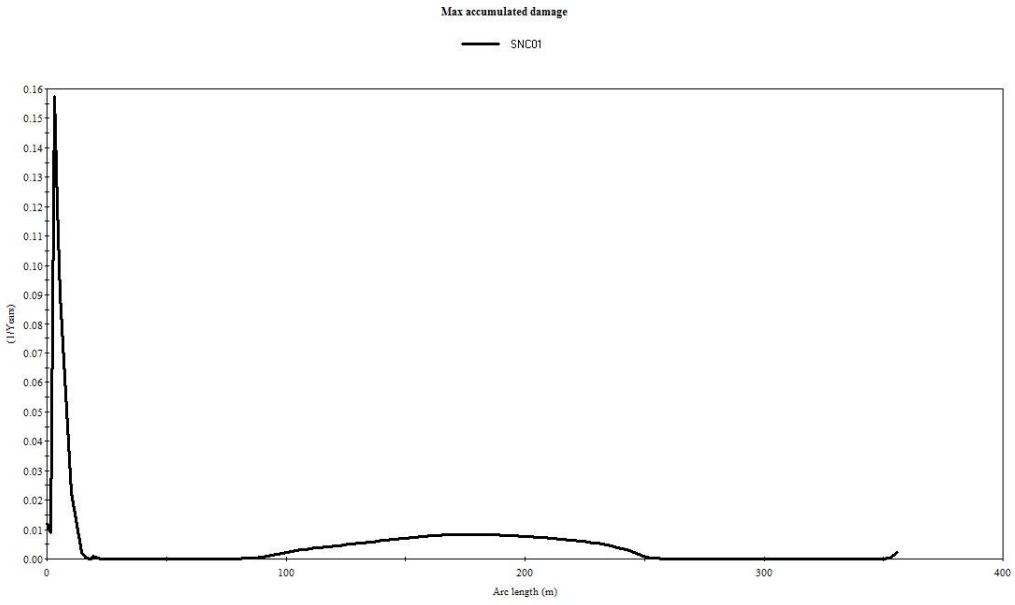

Figure 11.4 Fatigue damage for mesured current, base configuration

Table 11-8 below gives the accumulated fatigue damage for the staggered configuration. For the measured current profile, a significantly better fatigue result is found for the staggered configuration compared to the base configuration. For the remaining current profiles, the accumulated damages of the staggered configuration are fairly similar to the base configuration.

current profile	fatigue damage	fatigue life years	location
2/3-current	5,62E-02	17,79	WH/XMT interface
Linearly sheared	6,69E-03	149,47	WH/XMT interface
Measured current	4,85E-02	20,64	WH/XMT interface
Uniform	2,07E-01	4,83	WH/XMT interface

Table 11-8 Fatigue damage, staggered configuration

Figure 11.5 illustrates the accumulated damage. The largest spike is found at the WH/XMT interface.

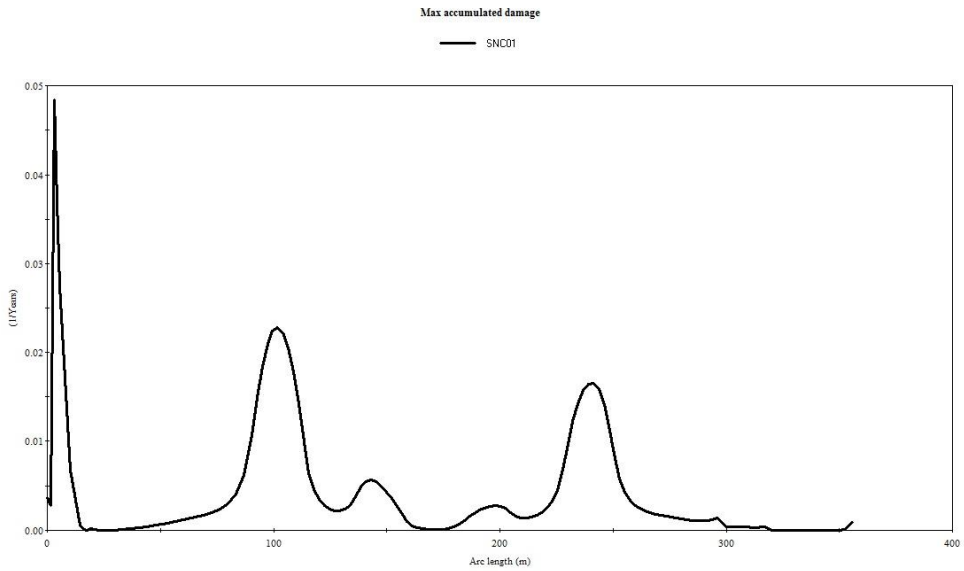

Figure 11.5 Fatigue damage for measured current, staggered configuration

The fatigue damage on the 321 m system decrease significantly when strakes were applied to the top section of the riser, see Table 11-9. No VIV is present for the linearly sheared current profiles.

current profile	fatigue damage	fatigue life years	location
2/3-current	9,81E-05	10194,51	WH/XMT interface
Linearly sheared	N/A	N/A	N/A
Measured current	1,44E-03	696,62	WH/XMT interface
Uniform	8,43E-04	1185,83	WH/XMT interface

Table 11-9 Fatigue damage, top strakes configuration

Figure 11.6 illustrates accumulated damage for the top strakes configuration in measured current.

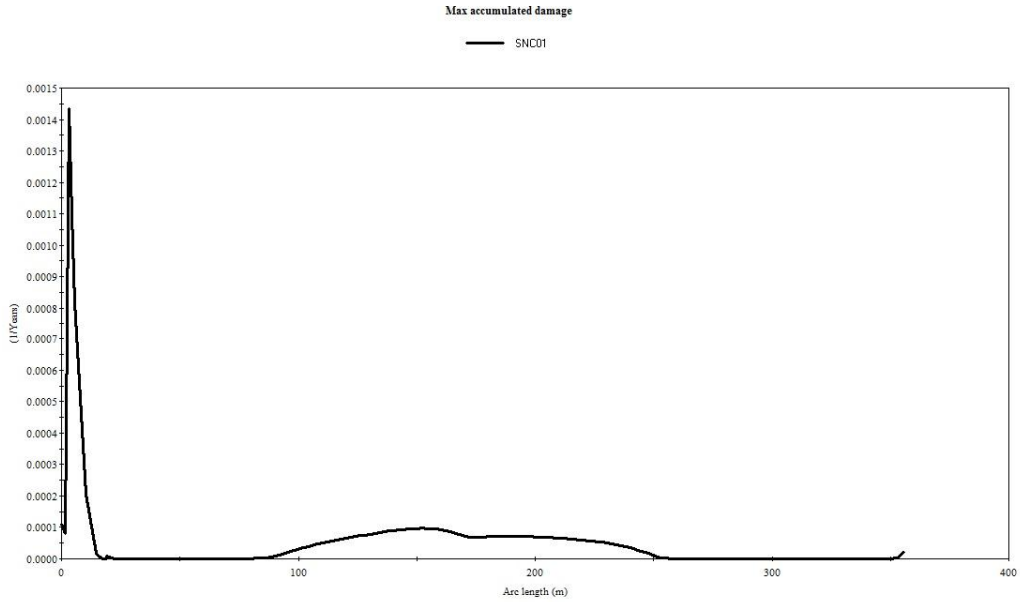

Figure 11.6 Fatigue damage for measured current, top strakes configuration

11.1.4 Static riser deflection and VIV amplification

This section presents the calculated static riser deflections and resulting deflections after added drag from VIV has been accounted for. Table 11-10 gives the static riser deflection of the base configuration before and after VIV amplification, as well as the increase in percentages.

Current profile	Maximum static riser deflection [m]	Maximum amplified static riser deflection [m]	Percentage increase [%]
2/3-current	0,505	0,905	79,21
Linearly sheared	0,278	0,402	44,60
Measured current	0,451	0,928	105,76
Uniform	0,747	1,545	106,83

Table 11-10 Static riser deflection, base configuration

As can be seen from Table 11-11, the decreased deflection of the staggered configuration is fairly small. In fact, added drag from VIV is found be larger for the staggered configuration when comparing the linearly sheared and uniform current profile results.

Current profile	Maximum static riser deflection [m]	Maximum amplified static riser deflection [m]	Percentage increase [%]
2/3-current	0,480	0,976	103,33
Linearly sheared	0,264	0,397	50,38
Measured current	0,433	0,821	89,61
Uniform	0,719	1,700	136,44

Table 11-11 Static riser deflection, staggered configuration

Table 11-12 illustrates how the added drag from the top straked section increases the static deflection of the riser. Accounting for VIV shows however a different picture, as the riser deflection decreases substantially compared to both the base and staggered configurations.

Current profile	Maximum static riser deflection [m]	Maximum amplified static riser deflection [m]	Percentage increase [%]
2/3-current	0,655	0,792	20,92
Linearly sheared	0,365	N/A	N/A
Measured current	0,556	0,764	37,41
Uniform	0,902	1,211	34,26

Table 11-12 Static riser deflection, top strakes configuration

11.1.5 Lower flex joint angles

As described in section 10.6 the flex joints are modelled as beam elements. In order to find the flex joint angles, simple trigonometry is used. Using the displacement of the end nodes of the flex joint element, the angle is found by use of Equation 11.1 below.

Equation 11.1: Lower flex joint angle

$$\theta_{LFJ} = \tan^{-1}\frac{(x_2 - x_1)}{l_{LFJ}}$$

where

x_2 = x-coordinate at end no. 2 of LFJ element

x_1 = x-coordinate at end no. 1 of LFJ element

l_{LFJ} = LFJ element length

Lower flex joint angles for the base configuration is given in Table 11-13 below. As can be seen very small flex joint angles are calculated, which are to be expected considering the small riser deflections given in Table 11-10.

Initial analysis				
Current profile	**LFJ element length [m]**	**End 1 deflection**	**End 2 deflection**	**LFJ angle [degrees]**
2/3-current	1,525	7,6061E-03	1,1407E-02	**0,14**
Linearly sheared	1,525	3,9536E-03	5,9298E-03	**0,07**
Measured current	1,525	1,0656E-02	1,5725E-02	**0,19**
Uniform current	1,525	1,9514E-02	2,8709E-02	**0,35**

Table 11-13 Lower flex joint angles, base configuration

VIV drag amplification gives the following lower flex joint angles, see Table 11-13.

VIV amplified analysis				
Current profile	**LFJ element length [m]**	**End 1 deflection**	**End 2 deflection**	**LFJ angle [degrees]**
2/3-current	1,525	1,3586E-02	2,0378E-02	**0,26**
Linearly sheared	1,525	5,6539E-03	8,4805E-03	**0,11**
Measured current	1,525	2,1042E-02	3,1244E-02	**0,38**
Uniform current	1,525	3,8541E-02	5,7116E-02	**0,70**

Table 11-14 Lower flex joint angles after VIV amplification, base configuration

As can be seen from Table 11-15 the lower flex joint angles of the staggered configuration are fairly similar to that of the base configuration, as the decrease in riser deflection from base to staggered configuration proved to be small.

Initial analysis				
Current profile	**LFJ element length [m]**	**End 1 deflection**	**End 2 deflection**	**LFJ angle [degrees]**
2/3-current	1,525	7,2752E-03	1,1009E-02	**0,14**
Linearly sheared	1,525	3,7783E-03	5,7175E-03	**0,07**
Measured current	1,525	1,0330E-02	1,5365E-02	**0,19**
Uniform current	1,525	1,8959E-02	2,8111E-02	**0,34**

Table 11-15 Lower flex joint angles, staggered configuration

The lower flex joint angles for the staggered configuration after VIV amplification are fairly similar to those of the base configuration, i.e. small flex joint angles, see Table 11-16. Compared to the base configuration, the largest difference is found for the uniform current profile, where an increase of 0.07 degrees of found for the staggered configuration.

VIV amplified analysis				
Current profile	**LFJ element length [m]**	**End 1 deflection**	**End 2 deflection**	**LFJ angle [degrees]**
2/3-current	1,525	1,4718E-02	2,2273E-02	**0,28**
Linearly sheared	1,525	5,6790E-03	8,5946E-03	**0,11**
Measured current	1,525	1,8716E-02	2,8005E-02	**0,35**
Uniform current	1,525	4,1442E-02	6,1978E-02	**0,77**

Table 11-16 Lower flex joint angles after VIV amplification, staggered configuration

As expected from the increased drag of the straked riser section, increase in lower flex joint angles were found for the top strakes configuration, see Table 11-17.

Initial analysis				
Current profile	**LFJ element length [m]**	**End 1 deflection**	**End 2 deflection**	**LFJ angle [degrees]**
2/3-current	1,525	9,3006E-03	1,3982E-02	**0,18**
Linearly sheared	1,525	4,9010E-03	7,3685E-03	**0,09**
Measured current	1,525	1,1893E-02	1,7619E-02	**0,22**
Uniform current	1,525	2,1399E-02	3,1606E-02	**0,38**

Table 11-17 Lower flex joint angles, top strakes configuration

By applying strakes to the top section of the riser, the increase in drag from VIV was substantially lower than for the other two configurations. Table 11-18 gives the resulting lower flex joint angles for the top strakes configuration after VIV amplification has been accounted for. While an angle increase is found compared to the initial analysis given in Table 11-17, the increase is smaller than what was found for both the base and staggered configurations.

VIV amplified analysis				
Current profile	**LFJ element length [m]**	**End 1 deflection**	**End 2 deflection**	**LFJ angle [degrees]**
2/3-current	1,525	1,1218E-02	1,6865E-02	**0,21**
Linearly sheared	1,525	N/A	N/A	**N/A**
Measured current	1,525	1,6039E-02	2,3831E-02	**0,29**
Uniform current	1,525	2,8022E-02	4,1521E-02	**0,51**

Table 11-18 Lower flex joint angles after VIV amplification, top strakes configuration

With references to Figure 7.3 and Figure 7.4, it is seen that VIV will have no operational consequences for the selected current profiles and configurations in the 321 m system. Neither the base configuration, staggered configuration nor the top strakes configuration give LFJ angles that exceeds the angle requirements given in the standards (ISO, 2009). The strictest requirement is found for running and retrieval of subsea equipment, for instance running of a XMT module, at ±1.0 degree. The highest LFJ angle is found for the staggered configuration in uniform current after VIV amplification, where a LFJ angle of 0.77 degrees was found, seeTable 11-16.

11.2 1300 m water depth VIV results

The following will give the calculated results for the 1300 m water depth system. In similar fashion as for the 321 m water depth, results for the base and staggered configurations are given, as well as results for the best performing strakes configuration.

11.2.1 Dominating frequency, duration and VIV amplitudes

Dominating frequencies and duration, in addition to excitation zone lengths and VIV amplitudes for the base configuration are given in Table 11-19. As can be seen the duration percentage of the dominating frequencies are considerably lower than what was found for the 321 m water depth system. While a maximum of 4 response frequencies were found for the 321 m system, more than 30 response frequencies were evaluated for each analysis of the 1300 m system. Consequently, a larger number of frequencies are competing to be the dominating one, and a shorter duration are found for the dominating frequency.

Current profile	Dominating frequency no.	Frequency [Hz]	Duration [%]	Length of excitation zone [m]	VIV amplitude [m]
2/3-current	9	0.1251	13.62	784.325	0.813447
Linearly Sheared	7	0.1038	14.18	352.0721	0.76736
Measured current	9	0.1287	9.68	950.502	0.447441
OL_2	10	0,1405	11.70	691.042	0.661432

Table 11-19 Dominating frequencies, durations and VIV amplitudes, base configuration

For the staggered configuration, the frequency number of the dominating frequency is lower for all current profiles compared to the base configuration. This is illustrated in Table 11-20 below.

Current profile	Dominating frequency no.	Frequency [Hz]	Duration [%]	Length of excitation zone [m]	VIV amplitude [m]
2/3-current	6	0.1248	16.37	539.498	0.894704
Linearly Sheared	5	0.1059	15.80	514.352	0.598257
Measured current	6	0.1267	10.70	660.870	0.906024
OL_2	7	0.1445	13.42	654.012	0.624586

Table 11-20 Dominating frequencies, durations and VIV amplitudes, staggered configuration

An opposite trend was found for the top 50_150 strakes configuration, see Table 11-21.

Current profile	Dominating frequency no.	Frequency [Hz]	Duration [%]	Length of excitation zone [m]	VIV amplitude [m]
2/3-current	9	0.1214	13.67	799.222	0.375753
Linearly Sheared	9	0.1195	15.53	616.266	0.216092
Measured current	12	0.1625	9.48	357.4664	0.15189
OL_2	11	0.1470	11.45	696.200	0.15106

Table 11-21 Dominating frequencies, durations and VIV amplitudes, top 50_150 strakes config.

The VIV amplitudes of the dominating frequencies for the staggered and base configurations are considerably higher than those of the top 50_150 strakes configuration. There is, however, no clear trend in the response amplitudes of the base and staggered configurations. For the linearly sheared and Ormen Lange 2 current models, higher response amplitudes are found for the dominating frequencies of the base configuration. The staggered configuration will however give higher VIV amplitudes for the 2/3-current and measured current profile.

11.2.2 Stress amplitudes

A clear pattern is seen when comparing the maximum stresses for the different configurations. The base configuration experiences the highest maximum stresses for all current profiles, and in particular for the measured current and Ormen Lange 2 profiles the calculated stresses were high, see Table 11-22.

Current profile	Frequency no.	Frequency [Hz]	Max stress amplitude [MPa]
2/3-current	7	0.1176	28.9914
Linearly sheared	8	0.1130	27.3267
Measured current	12	0.1698	37.3371
OL_2	12	0.1666	38.9866

Table 11-22 Stress amplitudes, base configuration

Figure 11.7 illustrates the maximum stresses for 19 of the calculated response frequencies of the base configuration subjected to the measured current profile. Note that there are several frequencies that induce higher stresses than the dominating frequency, which is marked with the black line in Figure 11.7. This will be discussed further later in the report.

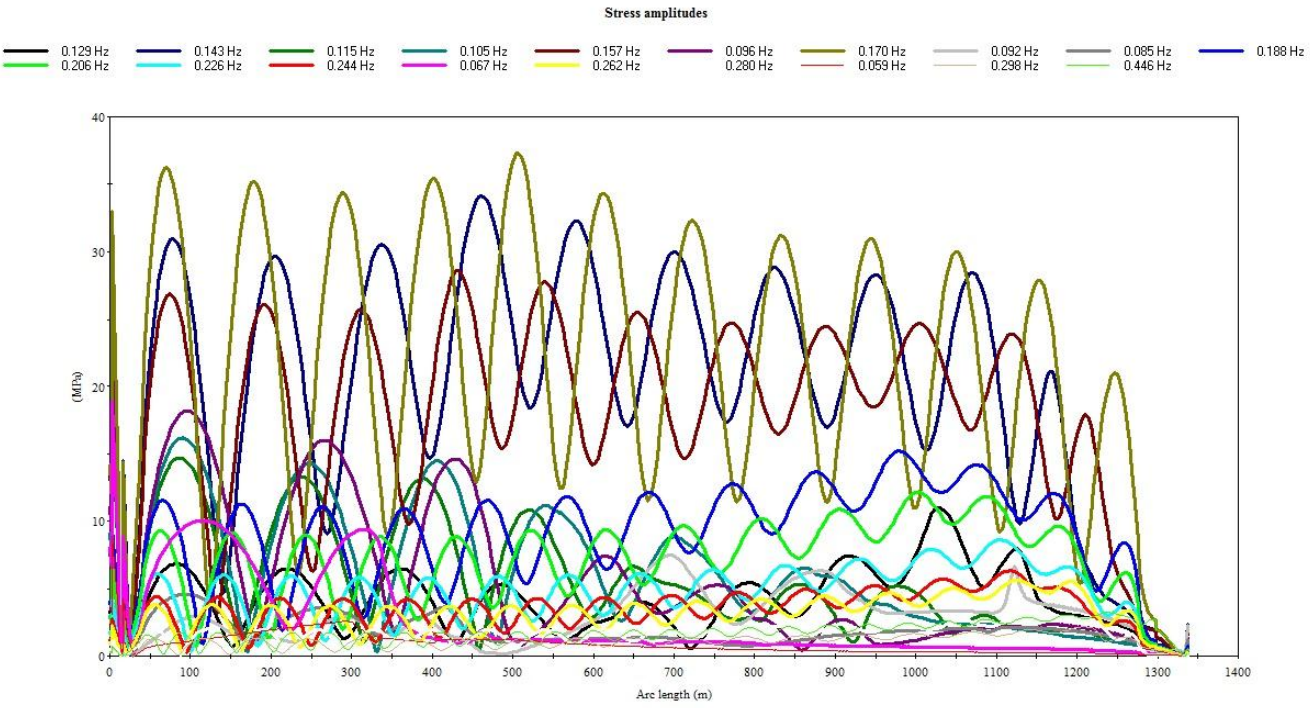

Figure 11.7 Stress amplitudes for measured current profile, base configuration

The staggered configuration experiences considerably lower stresses than the base configuration. The smallest difference between the two is seen for the 2/3-current model, where the staggered

configuration's maximum stress is roughly 3.3 MPa lower than the base configuration's highest stress, see Table 11-22.

Current profile	Frequency no.	Frequency [Hz]	Max stress amplitude [MPa]
2/3-current	5	0.1158	25.689
Linearly sheared	5	0.1059	14.4204
Measured current	6	0.1267	24.9908
OL_2	8	0.1634	22.1361

Table 11-23 Stress amplitudes, staggered configuration

Table 11-23 shows the highest stress amplitudes for the staggered configuration and measured current profile. The maximum stress is induced by frequency no. 6, which according to Table 11-20 is the dominating frequency for this configuration. Maximum stress if found to occur at the wellhead/BOP interface.

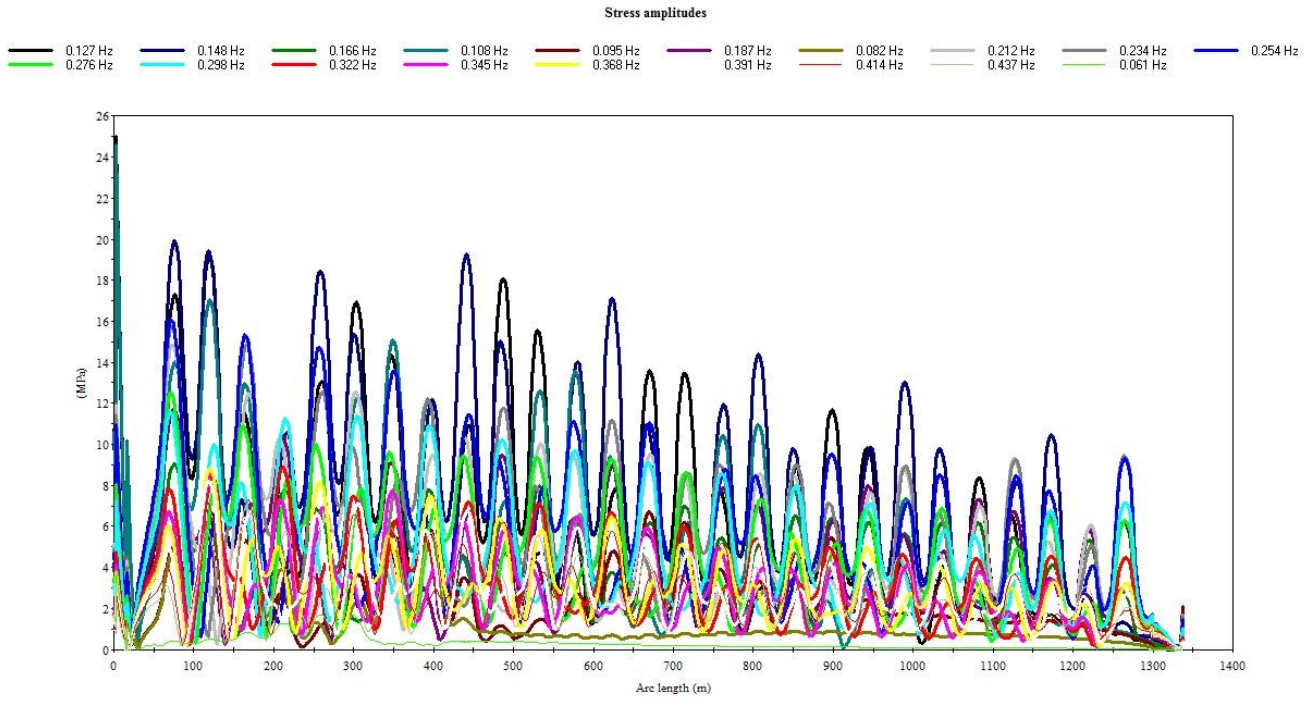

Figure 11.8 Stress amplitudes for measured current, staggered configuration

As for the 321 m water depth system, a drastic decrease in calculated stresses was found when applying the most efficient strakes configuration. From Table 11-24 it is seen that a decrease of more than 50% is found for the 2/3-current and linearly sheared current profiles, while a reduction of roughly 10 MPa is experienced for the last two current models when applying the relevant strakes configuration.

Current profile	Frequency no.	Frequency [Hz]	Max stress amplitude [MPa]
2/3-current	9	0.1214	7.40940
Linearly sheared	8	0.1108	6.05852
Measured current	13	0.1747	14.8849
OL_2	10	0.1394	13.6356

Table 11-24 Stress amplitudes, top 50_150 strakes configuration

Figure 11.9 illustrates the maximum stress amplitudes for the top 50_150 strakes configuration. The maximum stress is found roughly 125 m below the water surface, i.e. close to the start of the straked section, as the top 150 m of the riser is bare in this configuration.

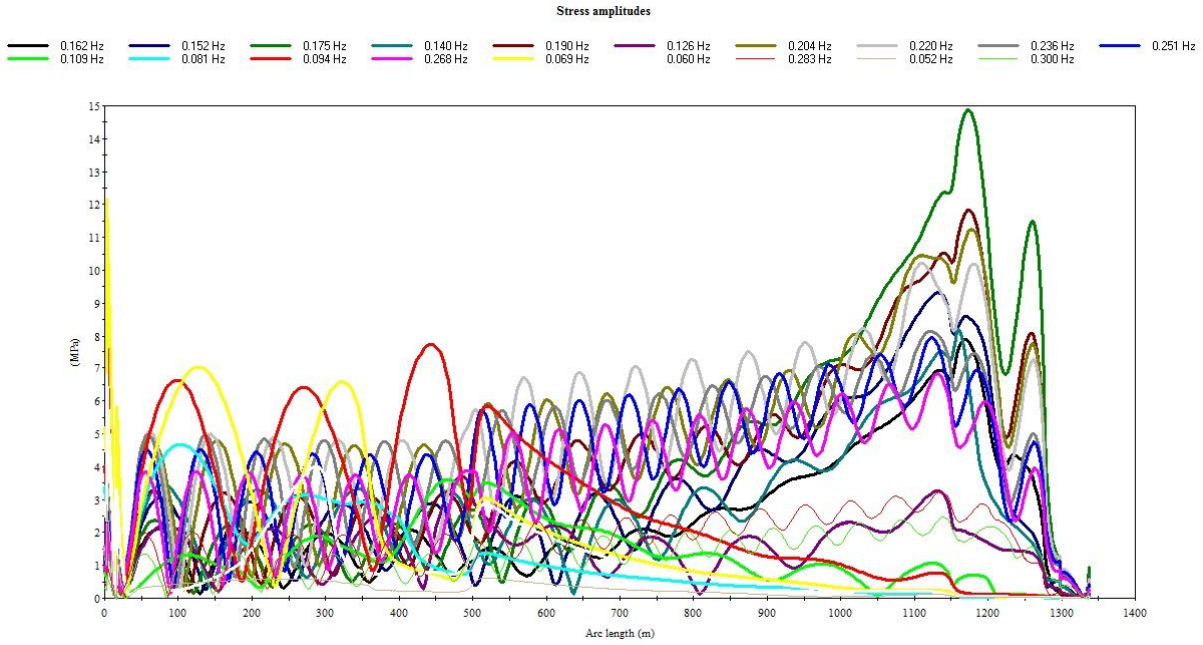

Figure 11.9 Stress amplitudes for measured current, top 50_150 strakes configuration

11.2.3 Fatigue damage

The same SN-curve for fatigue calculations used for the 321 m water depth, is used for all analyses of the 1300 m system.

The base configuration experiences the largest fatigue damage of all configurations, for all current profiles except the 2/3-current, see Table 11-25.

current profile	fatigue damage	fatigue life years	location
2/3-current	4,83E-01	2,07	WH/BOP interface
linearly sheared	4,85E-01	2,06	WH/BOP interface
measured current	1,17E+00	0,86	WH/BOP interface
OL_2	9,02E-01	1,11	z = -548 m

Table 11-25 Fatigue damage, base configuration

Figure 11.10 illustrates the accumulated damage for the base configuration in measured current. Max fatigue damage is located at the WH/BOP interface for the top three current profiles, a point which is associated with a large change in component bending stress.

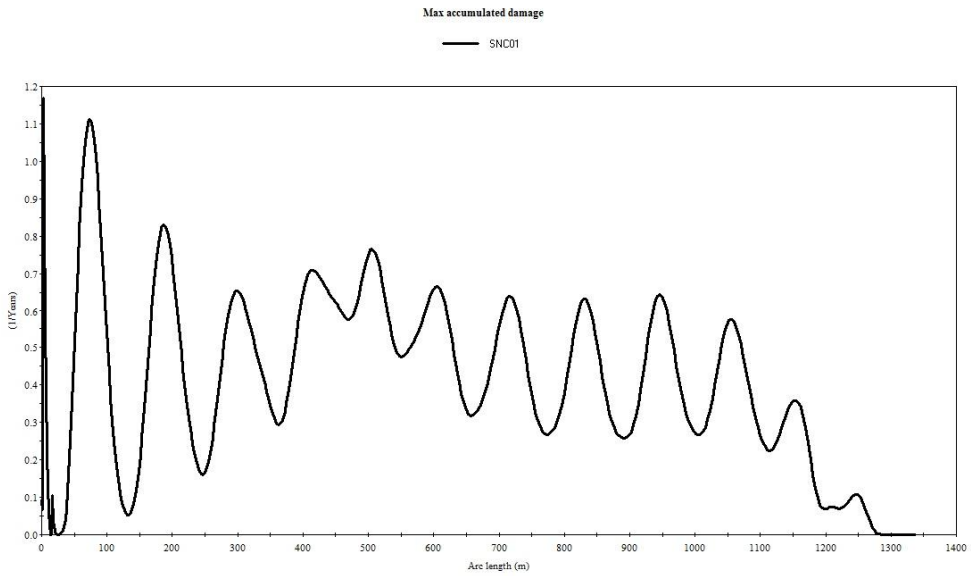

Figure 11.10 Fatigue damage for measured current, base configuration

Slightly better fatigue damage results are found for the staggered configuration, see Table 11-26.

current profile	fatigue damage	fatigue life years	location
2/3-current	7,19E-01	1,39	WH/BOP interface
linearly sheared	1,29E-01	7,73	WH/BOP interface
measured current	5,33E-01	1,87	WH/BOP interface
OL_2	4,52E-01	2,21	WH/BOP interface

Table 11-26 Fatigue damage, staggered configuration

Max accumulated damage is found at the WH/BOP interface for all current profiles. This is illustrated by the tallest spike in Figure 11.11.

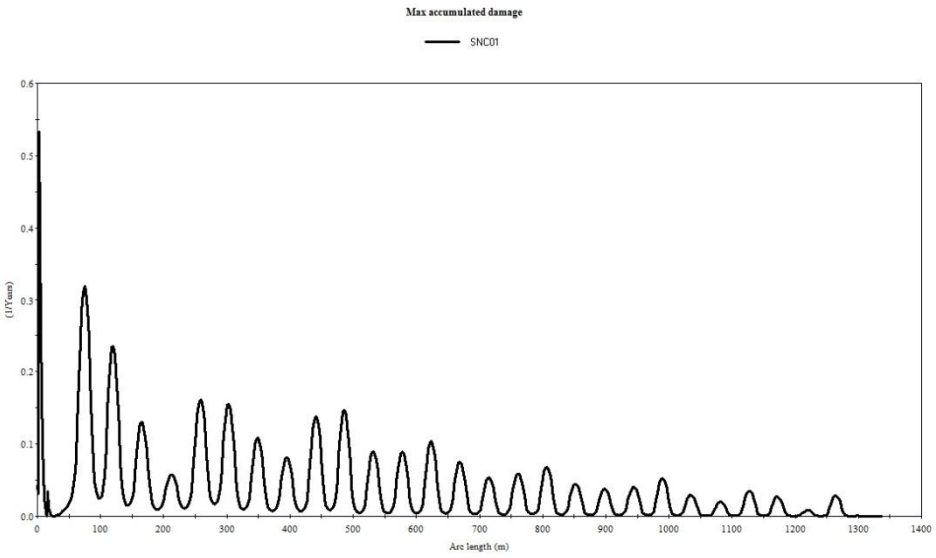

Figure 11.11 Fatigue damage for measured current, staggered configuration

Considerably better fatigue result are calculated for the top 50_150 strakes configuration, see Table 11-27, however the improvement is significantly smaller than what was found for the best strakes configuration of the 321 m water depth.

current profile	fatigue damage	fatigue life years	location
2/3-current	1,02E-02	98,45	z = -166.5 m
linearly sheared	5,43E-03	184,13	z = -164 m and z = -132 m
measured current	1,04E-01	9,57	z = -127 m
OL_2	5,72E-02	17,49	z = -165 m

Table 11-27 Fatigue damage, top 50_150 strakes configuration

Location of maximum accumulated damage for the top 50_150 strakes configuration is located close to the start of the straked section of the riser. The top 150 m of the riser is bare, and for the measured current profile the maximum accumulated damage is found at a water depth of 127 metres, see Figure 11.12.

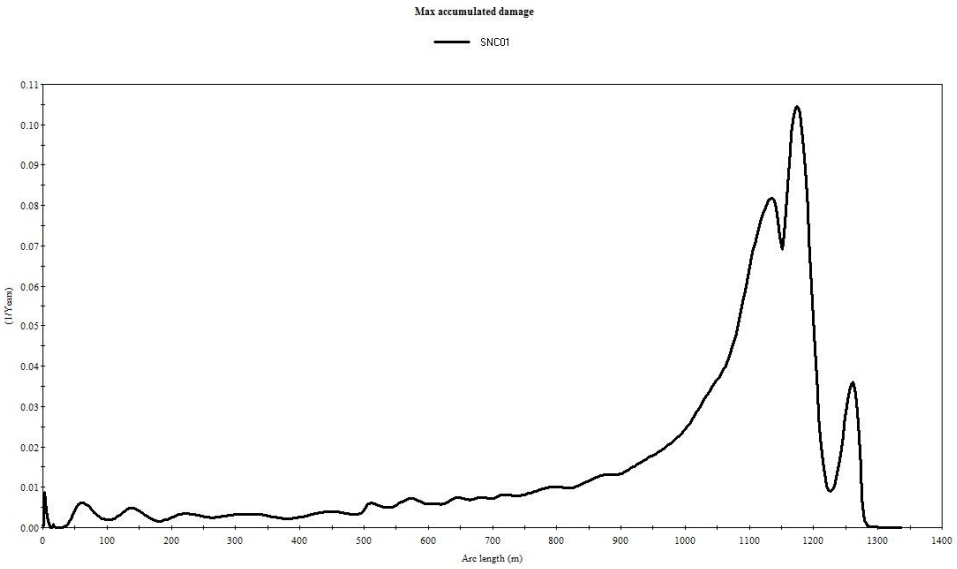

Figure 11.12 Fatigue damage for measured current, top 50_150 strakes configuration

11.2.4 Static riser deflection and VIV amplification

Static riser deflection of the base configuration is given in Table 11-28.

Current profile	Maximum initial static riser deflection [m]	Maximum amplified static riser deflection [m]	Percentage increase [%]
2/3-current	27,8838	58,2343	108,85
Linearly sheared	14,7735	27,2405	84,39
Measured current	28,1091	66,6406	137,08
OL_2	29,9215	68,8369	130,06

Table 11-28 Static riser deflection, base configuration

As expected the staggered configuration gave lower static deflections than the base configuration. This is valid both before and after VIV amplification has been accounted for. Note however, that for two of the current profiles the percentage increase in riser deflection from VIV drag amplification is greater for the staggered configuration than the base configuration, see Table 11-29.

Current profile	Maximum initial static riser deflection [m]	Maximum amplified static riser deflection [m]	Percentage increase [%]
2/3-current	18,8067	44,9866	139,21
Linearly sheared	9,81128	16,1116	64,22
Measured current	19,5559	49,2621	151,90
OL_2	20,1366	46,3198	130,03

Table 11-29 Static riser deflection, staggered configuration

While the addition of strakes to the riser drastically decreases the percentage increase in riser deflection from VIV amplification, the deflection in metres is still greater for the straked configuration than for the staggered configuration, see Table 11-30. Compared to the base configuration however, the static riser deflection after VIV amplification is lower for the top 50_150 strakes configuration.

Current profile	Maximum initial static riser deflection [m]	Maximum amplified static riser deflection [m]	Percentage increase [%]
2/3-current	36,357	47,4127	30,41
Linearly sheared	19,0397	20,0844	5,49
Measured current	35,3768	53,352	50,81
OL_2	38,3005	57,8753	51,11

Table 11-30 Static riser deflection, top 50_150 strakes configuration

11.2.5 Lower flex joint angles

As already discussed above, the base configuration has the highest riser deflection when increase in drag from VIV has been taken into account. This is also reflected in the lower flex joint angles, as is shown below.

Table 11-31 below gives the lower flex joint angles for the base configuration.

Initial analysis				
Current profile	**LFJ element length [m]**	**End 1 deflection**	**End 2 deflection**	**LFJ angle [degrees]**
2/3-current	1,525	6,3993E-02	1,1116E-01	**1,77**
Linearly sheared	1,525	3,2464E-02	5,6453E-02	**0,90**
Measured current	1,525	8,8977E-02	1,5390E-01	**2,44**
OL_2	1,525	8,7245-02	1,5105E-01	**2,39**

Table 11-31 Lower flex joint angles, base configuration

Taking VIV into account the following LFJ angels for the base configuration are found, see Table 11-32.

VIV amplified analysis				
Current profile	**LFJ element length [m]**	**End 1 deflection**	**End 2 deflection**	**LFJ angle [degrees]**
2/3-current	1,525	1,3769E-01	2,3679E-01	**3,71**
Linearly sheared	1,525	5,7635E-02	9,9621E-02	**1,58**
Measured current	1,525	2,0324E-01	3,4788E-01	**5,40**
OL_2	1,525	2,0805E-01	3,5527E-01	**5,49**

Table 11-32 Lower flex joint angles after VIV amplification, base configuration

The staggered configuration gives lower flex join angles for all current profiles, see Table 11-33.

Initial analysis				
Current profile	**LFJ element length [m]**	**End 1 deflection**	**End 2 deflection**	**LFJ angle [degrees]**
2/3-current	1,525	5,4638E-02	9,2357E-02	**1,42**
Linearly sheared	1,525	2,7496E-02	4,6506E-02	**0,71**
Measured current	1,525	7,8687E-02	1,3244E-01	**2,02**
OL_2	1,525	7,6653E-02	1,2898E-01	**1,96**

Table 11-33 Lower flex joint angles, staggered configuration

Also after VIV amplification, the staggered configuration provides better LFJ angle results, see Table 11-34, than the base configuration.

VIV amplified analysis				
Current profile	**LFJ element length [m]**	**End 1 deflection**	**End 2 deflection**	**LFJ angle [degrees]**
2/3-current	1,525	1,4485E-01	2,1952E-01	**2,80**
Linearly sheared	1,525	4,7201E-02	7,1788E-02	**0,92**
Measured current	1,525	2,2070E-01	3,3347E-01	**4,22**
OL_2	1,525	1,9580E-01	2,9595E-01	**3,75**

Table 11-34 Lower flex joint angles after VIV amplification, staggered configuration

The top 50_150 strakes configuration gives the poorest LFJ angle results for the initial analyses where no VIV amplification is considered, see Table 11-35.

Initial analysis				
Current profile	**LFJ element length [m]**	**End 1 deflection**	**End 2 deflection**	**LFJ angle [degrees]**
2/3-current	1,525	8,1112E-02	1,4095E-01	**2,25**
Linearly sheared	1,525	4,1014E-02	7,1265E-02	**1,14**
Measured current	1,525	1,0478E-01	1,8142E-01	**2,87**
OL_2	1,525	1,0382E-01	1,7980E-01	**2,85**

Table 11-35 Lower flex joint angles, top 50_150 strakes configuration

While not achieving as low LFJ angles as the staggered configuration, applying strakes will give smaller LFJ angles than the base configuration after increased drag from VIV has been added, as is seen in Table 11-36.

VIV amplified analysis				
Current profile	**LFJ element length [m]**	**End 1 deflection**	**End 2 deflection**	**LFJ angle [degrees]**
2/3-current	1,525	1,0923E-01	1,8821E-01	**2,96**
Linearly sheared	1,525	4,1472E-02	7,1730E-02	**1,14**
Measured current	1,525	1,7243E-01	2,9586E-01	**4,61**
OL_2	1,525	1,7115E-01	2,9333E-01	**4,57**

Table 11-36 Lower flex joint angles after VIV amplification, top 50_150 configuration

Considering the LFJ angle results solely, the staggered configuration is the best option as it provides the lowest flex joint angles for all current profiles, even after added drag from VIV has been accounted for. Still, with references to Figure 7.3 and Figure 7.4, it is clear that VIV may have operational consequences for all of the configurations given above. Operations like running and retrieval of subsea equipment will not be possible (ISO, 2006) under the presented current profiles, with the exception of the linearly sheared current where a LFJ angle of 0.92 degrees is found for the staggered configuration.

One important find is the drastic reduction in LFJ angle of the straked configuration compared to the base configuration after VIV drag amplification. For the measured and Ormen Lange 2 current profiles, drilling is not allowed for the base configuration as the LFJ angle exceeds the 5 degrees requirement, see Figure 7.3, set by the ISO 13624-1 standard (ISO, 2009). Applying the top 50_150 strakes configuration will however reduce the VIV amplified drag sufficiently so that a LFJ angle of 4.61 and 4.57 degrees are found for the measured and Ormen Lange 2 current profiles respectively, and thus allowing drilling.

12 Discussion

This chapter will give a discussion to the inputs of the model used in the analyses, as well as comment on the calculated results. Some of the arguments given are related to the definition of the model in INPMOD, and some related to the user defined inputs in VIVANA and how these inputs affect the analysis.

12.1 Model inputs

Certain simplifications have been made when the model was defined in INPMOD and STAMOD. The majority of these will have no effect on the comparison study of the various configurations in this thesis. However, if one was to compare the analyses in this thesis with independent, external VIV analyses, some of the simplifications may affect the results.

12.1.1 Geometry considerations

Compared to an in-house VIV-analysis in Aker Solutions, the presented model applies certain modifications. In particular three parameters stand out; structural properties of the wellhead, top tension used in the analysis and the boundary condition at the seabed.

As neither the inner diameter nor mass of the wellhead were clearly defined in the stack-up data made available from Aker Solutions, these values have been estimated. The estimations are made from wellhead structural properties of previous AKSO projects, but are nevertheless not project specific. Consequently, the volume of the component is also an estimation, which again will affect the density as defined in INPMOD of the component, see Equation 10.3. Still, as the same structural properties for the wellhead component are used for all analyses in the thesis, this simplification will have no effect on the comparison of the different configurations.

12.1.2 Boundary condition considerations

In presented analyses, the wellhead is modelled as fixed to the sea bed. As discussed in point 3 of section 10.1, the soil stiffness in the area around the wellhead will influence the structural properties of the wellhead/sea bed interaction. Based on thorough seismic study of the well bay area, collected geotechnical data may be “converted“ into a boundary condition of the wellhead which consists of a combination of springs. The interaction of the wellhead, conductor, soil and cement is typically modelled using a set of nonlinear rotational and translational springs. The prescribed properties of the springs allow certain levels of deflection of the wellhead. A local FEA analysis along with substantial soil data are required to determine the stiffness of the springs. Alteration to the boundary conditions will affect the system eigenfrequencies, which in turn will affect active response frequencies in the VIV analysis. If the presented analyses are to be examined and matched with an external VIV analysis, the simplification mentioned above should be considered as a source of error. Still, as the same boundary conditions are used for all analyses in the presented study, the mentioned modification will have no effect on the comparison study in this thesis.

12.1.3 Top tension considerations

The top tension in the models is, as described in section 10.4, determined by defining a positive axial force of roughly 400kN at the wellhead datum. The corresponding top tensions are given in Table 10-7 and Table 10-8. As can be seen from the tables, certain variations in the top tensions are present. According to Equation 12.1 (Larsen, 2009),a tensioned beam will have an eigenfrequency given as:

Equation 12.1: Eigenfrequency for beam subjected to tension force

$$\omega_o = \frac{n\pi}{l}\sqrt{\frac{T}{m} + \frac{n^2\pi^2}{l^2} * \frac{EI}{m}}$$

where

n = mode number

T = tension force

m = mass

l = length

Thus, variation in top tension will influence the eigenfrequency of the beam, which again will have an influence on the active response frequencies from VIV of the beam.

The largest variation in top tension is found for the non-staggered and staggered configurations for the 1300 m water depth system, as is expected as half of the buoyancy field is removed for the staggered configuration. For the base and straked configurations, top tension variations of 30-50kN are seen. Comparing the base and top 50_150 strakes configurations, Table 10-8 gives a difference of 30kN, or 0.5%, see Table 12-1.

1300 m water depth	
Configuration	**Top tension [kN]**
Base	6080
Top 50_150 strakes	6050

Table 12-1 Top tension variations base and top 150 strakes configuration

Adjusting the top tension of the top 50_150 strakes configuration to 6080 kN, i.e. equal to the base configuration, showes how sensitive the analysis is to top tension variation, see Table 12-2 and Table 12-3. Note that only the 2/3-current profile was applied in top tension sensitivity study.

Current profile	Dominating frequency no.	Frequency [Hz]	Duration [%]	Length of excitation zone [m]	VIV amplitude [m]
2/3-current	9	0.1214	13.72	799.222	0.347773

Table 12-2 Dominating frequency, VIV amplitude after adjusted top tension, top 50_150 strakes configuration

Current profile	Frequency no.	Frequency [Hz]	Max stress amplitude [MPa]
2/3-current	9	0.1214	6.83348

Table 12-3 Max stress after adjusted top tension, top 50_150 strakes configuration

Compared to the original results, see Table 11-21 and Table 11-24, one finds that the dominating response mode and frequency remains unchanged. The eigenfrequency of the dominating mode did change slightly, with a small increase for the increased top tension analysis, as is expected. The

duration of the dominating mode is marginally increased, from 13.67% of the original top tension analysis, to 13.72% of the increased top tension analysis. The excitation length is unchanged, however the VIV amplitude of the dominating mode is decreased from 0.376 m for 6050kN top tension, to 0.348 m for 6080kN top tension. Similarly, a reduction in the maximum stress amplitude is found for increased top tension. 6.833MPa maximum stress was found for 6080 kN top tension, which is a reduction of almost 8% compared to the original analysis, see Table 11-24.

While a reduction in VIV amplitudes and thus induces stresses is to be expected for increased top tension, the dramatic change found and discussed above may give hints to weaknesses in the model. Furthermore, inconsistencies related to dominating frequency number and the frequency number inducing maximum stresses laid the background for a sensitivity study related to the convergence limit in the model. This will now be discussed.

12.2 VIVANA inputs

12.2.1 Convergence and convergence limit

The results gathered from the analyses of the 1300 m system revealed certain inconsistencies. For the 2/3-current profile analysis of the base configuration, the highest stress amplitude was found to be excited by frequency no. 7, yet the dominating frequency of this configuration and current combination was frequency no. 9. The same result was found for several other configurations and current combinations, including the 2/3-current and staggered configuration, the linearly sheared current and middle strakes configuration, the linearly sheared current and top 50_150 strakes configuration as well as the measured current and top strakes configuration.

While it is common for the maximum stress inducing frequency to be of same mode order or higher than the dominating frequency, some of results from the presented analysis showed the opposite. Higher mode amplitudes will have increased curvature which will give higher bending stresses. That is, for a given response amplitude a higher mode response will give higher curvature at the peak of the amplitude than a lower mode response, which according to the derivation below will give higher bending stresses.

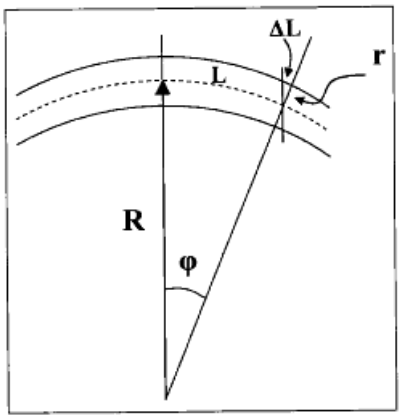

Figure 12.1 Bending stress form curvature (Larsen, 2009)

The bending stress is given by the curvature according to Equation 12.2, reference is made to Figure 12.1 above for explanation of the relationships:

Equation 12.2: Bending stress derivation

$$\varphi = \frac{L}{R} = \frac{\Delta L}{r}$$

$$\varepsilon = \frac{\Delta L}{L} = \frac{\varphi r}{\varphi R} = \frac{r}{R}$$

$$\sigma = \epsilon E = \frac{r}{R} E = Erw_{,xx}$$

where $w_{,xx}$ is the curvature of the beam. Now, from modal superposition we have the following relationship for the response (Larsen, 2009):

Equation 12.3: Modal superposition response

$$w(x,t) = \sum_{i=1}^{N} \psi_i(x) * q_i(t)$$

The eigenmode shapes are given as harmonic functions, see Equation 12.4:

Equation 12.4: Eigenmode shapes

$$\psi_i(x) = \sin\left(\frac{i\pi}{l} x\right)$$

Inserting Equation 12.4 into Equation 12.3 and differentiating twice with respect to x, gives the curvature as

Equation 12.5: Curvature

$$w_{,xx}(x,t) = \sum_{i=1}^{N} -\left(\frac{i\pi}{l}\right)^2 \sin\left(\frac{i\pi}{l} x\right) * q_i(t)$$

Consequently, the curvature is proportional to the square of the mode number i^2, which means that according to Equation 12.2 also the bending stress is proportional to the mode number squared. The derivation above explains why it is expected that the maximum induced stress on the riser occurs for a frequency number of same or higher order than the dominating frequency.

One reason for the unusual results may be linked to convergence of the response amplitude iteration process in VIVANA, reference is made to the VIVANA User's Manual (Yttervik, et al., 2009) for details. As discussed in section 10.5, all response frequencies were determined within the first 8 iterations, of a total of 30 iterations which was set as maximum. The value of the convergence limit for the iteration process in the presented analyses is set to $conlim = 0.0001$, and the order of magnitude was determined based on a recent VIV study at the Department of Marine Technology (Larsen, 2012). There an iteration limit of $conlim = 0.0005$ was used, thus a further 0.0004 was subtracted from the limit to assure successful convergence in the presented analyses.

However, based on the discrepancies in the results discussed above, a further narrowing of the convergence limit was applied and the limit for iteration was set to $conlim = 0.00005$. Analysing the

same base configuration of the 1300 m water depth subjected to 2/3-current, gave the following results:

Current profile	Dominating frequency no.	Frequency [Hz]	Duration [%]	Length of excitation zone [m]	VIV amplitude [m]
2/3-current	9	0.1251	13.62	784.325	0.813447

Table 12-4 Dominating frequency, base configuration, conlim=0.00005

Thus, from Table 12-4, there is no change to the dominating frequency for the base configuration in 2/3-current after the iteration limit was reduced. For the maximum stresses however, a drastic change was found, see Table 12-5.

Current profile	Frequency no.	Frequency [Hz]	Max stress amplitude [MPa]
2/3-current	12	0.1686	36.4682

Table 12-5 Stress amplitude, base configuration, conlim=0.00005

Compared to the initial analyses where an iteration limit of $conlim = 0.0001$ was used, see Table 11-22, the maximum stress occurs for frequency no. 12, against frequency no.7 of the initial analysis. Thus, maximum stress is found for a higher mode than the dominating mode, which according to the discussion above seems like a more reliable result that what was initially found. Additionally, the magnitude of the maximum stress amplitude has increased from 28.99MPa to 36.47MPa as seen in Table 12-5. These finds point to the conclusion that a stricter iteration limit than what was used in the presented analyses should be applied for future analyses.

12.3 Other observations

Previous case studies and experiments of straked risers (Vandiver, et al., 2006) have documented stress concentrations at locations close to the interface between the bare section and straked section of the riser, see section 6.3.4. A proposed explanation has been that travelling waves generated by VIV are reflected in the interface points, and thus giving a stress peak, when meeting the change in mass and hydrodynamic damping of the straked section. Similar results were observed in the presented case studies for two of the strakes configurations of the 1300 m water depth. For the middle strakes configuration, the interface between the bare and straked section is at z = -325 m, see Table 9-10. For this configuration maximum fatigue damage for the different current profiles were located close to the bare/straked riser interface depth, varying from z = -285 m to z = -337.5 m. Similarly, for the top 50_150 strakes configuration where the top 150 m of the riser is bare, see Table 9-11, maximum fatigue damage was located between z = -127 m to z = -166.5 m. One may therefore draw the conclusion that care should therefore be taken when determining location of the straked section of the riser. High stress amplitudes may occur at the interface between the straked and bare riser if high VIV amplitudes are present for the bare section.

13 Conclusion

The main objective of this Master Thesis was to provide basic insight into the physical aspects of Vortex Induced Vibrations (VIV), with emphasis on preventive measures, and in particular the use of strakes. Furthermore, two VIV case studies have been conducted where two Aker Solutions systems have been analysed; one 321 m water depth system and one 1300 m water depth system. The scope of the analyses was to study the effects from VIV on a base configuration, a staggered buoyancy and bare riser joint configuration as well as several strakes configurations. Interesting parameters were response frequencies and amplitudes, stress amplitudes from VIV and riser end angles, in addition to possible operational consequences from VIV.

13.1 321 m water depth

Results for the base, staggered and top strakes configuration have been presented in the main part of the report. The top strakes configuration was selected from the other strakes configurations as it delivered the lowest stress amplitudes and thus best fatigue results of the investigated strakes options.

For the 321 m water depth system, small differences in the dominating response frequencies were found between the base and staggered configurations. For the base configuration, frequency no. 1 was found to be the dominating frequency for all current profiles, which, with the exception of the sheared current profile, also was the case for the staggered configuration. Generally, the magnitude of frequency no. 1 increased for the staggered configuration.

As a general note, the durations of the dominating frequencies went down from the base configuration to the staggered, and reductions in excitation zones were also found for the staggered configuration. An opposite trend was found for the top strakes configuration where both the durations and excitation zones of the dominating frequencies increased. In terms of VIV amplitudes, small changes were found when comparing the base and staggered configuration. For the top strakes configuration however, amplitudes less than 20% of the base and staggered amplitudes were found. Furthermore, for the linearly sheared current profile, the top strakes configuration was the only configuration that supressed VIV completely.

With the exception of the linearly sheared current profile, the highest stress amplitudes were found for all current models on the base configuration. The differences in stress compared to the staggered configuration were not substantial; the largest variation was found for the measured current profile. This find is also reflected in the calculated fatigue lives, which were fairly similar for both the 2/3-current and uniform current profile. A large difference in fatigue lives was found for the linearly sheared current profile, where a fatigue life of nearly 3 times the staggered was found for the base configuration. Note however, that for this particular current profile the dominating frequency of the staggered configuration is frequency no. 2, as opposed to frequency no.1 for the base case. Frequency no. 2 of the staggered configuration is significantly higher than frequency no. 1 of the base configuration, $f_{staggered,2} = 0.1574\ Hz$ versus $f_{base,1} = 0.0597\ Hz$, which will give a higher number of response cycles and thus lower fatigue life.

For all current profiles, the fatigue life of the top strakes configuration was substantially better than both the base and staggered profile. Location of the maximum fatigue damage was the same for the three configurations and found at the WH/XMT interface.

As the static deflections of the riser, both before and after added drag from VIV, were small, according to ISO 13624-1 (ISO, 2009) and ISO 13628-7 (ISO, 2006) no operational consequences from VIV was reported for the 321 m water depth. Still it is noted that applying strakes to either the middle or top section of the riser reduced the static riser deflection after VIV amplification with more than 50% compared to the staggered or base configuration.

13.2 1300 m water depth

Similarly as for the 321 m system, results for the base and staggered configuration of the 1300 m water depth are presented in the result chapter of the thesis report. The lowest stress amplitudes of the strakes configurations were found for the top 50_150 strakes configuration, see Figure 9.9, and were thus also presented in the result chapter of the report.

No clear trends were found for the VIV amplitudes of the dominating frequencies for the base and staggered configurations. For the 2/3-current and measured current profiles, VIV amplitudes of the dominating frequencies are higher for the staggered configuration, while the base configuration experiences higher amplitudes for the linearly sheared and Ormen Lange 2 current profiles. It is noted however, that while the dominating response frequencies of the two configurations are fairly similar, the v frequencies of the base configuration are of higher mode number than those of the staggered configuration. This observation is also reflected in the calculated stress amplitudes, which are highest for all current profiles on the base configuration. From the discussion in section 12.2.1 it is stated that for similar VIV amplitudes, response at higher modes will induce higher bending stresses, which is in correspondence with what is observed from the results of the base and staggered VIV amplitudes and response mode numbers.

For the top 50_150 strakes configuration the VIV amplitudes of the dominating frequencies were between 50% and 75% lower than those of the base configuration. The excited mode numbers were found to be higher for the top 50_150 strakes configuration, where mode number 9, 11 and 12 were found to be the dominating, versus mode number 9,7 and 10 for the base configuration. The durations of the dominating frequencies were found to be fairly similar for the base and top 50-150 strakes configurations at 9.5-15.5%, depending on the current profile. For the staggered profile, durations of 10.7-16.4% were found.

The low amplitudes of the top 50_150 strakes configuration gave similarly low stress amplitudes, and compared to the base configuration reductions in stress amplitudes of more than 60% were found. The largest reduction was found for the linearly sheared current profile where the top 50_150 strakes configuration gave 78% lower stress amplitudes than the base configuration.

Lower fatigue life was found for all current profiles, except for 2/3-current, when comparing the base to the staggered configuration. Lowest calculated fatigue life was found for the base configuration in measured current profile, where a fatigue life of 0.86 years or 313 days was found. In measure current, a fatigue life of 1.87 years or 682 days was found as the poorest fatigue result of the staggered configuration. Applying the top 50_150 strakes configuration to the riser increased the fatigue life of a bit more than a decade compared to the base configuration, which is lower than reported in previous experiments and case studies (Larsen, et al., 2005). This will be further discussed later.

In general maximum fatigue damage was found to occur at the interface between the WH and BOP for both the base and staggered configurations. For the Ormen Lange 2 current profile however, maximum fatigue damage was found 548 m below the surface, or 100 m above the mid-point of the riser. For the top 50_150 strakes configuration maximum fatigue damage was located close to the point on the riser where the straked section starts, i.e. in the neighbourhood of z = -150 m.

As anticipated, significantly larger static riser deflections were found for the 1300 m system compared to the 321 m system. The added drag associated with addition of strakes gave largest riser deflection for the top 50_150 strakes configuration before VIV was accounted for. With the added drag from VIV however, largest riser deflections were found for the base configuration. Both before and after added drag from VIV, the staggered configuration had the lowest riser deflections.

A central observation from the case studies is the effectiveness of the strakes to reduce the amplified riser defection from VIV. Averaging over the four current profiles used in the analyses, the percentage increase in static riser deflection from VIV was reduced by roughly 80% when comparing the top strakes 50_150 to the base configuration.

The significant decrease in static riser deflection from VIV for the top 50_150 strakes configuration means that drilling operations may be performed for the measured and Ormen Lange current profile, as the LFJ angle only reaches angles of 4.61 and 4.57 degrees respectively for the two current profiles. At a maximum allowable LFJ angle during drilling of 5 degrees (ISO, 2009), drilling operations for the base configuration will not be possible in the same current profiles, as LFJ angles of 5.40 and 5.49 respectively are seen for the measure and Ormen Lange 2 current models.

For normal workover operations the maximum flex joint angle should not exceed 3 degrees (ISO, 2006). For the base configuration this means that workover operation may only be executed for the sheared current profile. Applying the top 50_150 strakes configuration will however also make normal workover operations possible in the 2/3-current profile, as a LFJ angle 2.96 degrees is found for this current.

13.3 Final remarks and recommendations

For the 321 m water depth where none of the calculated LFJ angles will have operational consequences for the system, appliance of the top strakes configuration will drastically reduce the VIV induced bending stresses and consequently more or less eliminate any danger of fatigue induced damage.

For the 1300 m water depth where higher static riser deflections were found, the situation is somewhat more complex. The top 50_150 strakes configuration will see LFJ angles that are higher than those of the staggered configuration, even after VIV amplification has been added. Still, as a general note the fatigue life of the top 50_150 strakes configuration is significantly higher than the staggered configuration, and is thus recommended. The analysis did however reveal large differences in fatigue results between the different current profiles, which indicate that separate VIV analyses for specific current profiles should be performed.

14 Further work

As mentioned earlier, a total of 40 analysis runs have been performed in the presented report, and a large amount of data has been collected. Focus has been given to the base, staggered and best performing strakes configurations for both systems, while a total overview of the results is given in Appendix A.

14.1 Model

As was discussed in the chapter 12, section 12.2.1, certain discrepancies were found for some of the current/configuration combinations. Indications pointed to a too loose convergence limit in the model; which was validated by a new analysis where a stricter convergence limit was used. Note however that analysis runs for verification were only performed for one of the current/configuration combinations. For confirmation of the presented results, verification analyses with a stricter convergence limit should be run for each of the current-configuration combinations.

14.2 Post-processing

The presented results for duration, excitation zone length and VIV amplitude are only applicable for the dominating response frequency. For the 321 m water depth analyses where a maximum of 4 response frequency were active, these results give a good picture of the VIV response. However, for the 1300 m water depth where more than 30 active frequencies were observed, further emphasis should be given to the remaining response frequencies in addition to the dominating frequency. From the present analyses the top 5 dominating frequencies are active between 45% and 65% of the time, and the remaining 55% to 35% are divided between the remaining 25 or more response frequencies. A broader picture of the VIV response is thus found if more of the response frequencies are discussed and evaluated. This will however increase the amount of time and energy for post-processing, as the collected amount of data will increase significantly. Finding the best method for presenting results from VIV analyses is an on-going process, and new ways have been proposed recently at the Department of Marine Technology (Larsen, et al., 2012).

14.3 Coverage density

In the presented analyses coverage densities of between 45 and 50% have been used for various different strakes locations on the riser. As discussed earlier, previous experiments and case studies have analysed straked risers with a coverage density of between 40 to 75%. A larger straked riser length and thus larger coverage density will give more damping and thus lower VIV response. While added drag may have operational consequences, further analyses of higher coverage densities should be performed to investigate VIV response and riser deflection after added drag from VIV has been accounted for. In particular for the measured and Ormen Lange 2 current profiles of the 1300 m water depth, lower fatigue life improvements were found for the presented analyses than from previous case studies (Larsen, et al., 2005).

Bibliography

Allen, D. W., Lee, L. & Henning, D. L., 2008. *Fairings versus Helical Strakes for Suppression of Vortex-Induced Vibration: Technical Comparison.* Houston, Offshore Technology Conference.

Amdahl, J. et al., 2005. *TMR 4100-Marin Teknikk Intro, TMR4105 Marin Teknikk 1.* Trondheim: Marin Teknisk Senter, NTNU.

api.org, 2011. *API Overview and Mission.* [Internett]
Available at:
http://www.api.org/globalitems/globalheaderpages/~/link.aspx?_id=A24EF54CAFFB4AD3A57630BE53971B24&_z=z
[Funnet 23 May 2012].

API, 1998. *Design of Risers for Floating Production Systems and Tension-Leg Platforms, RP 2RD,* s.l.: American Petrolium Institute.

Blevins, R. D., 1994. *Flow-Induced Vibration.* s.l.:Krieger Publishing Company.

DNV, 2010. *DNV-RP-C205 Environmental Conditions and Environmental Loads,* Høvik: Det Norske Veritas.

DNV, 2010. *DNV-RP-F204 Riser Fatigue,* s.l.: Det Norske Veritas.

Faltinsen, O., 1990. *Sea Loads on Ships and Offshore Structures.* New York: Cambridge University Press.

Faltinsen, O. M., 2007. *Hydrodynamics of High Speed Craft.* New York: Cambridge University Press.

ISO, 2006. *ISO 13628-7 Completion/workover riser system,* s.l.: International Organization for Standardization, British Standard Institution.

ISO, 2009. *EN ISO 13624-1 Design and operation of marine drilling riser equipment,* s.l.: International Organization for Standardization, British Standards Institution.

Knardahl, G. M., 2011. *Vortex Induced Vibrations of Workover Risers - Project Thesis,* Trondheim: s.n.

Kumar, R. A., Sohn, C.-H. & Gowda, B. H., 2007. *Passive Control of Vortex-Induced Vibrations: An Overview,* Daegu: School of Mechanical Engineering, Kyungpook National University.

Lamb, W. S., 1991. *Suppression of the Vortex Induced Vibration of Slender Cylidrical Structures,* s.l.: Cranfield Institute of Technology, Department of Fluid Engineering and Instrumentation.

Larsen, C. M., 2009. *TMR 4180 Marin Dynamikk.* 5th red. Trondheim: Department of Marine Technology.

Larsen, C. M., 2011. *Vortex Induced Vibrations-A short and incomplete introduction to fundamental concepts,* Trondheim: Department of Marine Technology, NTNU.

Larsen, C. M., 2012. *Meeting with supervisor* [Intervju] (23 March 2012).

Larsen, C. M. & Bech, A., 1986. *Stress Analysis of Marine Risers under Lock-In Condition,* s.l.: International Offshore Mechanics and Arctic Engineering Symposium.

Larsen, C. M., Lie, H. & Baarholm, G. S., 2005. *Incluence from Helical Stakes on Vortex Induced Vibrations and Static Deflection of Drilling Risers,* Halkidiki: Conference on Offshore Mechanics and Arctic Engineering.

Larsen, C. M. et al., 2009. *Vivana-Theory Manual Version 3.7,* Trondheim: Norwegian Marine Technology Research Institute, Marintek.

Larsen, C. M., Lie, H. & Zhao, Z., 2012. *Frequency Components of Vortex Induced Vibrations in Sheared Current,* Rio de Janeiro: International Conference on Ocean, Offshore and Arctic Engineering.

Lie, H. & Larsen, C. M., u.d. *Vortex Induced Vibrations of Deepwater Risers and Pipelines-Review of Model Test Results,* Trondheim: Norwegian marine Technology Research Institute, The Norwegian University of Science and Technology.

Myrhaug, D., 2005. *Oceanography TMR 4230, Current.* Trondheim: Marine Technology Centre.

Rustad, A. M., 2007. *Modeling and Control of Top Tensioned Risers,* Trondheim: Department of Marine Technology, Norwegian University of Science and Technology.

Schlichting, H. & Gertsen, K., 2000. *Boundary Layer Theory.* Darmstadt, Germany: Springer.

Stangeland, G., 2011. *Blant tidenes største på norsk sokkel.* [Internett]
Available at: http://www.offshore.no/sak/Blant_tidenes_st%C3%B8rste_p%C3%A5_norsk_sokkel
[Funnet 2 May 2010].

Statistisk Sentralbyrå, 2011. *Produksjon og reserver, 1.kvartal 2011.* [Internett]
Available at: http://www.ssb.no/ogprodre/arkiv/art-2011-07-06-01.html
[Funnet 2 May 2012].

Vandiver, J. K. & Li, L., 2005. *Shear7 V4.4 Program Theoretical Manual,* s.l.: Department of Ocean Engineering, Massachusetts Institute of Technology.

Vandiver, J. K., Swithenbank, S. & Jaiswal, V., 2006. *The Effectiveness of Helical Strakes in the Suppression of High Mode Number VIV,* Houston: Offshore Technology Conference.

Vikestad, K., 1998. *Multi-frequency response of a cylinder subjected to vortex shedding and support motions,* Trondheim: Department of Marine Structures, Faculty of Marine Technology, NTNU.

VIV Solutions, 2010. *VIV Solutions "The VIV Suppression Experts".* [Internett]
Available at: http://www.vivsolutions.com/index.asp
[Funnet 20 March 2012].

White, F. M., 2003. *Fluid Mechanics,* New York: McGraw-Hill.

Yttervik, R. et al., 2009. *VIVANA- User's Manual Version 3.7-Draft,* Trondheim: Norwegian Marine Technology Research Institute.

Yttervik, R. et al., 2011. *RIFLEX User's Manual,* Trondheim: Marintek.

Appendix A

A.1 321 m water depth VIV results

A.1.1 Base case

The base configuration applies no strakes and is illustrated in Figure 9.1. Key results for the dominating response frequencies are given in Table A-1 below.

Current profile	Dominating frequency no.	Frequency [Hz]	Duration [%]	Length of excitation zone [m]	VIV amplitude [m]
2/3-current	1	0.0583	83.67	182.332	0.656
Linearly sheared	1	0.0597	54.43	95.384	0.215
Measured current	1	0.0514	81.19	174.525	1.0199
Uniform	1	0.0673	86.71	177.525	1.0290

Table A-1 Dominating response frequency results, base configuration

As can be seen from Table A-2, frequency number 1 induces the highest stress for all current distributions.

Current profile	Frequency no.	Frequency [Hz]	Max stress amplitude [MPa]
2/3-current	1	0.0583	11.213
Linearly sheared	1	0.0597	3.536
Measured current	1	0.0514	16.829
Uniform	1	0.0673	17.264

Table A-2 Stress amplitudes, base configuration

Calculated fatigue damage for the base case configuration is given in Table A-3.

current profile	fatigue damage	fatigue life years	location
2/3-current	5,43E-02	18,40	WH/XMT interface
Linearly sheared	2,34E-03	427,83	WH/XMT interface
Measured current	1,57E-01	6,36	WH/XMT interface
Uniform	2,15E-01	4,65	WH/XMT interface

Table A-3 Fatigue damage, base configuration

A.1.2 Staggered configuration

Dominating frequency results for the different current profiles are given in Table A-4 below.

Current profile	Dominating frequency no.	Frequency [Hz]	Duration [%]	Length of excitation zone [m]	VIV amplitude [m]
2/3-current	1	0.0707	60.59	124.794	0.6089
Linearly Sheared	2	0.1574	54.43	92.202	0.1328
Measured current	1	0.0727	51.98	94.565	0.4868
Uniform	1	0.0666	68.12	108.965	0.9834

Table A-4 Dominating response frequency results, staggered configuration

Stress amplitudes for the staggered configuration given in Table A-6.

Current profile	Frequency no.	Frequency [Hz]	Max stress amplitude [MPa]
2/3-current	1	0.0707	10.499
Linearly sheared	2	0.1574	4.382
Measured current	2	0.155	8.528
Uniform	1	0.0666	14.24

Table A-5 Stress amplitudes, staggered configuration

Fatigue damage is given in Table A-6.

current profile	fatigue damage	fatigue life years	location
2/3-current	5,62E-02	17,79	WH/XMT interface
Linearly sheared	6,69E-03	149,47	WH/XMT interface
Measured current	4,85E-02	20,64	WH/XMT interface
Uniform	2,07E-01	4,83	WH/XMT interface

Table A-6 Fatigue damage, staggered configuration

A.1.3 Bottom strakes configuration

See Table A-7 below for the dominating response frequency results.

Current profile	Dominating frequency no.	Frequency [Hz]	Duration [%]	Length of excitation zone [m]	VIV amplitude [m]
2/3-current	1	0.0572	81.77	193.896	0.3359
Linearly Sheared	1	0.0530	58.50	134.076	0.3495
Measured current	1	0.0513	74.18	245.805	0.2560
Uniform	1	0.0576	86.17	245.680	0.1962

Table A-7 Dominating response frequency results, bottom strakes configuration

The different current profiles gave the following stress amplitudes for the bottom strakes configuration, see Table A-8.

Current profile	Frequency no.	Frequency [Hz]	Max stress amplitude [MPa]
2/3-current	1	0.0572	6.024
Linearly sheared	1	0.0530	5.943
Measured current	1	0.0513	4.227
Uniform	1	0.0576	3.548

Table A-8 Stress amplitudes, bottom strakes configuration

Fatigue damage and fatigue life for the bottom strakes configuration is given in Table A-9 below.

current profile	fatigue damage	fatigue life years	location
2/3-current	8,48E-03	117,915	WH/XMT interface
Linearly sheared	5,64E-03	177,28	WH/XMT interface
Measured current	2,40E-03	417,41	WH/XMT interface
Uniform	1,80E-03	556,61	WH/XMT interface

Table A-9 Fatigue damage, bottom strakes configuration

A.1.4 Middle strakes configuration

Dominating response frequency for the different current profiles is given in Table A-10.

Current profile	Dominating frequency no.	Frequency [Hz]	Duration [%]	Length of excitation zone [m]	VIV amplitude [m]
2/3-current	2	0.1213	45.09	69.344	0.0227
Linearly Sheared	2	0.1205	62.06	69.344	0.0574
Measured current	2	0.1199	52.96	140.624	0.0725
Uniform	2	0.1224	27.31	143.749	0.0351

Table A-10 Dominating response frequency results, middle strakes configuration

Stress amplitudes for the frequencies that induce maximum stresses on the riser stack-up are given in Table A-11 below. As can be seen, the dominating frequency, i.e. the frequency with longest duration, is not the same as the frequency which induces the highest stresses on system.

Current profile	Frequency no.	Frequency [Hz]	Max stress amplitude [MPa]
2/3-current	3	0.1970	5.975
Linearly sheared	3	0.1979	3.819
Measured current	3	0.1972	3.772
Uniform	3	0.1954	9.703

Table A-11 Stress amplitudes, middle strakes configuration

Calculated fatigue life for the middle strakes section is given in Table A-12.

current profile	fatigue damage	fatigue life years	location
2/3-current	1,45E-02	69,08	z=-146 m, middle of straked section
Linearly sheared	3,27E-03	305,60	z=-146 m, middle of straked section
Measured current	2,92E-03	342,99	z=-146.5 m, middle of straked section
Uniform	5,95E-02	16,82	z=-146 m, middle of straked section

Table A-12 Fatigue damage, middle strakes configuration

A.1.5 Top strakes configuration

For the top strakes configuration the following response frequencies were found to be dominating, see Table A-13. Note that for the linearly sheared current profile the induced amplitudes are less than 6 mm, which in practice means that no VIV occur.

Current profile	Dominating frequency no.	Frequency [Hz]	Duration [%]	Length of excitation zone [m]	VIV amplitude [m]
2/3-current	1	0.0528	92.61	195.896	0.0814
Linearly Sheared	2	0.1309	50.45	69.344	less than 0.533E-2
Measured current	1	0.0512	87.54	206.529	0.2042
Uniform	1	0.0580	85.94	240.620	0.1757

Table A-13 Dominating response frequencies results, top strakes configuration

Response frequencies inducing maximum stresses on the riser, and corresponding maximum stress amplitudes are given in Table A-14 below. As can be seen no maximum stress amplitude is calculated for the linearly sheared current profile. VIVANA sets a lower limit for calculated response amplitude equal to $0.533 * 10^{-2}$. The response amplitude for the sheared current profile was lower than the limit, thus no stress amplitude is calculated.

Current profile	Frequency no.	Frequency [Hz]	Max stress amplitude [MPa]
2/3-current	1	0.0528	1.332
Linearly sheared	2	0.1309	N/A
Measured current	1	0.0512	3.420
Uniform	1	0.0580	2.771

Table A-14 Stress amplitudes, top strakes configuration

Calculated fatigue damage given in Table A-15.

current profile	fatigue damage	fatigue life years	location
2/3-current	9,81E-05	10194,51	WH/XMT interface
Linearly sheared	N/A	N/A	N/A
Measured current	1,44E-03	696,62	WH/XMT interface
Uniform	8,43E-04	1185,83	WH/XMT interface

Table A-15 Fatigue damage, top strakes configuration

A.2 Static drag and drag amplification, 321 m water depth

As discussed in chapter 7, drag forces on the riser will give a static deflection in the downstream direction. A riser in VIV conditions will experience a larger static deflection due to the increased drag forces from the oscillating amplitudes. In the following static riser deflections for the various configurations and current profiles are given. Both initial and VIV amplified deflection results are presented.

A.2.1 Base configuration

Analyses of the base configuration of 321 m water depth system revealed the following results see Table A-16.

Current profile	Maximum static riser deflection [m]	Maximum amplified static riser deflection [m]	Percentage increase [%]
2/3-current	0,505	0,905	79,21
Linearly sheared	0,278	0,402	44,60
Measured current	0,451	0,928	105,76
Uniform	0,747	1,545	106,83

Table A-16 Static deflections, base configuration

A.2.2 Staggered configuration

Deflection results for the staggered configuration are given in Table A-17 below.

Current profile	Maximum static riser deflection [m]	Maximum amplified static riser deflection [m]	Percentage increase [%]
2/3-current	0,480	0,976	103,33
Linearly sheared	0,264	0,397	50,38
Measured current	0,433	0,821	89,61
Uniform	0,719	1,700	136,44

Table A-17 Static deflections, staggered configuration

A.2.3 Bottom strakes configuration

For the bottom strakes configuration static riser deflection were found to be, see Table A-18.

Current profile	Maximum static riser deflection [m]	Maximum amplified static riser deflection [m]	Percentage increase [%]
2/3-current	0,551	0,833	51,18
Linearly sheared	0,299	0,465	55,52
Measured current	0,523	0,752	43,79
Uniform	0,889	1,217	36,90

Table A-18 Static deflections, bottom strakes configuration

A.2.4 Middle strakes configuration

Applying strakes at the middle section of the riser gave the following static deflections, see Table A-19.

Current profile	Maximum static riser deflection [m]	Maximum amplified static riser deflection [m]	Percentage increase [%]
2/3-current	0,640	0,771	20,47
Linearly sheared	0,341	0,427	25,22
Measured current	0,567	0,707	24,69
Uniform	0,951	1,211	27,34

Table A-19 Static deflections, middle strakes configuration

A.2.5 Top strakes configuration

See Table A-20 below for deflection results.

Current profile	Maximum static riser deflection [m]	Maximum amplified static riser deflection [m]	Percentage increase [%]
2/3-current	0,655	0,792	20,92
Linearly sheared	0,365	N/A	N/A
Measured current	0,556	0,764	37,41
Uniform	0,902	1,211	34,26

Table A-20 Static deflections, top strakes configuration

A.3 Lower flex joint angles, 321 m water depth

Presented below are the calculated flex joint angles for the Lower Flex Joint (LFJ).

A.3.1 Base configuration

Flex joint angles for varying current profile are given in Table A-21.

Initial analysis				
Current profile	**LFJ element length [m]**	**End 1 deflection**	**End 2 deflection**	**LFJ angle [degrees]**
2/3-current	1,525	7,6061E-03	1,1407E-02	**0,14**
Linearly sheared	1,525	3,9536E-03	5,9298E-03	**0,07**
Measured current	1,525	1,0656E-02	1,5725E-02	**0,19**
Uniform current	1,525	1,9514E-02	2,8709E-02	**0,35**

Table A-21 Lower flex joint angles, base configuration

Lower flex joint angles after amplified static riser deflection are presented in Table A-22.

VIV amplified analysis				
Current profile	**LFJ element length [m]**	**End 1 deflection**	**End 2 deflection**	**LFJ angle [degrees]**
2/3-current	1,525	1,3586E-02	2,0378E-02	**0,26**
Linearly sheared	1,525	5,6539E-03	8,4805E-03	**0,11**
Measured current	1,525	2,1042E-02	3,1244E-02	**0,38**
Uniform current	1,525	3,8541E-02	5,7116E-02	**0,70**

Table A-22 Lower flex joint angles after VIV amplification, base configuration

A.3.2 Staggered configuration

Lower flex joints angles for the staggered configuration are given in Table A-23 below.

Initial analysis				
Current profile	**LFJ element length [m]**	**End 1 deflection**	**End 2 deflection**	**LFJ angle [degrees]**
2/3-current	1,525	7,2752E-03	1,1009E-02	**0,14**
Linearly sheared	1,525	3,7783E-03	5,7175E-03	**0,07**
Measured current	1,525	1,0330E-02	1,5365E-02	**0,19**
Uniform current	1,525	1,8959E-02	2,8111E-02	**0,34**

Table A-23 Lower flex joint angles, staggered configuration

Lower flex joint angles after amplified static riser deflection are presented in Table A-24.

VIV amplified analysis				
Current profile	**LFJ element length [m]**	**End 1 deflection**	**End 2 deflection**	**LFJ angle [degrees]**
2/3-current	1,525	1,4718E-02	2,2273E-02	**0,28**
Linearly sheared	1,525	5,6790E-03	8,5946E-03	**0,11**
Measured current	1,525	1,8716E-02	2,8005E-02	**0,35**
Uniform current	1,525	4,1442E-02	6,1978E-02	**0,77**

Table A-24 Lower flex joint angles after VIV amplification, staggered configuration

A.3.3 Bottom strakes configuration

Lower flex joints angles for the bottom strakes configuration are given in Table A-25.

Initial analysis				
Current profile	**LFJ element length [m]**	**End 1 deflection**	**End 2 deflection**	**LFJ angle [degrees]**
2/3-current	1,525	8,6152E-03	1,2981E-02	**0,16**
Linearly sheared	1,525	4,4041E-03	6,6364E-03	**0,08**
Measured current	1,525	1,3085E-02	1,9418E-02	**0,24**
Uniform current	1,525	2,4318E-02	3,5994E-02	**0,44**

Table A-25 Lower flex joint angles, bottom strakes configuration

Lower flex joint angles after amplified static riser deflection are presented in Table A-26 below.

VIV amplified analysis				
Current profile	**LFJ element length [m]**	**End 1 deflection**	**End 2 deflection**	**LFJ angle [degrees]**
2/3-current	1,525	1,3045E-02	1,9657E-02	**0,25**
Linearly sheared	1,525	6,8177E-03	1,0274E-02	**0,13**
Measured current	1,525	1,8424E-02	2,7429E-02	**0,34**
Uniform current	1,525	3,2768E-02	4,8663E-02	**0,60**

Table A-26 Lower flex joint angles after VIV amplification, bottom strakes configuration

A.3.4 Middle strakes configuration

Lower flex joints angles for the middle strakes configuration given in Table A-27 below.

Initial analysis				
Current profile	**LFJ element length [m]**	**End 1 deflection**	**End 2 deflection**	**LFJ angle [degrees]**
2/3-current	1,525	9,5893E-03	1,4416E-02	**0,18**
Linearly sheared	1,525	4,8748E-03	7,3291E-03	**0,09**
Measured current	1,525	1,2628E-02	1,8724E-02	**0,23**
Uniform current	1,525	2,3037E-02	3,4069E-02	**0,41**

Table A-27 Lower flex joint angles, middle strakes configuration

Lower flex joint angles after amplified static riser deflection are presented in Table A-28 below.

VIV amplified analysis				
Current profile	**LFJ element length [m]**	**End 1 deflection**	**End 2 deflection**	**LFJ angle [degrees]**
2/3-current	1,525	1,1501E-02	1,7291E-02	**0,22**
Linearly sheared	1,525	6,0357E-03	9,0747E-03	**0,11**
Measured current	1,525	1,5818E-02	2,3499E-02	**0,29**
Uniform current	1,525	2,9628E-02	4,3919E-02	**0,54**

Table A-28 Lower flex joint angles after VIV amplification, middle strakes configuration

A.3.5 Top strakes configuration

Table A-29 gives the lower flex joint angles for the top strakes configuration.

Initial analysis				
Current profile	**LFJ element length [m]**	**End 1 deflection**	**End 2 deflection**	**LFJ angle [degrees]**
2/3-current	1,525	9,3006E-03	1,3982E-02	**0,18**
Linearly sheared	1,525	4,9010E-03	7,3685E-03	**0,09**
Measured current	1,525	1,1893E-02	1,7619E-02	**0,22**
Uniform current	1,525	2,1399E-02	3,1606E-02	**0,38**

Table A-29 Lower flex joint angles, top strakes configuration

Lower flex joints angles after VIV amplification is given below.

VIV amplified analysis				
Current profile	**LFJ element length [m]**	**End 1 deflection**	**End 2 deflection**	**LFJ angle [degrees]**
2/3-current	1,525	1,1218E-02	1,6865E-02	**0,21**
Linearly sheared	1,525	N/A	N/A	**N/A**
Measured current	1,525	1,6039E-02	2,3831E-02	**0,29**
Uniform current	1,525	2,8022E-02	4,1521E-02	**0,51**

Table A-30 Lower flex joint angles after VIV amplification, top strakes configuration

A.4 1300 m water depth VIV results

A.4.1 Base configuration

Dominating frequencies for the base configuration is given in Table A-31 below.

Current profile	Dominating frequency no.	Frequency [Hz]	Duration [%]	Length of excitation zone [m]	VIV amplitude [m]
2/3-current	9	0.1251	13.62	784.325	0.813447
Linearly Sheared	7	0.1038	14.18	352.0721	0.76736
Measured current	9	0.1287	9.680	950.502	0.447441
OL_2	10	0,1405	11.700	691.042	0.661432

Table A-31 Dominating response frequency results, base configuration 1300 m system

Maximum stress amplitude and corresponding frequency inducing the maximum stress is given in the table below.

Current profile	Frequency no.	Frequency [Hz]	Max stress amplitude [MPa]
2/3-current	7	0.1176	28.9914
Linearly sheared	8	0.1130	27.3267
Measured current	12	0.1698	37.3371
OL_2	12	0.1666	38.9866

Table A-32 Stress amplitudes, base configuration 1300 m system

Calculated fatigue damage and location is given below.

current profile	fatigue damage	fatigue life years	location
2/3-current	4,83E-01	2,07	WH/BOP interface
linearly sheared	4,85E-01	2,06	WH/BOP interface
measured current	1,17E+00	0,86	WH/BOP interface
OL_2	9,02E-01	1,11	z = -548 m

Table A-33 Fatigue damage, base configuration 1300 m system

A.4.2 Staggered configuration

Dominating frequencies for the staggered configuration given below.

Current profile	Dominating frequency no.	Frequency [Hz]	Duration [%]	Length of excitation zone [m]	VIV amplitude [m]
2/3-current	6	0.1248	16.37	539.498	0.894704
Linearly Sheared	5	0.1059	15.80	514.352	0.598257
Measured current	6	0.1267	10.700	660.870	0.906024
OL_2	7	0.1445	13.42	654.012	0.624586

Table A-34 Dominating response frequency results, staggered configuration 1300 m system

Maximum calculated stress amplitude given in Table A-35.

Current profile	Frequency no.	Frequency [Hz]	Max stress amplitude [MPa]
2/3-current	5	0.1158	25.689
Linearly sheared	5	0.1059	14.4204
Measured current	6	0.1267	24.9908
OL_2	8	0.1634	22.1361

Table A-35 Stress amplitudes, staggered configuration 1300 m system

Calculated fatigue damage and fatigue life given below.

current profile	fatigue damage	fatigue life years	location
2/3-current	7,19E-01	1,39	WH/BOP interface
linearly sheared	1,29E-01	7,73	WH/BOP interface
measured current	5,33E-01	1,87	WH/BOP interface
OL_2	4,52E-01	2,21	WH/BOP interface

Table A-36 Fatigue damage, staggered configuration 1300 m system

A.4.3 Middle strakes configuration

The following results were found for the dominating frequencies of the middle strakes configuration, see below.

Current profile	Dominating frequency no.	Frequency [Hz]	Duration [%]	Length of excitation zone [m]	VIV amplitude [m]
2/3-current	9	0.1228	13.69	820.968	0.975628
Linearly Sheared	9	0.1172	14.110	627.878	0.312376
Measured current	12	0.1610	9.740	892.145	0.459737
OL_2	11	0.1438	12.090	705.056	0.773382

Table A-37 Dominating response frequency results, middle strakes config. 1300 m system

Analyses of the middle strakes configuration gave the following maximum stress amplitudes.

Current profile	Frequency no.	Frequency [Hz]	Max stress amplitude [MPa]
2/3-current	10	0.1300	21.6842
Linearly sheared	5	0.0768	14.423
Measured current	12	0.1610	20.3256
OL_2	11	0.1438	31.7006

Table A-38 Stress amplitudes, middle strakes configuration 1300 m system

Table A-39 presents the calculated fatigue damage.

current profile	fatigue damage	fatigue life years	location
2/3-current	3,54E-01	2,83	z = -337.5 m
linearly sheared	1,12E-01	8,89	z = -285.0 m
measured current	2,88E-01	3,47	z = -289.0 m
OL_2	9,14E-01	1,09	z = -297.0 m

Table A-39 Fatigue damage, middle strakes configuration 1300 m system

A.4.4 Top 50_150 strakes configuration

The dominating frequencies for the different current profiles are given in Table A-40.

Current profile	Dominating frequency no.	Frequency [Hz]	Duration [%]	Length of excitation zone [m]	VIV amplitude [m]
2/3-current	9	0.1214	13.67	799.222	0.375753
Linearly Sheared	9	0.1195	15.53	616.266	0.216092
Measured current	12	0.1625	9.480	357.4664	0.15189
OL_2	11	0.1470	11.450	696.200	0.15106

Table A-40 Dominating response frequency results, top 50_150 strakes config. 1300 m system

Calculated maximum stresses are given in Table A-41.

Current profile	Frequency no.	Frequency [Hz]	Max stress amplitude [MPa]
2/3-current	9	0.1214	7.40940
Linearly sheared	8	0.1108	6.05852
Measured current	13	0.1747	14.8849
OL_2	10	0.1394	13.6356

Table A-41 Stress amplitudes, top 50_150 strakes configuration 1300 m system

Resulting fatigue damage is given in Table A-42.

current profile	fatigue damage	fatigue life years	location
2/3-current	1,02E-02	98,45	z = -166.5 m
linearly sheared	5,43E-03	184,13	z = -164 m and z = -132 m
measured current	1,04E-01	9,57	z = -127 m
OL_2	5,72E-02	17,49	z = -165 m

Table A-42 Fatigue damage, top 50_150 strakes configuration 1300 m system

A.4.5 Top strakes configuration

The dominating frequencies for the top strakes configuration are given in Table A-43.

Current profile	Dominating frequency no.	Frequency [Hz]	Duration [%]	Length of excitation zone [m]	VIV amplitude [m]
2/3-current	6	0.0791	18.780	960.347	0.43461
Linearly Sheared	4	0.0517	25.550	965.375	0.36445
Measured current	8	0.1009	15.830	1237.463	0.51029
OL_2	5	0.0665	19.680	1249.338	1.12586

Table A-43 Dominating response frequency results, top strakes configuration 1300 m system

Maximum stresses are given in Table A-44.

Current profile	Frequency no.	Frequency [Hz]	Max stress amplitude [MPa]
2/3-current	6	0.0791	9.28212
Linearly sheared	4	0.0517	5.1869
Measured current	7	0.0917	26.3865
OL_2	6	0.0728	18.068

Table A-44 Stress amplitudes, top strakes configuration 1300 m system

Calculated fatigue life and damage is given Table A-45.

current profile	fatigue damage	fatigue life years	location
2/3-current	1,54E-02	64,91	WH/BOP interface
linearly sheared	1,77E-03	565,32	WH/BOP interface
measured current	2,56E-01	3,91	WH/BOP interface
OL_2	1,25E-01	8,02	WH/BOP interface

Table A-45 Fatigue damage, top strakes configuration 1300 m system

A.5 Static drag and drag amplification 1300 m water depth

A.5.1 Base configuration

Table A-46 below gives the maximum riser deflections from drag forces for both initial and VIV amplified analyses.

Current profile	Maximum initial static riser deflection [m]	Maximum amplified static riser deflection [m]	Percentage increase [%]
2/3-current	27,8838	58,2343	108,85
Linearly sheared	14,7735	27,2405	84,39
Measured current	28,1091	66,6406	137,08
OL_2	29,9215	68,8369	130,06

Table A-46 Static deflections, base configuration 1300 m system

A.5.2 Staggered configuration

Maximum riser deflections for the staggered configuration are given below.

Current profile	Maximum initial static riser deflection [m]	Maximum amplified static riser deflection [m]	Percentage increase [%]
2/3-current	18,8067	44,9866	139,21
Linearly sheared	9,81128	16,1116	64,22
Measured current	19,5559	49,2621	151,90
OL_2	20,1366	46,3198	130,03

Table A-47 Static deflections, base configuration 1300 m system

A.5.3 Middle strakes configuration

Static deflection of the riser in middle strakes configuration is given in the table below.

Current profile	Maximum initial static riser deflection [m]	Maximum amplified static riser deflection [m]	Percentage increase [%]
2/3-current	34,8038	61,3773	76,35
Linearly sheared	17,9618	24,3815	35,74
Measured current	35,1399	56,2598	60,10
OL_2	36,6382	66,3338	81,05

Table A-48 Static deflection, middle strakes configuration 1300 m system

A.5.4 Top 50_150 strakes configuration

Static deflection of the riser for the top 50_150 strakes configuration is given in Table A-49.

Current profile	Maximum initial static riser deflection [m]	Maximum amplified static riser deflection [m]	Percentage increase [%]
2/3-current	36,357	47,4127	30,41
Linearly sheared	19,0397	20,0844	5,49
Measured current	35,3768	53,352	50,81
OL_2	38,3005	57,8753	51,11

Table A-49 Static deflection, top 50_150 strakes configuration 1300 m system

A.5.5 Top strakes configuration

Static deflection is given in Table A-50 below.

Current profile	Maximum initial static riser deflection [m]	Maximum amplified static riser deflection [m]	Percentage increase [%]
2/3-current	35,8967	55,3624	54,23
Linearly sheared	19,1587	19,8859	3,80
Measured current	34,4379	62,9544	82,81
OL_2	38,2469	75,1811	96,57

Table A-50 Static deflection, top strakes configuration 1300 m system

A.6 Lower flex joint angles, 1300 m water depth

A.6.1 Base configuration

The table below gives the LFJ angles from the initial analyses, i.e. no effects from VIV have been considered.

Initial analysis				
Current profile	**LFJ element length [m]**	**End 1 deflection**	**End 2 deflection**	**LFJ angle [degrees]**
2/3-current	1,525	6,3993E-02	1,1116E-01	**1,77**
Linearly sheared	1,525	3,2464E-02	5,6453E-02	**0,90**
Measured current	1,525	8,8977E-02	1,5390E-01	**2,44**
OL_2	1,525	8,7245E-02	1,5105E-01	**2,39**

Table A-51 Lower flex joint angles, base configuration 1300 m system

In Table A-52 VIV amplification has been accounted for when the LFJ angles were calculated.

VIV amplified analysis				
Current profile	**LFJ element length [m]**	**End 1 deflection**	**End 2 deflection**	**LFJ angle [degrees]**
2/3-current	1,525	1,3769E-01	2,3679E-01	**3,71**
Linearly sheared	1,525	5,7635E-02	9,9621E-02	**1,58**
Measured current	1,525	2,0324E-01	3,4788E-01	**5,40**
OL_2	1,525	2,0805E-01	3,5527E-01	**5,49**

Table A-52 Lower flex joint angles after VIV amplification, base config. 1300 m system

A.6.2 Staggered configuration

Initial analyses of the staggered configuration revealed the following flex joint angles, see below.

Initial analysis				
Current profile	**LFJ element length [m]**	**End 1 deflection**	**End 2 deflection**	**LFJ angle [degrees]**
2/3-current	1,525	5,4638E-02	9,2357E-02	**1,42**
Linearly sheared	1,525	2,7496E-02	4,6506E-02	**0,71**
Measured current	1,525	7,8687E-02	1,3244E-01	**2,02**
OL_2	1,525	7,6653E-02	1,2898E-01	**1,96**

Table A-53 Lower flex joint angles, staggered configuration 1300 m system

VIV amplified analysis				
Current profile	**LFJ element length [m]**	**End 1 deflection**	**End 2 deflection**	**LFJ angle [degrees]**
2/3-current	1,525	1,4485E-01	2,1952E-01	**2,80**
Linearly sheared	1,525	4,7201E-02	7,1788E-02	**0,92**
Measured current	1,525	2,2070E-01	3,3347E-01	**4,22**
OL_2	1,525	1,9580E-01	2,9595E-01	**3,75**

Table A-54 Lower flex joint angles after VIV amplification, staggered config. 1300 m system

A.6.3 Middle strakes configuration

LFJ angles for the middle strakes configuration given below.

Initial analysis				
Current profile	**LFJ element length [m]**	**End 1 deflection**	**End 2 deflection**	**LFJ angle [degrees]**
2/3-current	1,525	8,0448E-02	1,3960E-01	**2,22**
Linearly sheared	1,525	4,0027E-02	6,9566E-02	**1,11**
Measured current	1,525	1,0755E-01	1,8631E-01	**2,95**
OL_2	1,525	1,0359E-01	1,7927E-01	**2,84**

Table A-55 Lower flex joint angles, middle strakes configuration 1300 m system

Accounting for added drag from VIV gave the following LFJ angles, see below.

VIV amplified analysis				
Current profile	**LFJ element length [m]**	**End 1 deflection**	**End 2 deflection**	**LFJ angle [degrees]**
2/3-current	1,525	1,3857E-01	2,3791E-01	**3,72**
Linearly sheared	1,525	5,1558E-02	8,9136E-02	**1,41**
Measured current	1,525	1,7309E-01	2,9684E-01	**4,63**
OL_2	1,525	1,8453E-01	3,1532E-01	**4,89**

Table A-56 Lower flex joint angles after VIV amplification, middle strakes config. 1300 m system

A.6.4 Top 50_150 strakes configuration

Lower flex joint angles are given in Table A-57.

Initial analysis				
Current profile	**LFJ element length [m]**	**End 1 deflection**	**End 2 deflection**	**LFJ angle [degrees]**
2/3-current	1,525	8,1112E-02	1,4095E-01	**2,25**
Linearly sheared	1,525	4,1014E-02	7,1265E-02	**1,14**
Measured current	1,525	1,0478E-01	1,8142E-01	**2,87**
OL_2	1,525	1,0382E-01	1,7980E-01	**2,85**

Table A-57 Lower flex joint angles, top 50_150 strakes configuration 1300 m system

Added drag from VIV gives the following flex joint angles, see Table A-58.

VIV amplified analysis				
Current profile	**LFJ element length [m]**	**End 1 deflection**	**End 2 deflection**	**LFJ angle [degrees]**
2/3-current	1,525	1,0923E-01	1,8821E-01	**2,96**
Linearly sheared	1,525	4,1472E-02	7,1730E-02	**1,14**
Measured current	1,525	1,7243E-01	2,9586E-01	**4,61**
OL_2	1,525	1,7115E-01	2,9333E-01	**4,57**

Table A-58 Lower flex joint angles after VIV amplification, top 50_150 strakes configuration 1300 m system

A.6.5 Top strakes configuration

Lower flex joint angles are given in Table A-59.

Initial analysis				
Current profile	**LFJ element length [m]**	**End 1 deflection**	**End 2 deflection**	**LFJ angle [degrees]**
2/3-current	1,525	7,8658E-02	1,3666E-01	**2,18**
Linearly sheared	1,525	4,0384E-02	7,0161E-02	**1,12**
Measured current	1,525	1,0110E-01	1,7496E-01	**2,77**
OL_2	1,525	1,0239E-01	1,7724E-01	**2,81**

Table A-59 Lower flex joint angles, top strakes configuration 1300 m system

When VIV is accounted for the following flex joint angles are found, see

VIV amplified analysis				
Current profile	**LFJ element length [m]**	**End 1 deflection**	**End 2 deflection**	**LFJ angle [degrees]**
2/3-current	1,525	1,2624E-01	2,1717E-01	**3,41**
Linearly sheared	1,525	4,0830E-02	7,0617E-02	**1,12**
Measured current	1,525	1,9353E-01	3,3093E-01	**5,13**
OL_2	1,525	2,1294E-01	3,6304E-01	**5,60**

Table A-60 Lower flex joint angles after VIV amplification, top strakes config. 1300 m system

Apppendix B

B.1 Input files staggered configuration, 321 m water depth

B.1.1 INPMOD

```
'
' ************************************************************
' #                                                          #
' #  Inputfile for test of VIVANA                            #
' #                                                          #
' #  Test case  : 321 m in-marine drilling riser with buoyancy,#
' #               MT, staggered buoyancy/bare joints         #
' #                                                          #
' #                                                          #
' #  Module     : RIFLEX INPMOD                             #
' #                                                          #
' #  VIVANA input file  : med_staggerd_vivana.inp            #
' #                                                          #
' #  RIFLEX input files : med_staggered_inpmod.inp           #
' #                       med_staggered__stamod.inp          #
' #  Date        : 10/4 - 2012   GMK                         #
' ************************************************************
'
'-------------------------------------------------------
        INPMOD IDENTIFICATION TEXT  3.8
'-------------------------------------------------------
   - VIVANA Test case
   - Drilling riser with buoyancy
   - 321 m water depth, upper end above water
'-------------------------------------------------------
        UNIT NAME SPECIFICATION
         s   m   Mg  kN  9.81  1.
'-------------------------------------------------------
        NEW SINGLE RISER
'-------------------------------------------------------
         AR     VERTIC
         ARBITRARY SYSTEM AR
'        nsnod  nlin nsnfix  nves nricon  nspr  nakc
         4      3    2       0    0       0     0
'        ibtang  zbot     ibot3d
         0       -321.    0
'
'-------------------------------------------------------
'        ilinty   isnod1     isnod2
          1         1          2
          2         2          3
          3         3          4
'-------------------------------------------------------
'
'    BOTTOM NODE COORDINATES AND BC
'    isnod  ipos   ix      iy     iz     irx    iry      irz    chref
     1      0      1       1      1      1      1        1      GLOBAL
'    xo     yo     zo      x1     y1     z1      rot     dir
     0.0    0.0    -321.0  0.0    0.0    -321.0  0.0     0.0
'
'    TOP NODE COORDINATES AND BC
'    isnod  ipos   ix      iy     iz     irx    iry      irz    chref
     4      0      1       1      0      1      1        1      GLOBAL
'    xo     yo     zo      x1     y1     z1     rot      dir
     0.0    0.0    34.57   0.0    0.0    34.57   0.0      0.0
'
'
'    BOUNDARY CONDITIONS : Free supernodes
'
'    ISNOD      X0      Y0      Z0
     2          0.      0.     -301.875
```

```
     3          0.      0.      26.865
'
' ------------------------------------------------------------
'       LINE AND SEGMENT SPECIFICATION
'
        NEW LINE DATA
'
'       ilinty  nseg  icnlty  ifluty
        1       5     0       13
'
'   segment data
'   NOTE: Segment 1 is at seafloor
'
'      icmpty  icn1ty  iexwty  nelseg    slgth nstrps nstrpd slgth0
        1       0       0       2         3.2
        2       0       0       2         2.4
        3       0       0       2         9.0
        4       0       0       2         3.0
        44      0       0       1         1.525
'
'
      NEW LINE DATA
'
'       ilinty  nseg    icnlty  ifluty
        2       12       0       13
'
'       icmpty  icn1ty  iexzty  nelseg   slgth   nstrps   nstrpd   slgth0
        5       0       0       20       71.28
'-------------------------------------------------------------------------
        6       0       0       10       22.86
        7       0       0       10       22.86
        6       0       0       10       22.86
        7       0       0       10       22.86
        6       0       0       10       22.86
        7       0       0       10       22.86
        6       0       0       10       22.86
'-------------------------------------------------------------------------
        7       0       0       20       45.72
       8       0       0       2        7.63
        9       0       0       3        12.87
       10      0       0       10       31.24
'
       NEW LINE DATA
'
'       ilinty  nseg    icnlty  ifluty
        3       2       0       13
'
'       icmpty  icn1ty  iexzty  nelseg   slgth   nstrps   nstrpd   slgth0
        55      0       0       1        1.525
       11     0      0      2       6.18
'-----------------------------------------------------------
'            Total length : 355.12 m
'===========================================================
'
'          C O M P O N E N T     D A T A
'  -------------------------------------------------------
'       Pipe cross sections.
'  -------------------------------------------------------
'
        NEW COMPONENT CRS1
'       Wellhead
'      icmpty  temp   alpha   beta
        1       5.0    0.0     0.0
'       ams     ae      ai     rgyr   ast   wst    dst    thst    r-extcnt    r-
intcnt
        18.750  0.7854  0.1605 0.0    /      /      /      /       0.0          0.0
'
'       iea     iej    igt   ipress   imf   harpar
```

```
         1       1      1      0       0     0.0
'
'       ea
        1.649e+08
'
'       ei
        9.88e+06
'
'       gt
        1.0e+08
'
'       dh is the hydrodynamic diameter used by VIVANA
'
'      cqx      cqy      cax     cay     clx   cly    icode   dh
        0.0      1.0      0.      1.0     0.    0.     1       1.0
'
'      tb      ycurmx
        /         /
'
' ---------------------------------------------------------------
'
        NEW COMPONENT CRS1
'       XMT
'      icmpty  temp   alpha   beta
        2       5.0     0.0     0.0
'       ams     ae      ai      rgyr   ast   wst    dst    thst    r-extcnt    r-
intcnt
        22.917  0.4266  0.1780  0.0     /     /      /       /        0.0
0.0
'
'       iea     iej    igt   ipress   imf    harpar
         1       1      1       0      0       0
'
'       ea
        8.959e+07
'
'       ei
        2.51e+06
'
'       gt
        1.0e+08
'
'       dh is the hydrodynamic diameter used by VIVANA
'
'      cqx      cqy      cax     cay     clx   cly    icode   dh
        0.0      1.0      0.      1.0     0.    0.      1       1.982
'
'      tb      ycurmx
        /         /
'
' ------------------------------------------------------------
'
        NEW COMPONENT CRS1
'       BOP
'      icmpty  temp   alpha   beta
        3       5.0     0.0     0.0
'       ams     ae      ai      rgyr   ast   wst    dst    thst    r-extcnt    r-
intcnt
        21.621  0.4266  0.1780  0.0     /     /      /       /        0.0
0.0
'
'       iea     iej    igt   ipress   imf    harpar
         1       1      1       0      0       0
'
'       ea
        8.959e+07
'
'       ei
```

```
        2.51e+06
'
'       gt
        1.0e+08
'
'       dh is the hydrodynamic diameter used by VIVANA
'
'      cqx      cqy      cax     cay     clx   cly    icode   dh
        0.0      1.0      0.      1.0    0.    0.      1       1.94
'
'      tb      ycurmx
        /         /
'
' ------------------------------------------------------------
'
        NEW COMPONENT CRS1
'       LMRP
'      icmpty  temp   alpha   beta
        4       5.0     0.0     0.0
'       ams     ae      ai      rgyr   ast   wst    dst    thst    r-extcnt    r-
intcnt
        28.570  0.4266  0.1780  0.0     /     /      /      /          0.0
0.0
'
'       iea     iej    igt   ipress   imf    harpar
         1       1      1       0      0       0
'
'       ea
        8.959e+07
'
'       ei
        2.51e+06
'
'       gt
        1.0e+08
'
'       dh is the hydrodynamic diameter used by VIVANA
'
'      cqx      cqy      cax     cay     clx   cly    icode   dh
        0.0      1.0      0.      1.0    0.    0.      1       2.20
'
'      tb      ycurmx
        /          /
'
'-----------------------------------------------------------------
'
        NEW COMPONENT CRS1
'       Lower flex joint
'      icmpty  temp   alpha   beta
        44       5.0     0.0     0.0
'       ams     ae      ai      rgyr   ast   wst    dst    thst    r-extcnt    r-
intcnt
        3.485  0.7854  0.0      0.0     /     /      /      /          0.0
0.0
'
'       iea     iej    igt   ipress   imf    harpar
         1       1      1       0      0       0
'
'       ea
        5.0e+06
'
'       ei
        4.019e+03
'
'       gt
        1.0e+07
'
'
```

```
'       dh is the hydrodynamic diameter used by VIVANA
'
'      cqx      cqy      cax     cay     clx   cly    icode   dh
        0.0      1.0      0.      1.0    0.    0.      1       1.0
'
'      tb      ycurmx
        /          /
'
'-----------------------------------------------------------------
'
        NEW COMPONENT CRS1
'       Upper flex joint
'      icmpty  temp   alpha   beta
        55       5.0     0.0     0.0
'       ams     ae      ai      rgyr   ast   wst    dst    thst    r-extcnt    r-
intcnt
        3.485  0.7854  0.0      0.0     /     /      /      /          0.0
0.0
'
'       iea     iej    igt   ipress   imf    harpar
         1       1      1       0      0       0
'
'       ea
        2.5e+06
'
'       ei
        1.136e+03
'
'       gt
        1.0e+05
'
'
'       dh is the hydrodynamic diameter used by VIVANA
'
'      cqx      cqy      cax     cay     clx   cly    icode   dh
        0.0      1.0      0.      1.0    0.    0.      1       1.0
'
'      tb      ycurmx
        /          /
'
' ----------------------------------------------------------
'
        NEW COMPONENT CRS0
'       riser joint bare
'      icmpty  temp
        5       5.0
'
'       diast   thst   densst  thex     densex
        0.533    0.019  19.08   0.0        0.0
'       metkind emod       gmod
        1       210000000. 80000000.
'
'       dh is the hydrodynamic diameter used by VIVANA
'
'      cqx      cqy      cax     cay     clx   cly    icode   dh
        0.0      1.0      0.      1.0    0.    0.       1      0.533
'
'      tb      ycurmx
        /          /
'
' ----------------------------------------------------------
'
        NEW COMPONENT CRS0
'       riser joint buoyant
'      icmpty  temp
        6       5.0
'
'       diast   thst   densst  thex     densex
```

```
        0.533   0.019  19.84   0.432     0.4125
'       metkind emod       gmod
        1       210000000. 80000000.
'
'       dh is the hydrodynamic diameter used by VIVANA
'
'      cqx      cqy      cax     cay     clx   cly    icode    dh
        0.0      1.0      0.      1.0    0.    0.       1       1.397
'
'      tb      ycurmx
        /          /
'
' ------------------------------------------------
'
        NEW COMPONENT CRS0
'       riser joint bare
'      icmpty  temp
        7       5.0
'
'       diast   thst   densst  thex     densex
        0.533   0.019   19.83    0      0.0
'       metkind emod       gmod
        1       210000000. 80000000.
'
'       dh is the hydrodynamic diameter used by VIVANA
'
'      cqx      cqy      cax     cay     clx   cly    icode   dh
        0.0      1.0      0.      1.0     0.    0.     1       0.533
'
'      tb      ycurmx
        /           /
'
' ------------------------------------------------
'
        NEW COMPONENT CRS0
'       pup joint
'      icmpty  temp
        8       5.0
'
'       diast   thst   densst  thex     densex
        0.556   0.0305  16.215    0      0.0
'       metkind emod       gmod
        1       210000000. 80000000.
'
'       dh is the hydrodynamic diameter used by VIVANA
'
'      cqx      cqy      cax     cay     clx   cly    icode   dh
        0.0      1.0      0.      1.0    0.    0.      1       0.556
'
'      tb      ycurmx
        /          /
'
'
'


' ------------------------------------------------
'
        NEW COMPONENT CRS0
'       spacer joint
'      icmpty  temp
        9       5.0
'
'       diast   thst   densst  thex     densex
        0.556   0.0305  16.233    0      0.0
'       metkind emod       gmod
        1       210000000. 80000000.
'
'       dh is the hydrodynamic diameter used by VIVANA
```

```
'
'      cqx      cqy      cax      cay      clx    cly     icode   dh
        0.0      1.0      0.       1.0     0.     0.       1       0.556
'
'      tb      ycurmx
        /          /
'
' ------------------------------------------------
'
        NEW COMPONENT CRS0
'       Telescopic joint
'      icmpty  temp
        10       5.0
'
'       diast   thst    densst  thex     densex
        0.66    0.0885  8.085   0      0.0
        1       210000000. 80000000.
'
'       dh is the hydrodynamic diameter used by VIVANA
'
'      cqx      cqy      cax      cay      clx    cly     icode   dh
        0.0      1.0      0.       1.0      0.0   0.0       1     0.66
'
'      tb      ycurmx
        /          /
'
' ------------------------------------------------
'
        NEW COMPONENT CRS0
'       Diverter
'      icmpty  temp
        11       5.0
'
'       diast   thst   densst  thex     densex
        1.575    0.032  5.435   0      0.0
        1       210000000. 80000000.
'
'       dh is the hydrodynamic diameter used by VIVANA
'
'      cqx      cqy      cax      cay      clx    cly     icode   dh
        0.0      1.0      0.       1.0      0.0   0.0       1     1.575
'
'      tb      ycurmx
        /          /
'  ------------------------------------------------------
'
        NEW COMPONENT FLUID
'       icmpty
        13
'       rhoi    vveli    pressi    dpress    idir
        1.250     0        0         0         1
'
' ------------------------------------------------------
'
         ENVIRONMENT IDENTIFICATION
'
         Current conditions
'        idenv
         ENV22
'
         WATERDEPTH AND WAVETYPE
'        wdepth   noirw  norw    ncusta
         321.0    0      0       10
'
         ENVIRONMENT CONSTANTS
'        airden   watden   wakivi
         .0013    1.000    1.188e-6
'             --------------- Case 1  Low speed
```

```
         NEW CURRENT STATE
'        icusta   nculev
         1        7
'        curlev   curdir  curvel
         0.0      0.      0.18
        -1.5    0.     0.18
        -54     0.     0.17
        -134    0.     0.16
        -214    0.     0.16
        -294    0.     0.16
        -321    0.     0.16
'
'              -------------- Case 2   Low speed
         NEW CURRENT STATE
'        icusta   nculev
         2        7
'        curlev   curdir  curvel
         0.0      0.      0.21
         -1.5  0.     0.21
        -54     0.     0.19
        -134    0.     0.19
        -214    0.     0.18
        -294    0.     0.18
        -321    0.     0.18
'
'             --------------- Case 3   Low speed
         NEW CURRENT STATE
'        icusta   nculev
         3        7
'        curlev   curdir  curvel
         0.0      0.      0.24
         -1.5  0.     0.24
        -54     0.     0.22
        -134    0.     0.21
        -214    0.     0.2
        -294    0.     0.2
        -321    0.     0.2
'
'            ------------------ Case 4   Medium speed
         NEW CURRENT STATE
'        icusta   nculev
         4        7
'        curlev   curdir  curvel
         0.0      0.      0.28
         -1.5  0.     0.28
        -54     0.     0.25
        -134    0.     0.24
        -214    0.     0.23
        -294    0.     0.22
        -321    0.     0.22
'
'             ----------------- Case 5   Medium speed
         NEW CURRENT STATE
'        icusta   nculev
         5        7
'        curlev   curdir  curvel
         0.0      0.      0.34
         -1.5  0.     0.34
        -54     0.     0.29
        -134    0.     0.28
        -214    0.     0.26
        -294    0.     0.26
        -321    0.     0.26
'
'             ----------------- Case 6   Medium speed
         NEW CURRENT STATE
'        icusta   nculev
         6        7
```

```
'        curlev   curdir  curvel
         0.0      0.      0.38
         -1.5  0.     0.38
        -54     0.     0.33
        -134    0.     0.31
        -214    0.     0.29
        -294    0.     0.29
        -321    0.     0.29
'
'            ----------------- Case 7   Medium speed
         NEW CURRENT STATE
'        Measured current
'        icusta   nculev
         7        7
'        curlev   curdir  curvel
         0.0      0.      0.56
         -1.5  0.     0.56
        -54     0.     0.41
        -134    0.     0.38
        -214    0.     0.36
        -294    0.     0.34
        -321    0.     0.34
'
'            ----------------- Case 8
         NEW CURRENT STATE
'        2/3 current
'        icusta   nculev
         8        3
'        curlev   curdir  curvel
         0.0      0.      0.5
         -107  0.     0.5
         -321     0.      0
'
'            ----------------- Case 9
         NEW CURRENT STATE
'        Linearly sheared
'        icusta   nculev
         9        3
'        curlev   curdir  curvel
         0.0      0.      0.5
         -160.5       0.     0.25
        -321    0.     0.0
'
'            ----------------- Case 10
         NEW CURRENT STATE
'        Uniform current state
'        icusta   nculev
         10        7
'        curlev   curdir  curvel
         0.0      0.      0.5
         -1.5  0.     0.5
        -54     0.     0.5
        -134    0.     0.5
        -214    0.     0.5
        -294    0.     0.5
        -321    0.     0.5
'
     END
```

_

B.1.2 STAMOD

```
'
' ************************************************************
' #                                                          #
' #  Inputfile for test of VIVANA                            #
' #                                                          #
' #  Test case :  321 m in-marine drilling riser with buoyancy,#
' #               XM   T                                     #
' #                                                          #
' #                                                          #
' #  Module    : RIFLEX STAMOD                               #
' #                                                          #
' #  VIVANA input file  : med_staggared_vivana.inp            #
' #                                                          #
' #  RIFLEX input files : med_staggared_inpmod.inp            #
' #                       med_staggared_stamod.inp            #
' #  Date        : 10/4 - 2012    GMK                       #
' ************************************************************
'
' ------------------------------------------------------------
       STAMOD CONTROL INFORMATION 3.8
' ------------------------------------------------------------
   - VIVANA Test case.
   - Drilling rise with buoyancy, no strakes, staggered buoyancy/bare joints
   - 321 m water depth, upper end above water
' ------------------------------------------------------------
'
'       irunco   idris    ianal iprdat iprcat  iprfem  ipform iprnor
        1        VERTIC   1     5      1       1       1      1
'
' ------------------------------------------------------------
       RUN IDENTIFICATION
' ------------------------------------------------------------
'       idsta
        STVERT
'
' ------------------------------------------------------------
'
       ENVIRONMENT REFERENCE IDENTIFIER
'       idenv
        ENV22
'
' ------------------------------------------------------------
'            STATIC ANALYSIS WITH FIXED PARAMETERS
' ------------------------------------------------------------
       STATIC CONDITION INPUT
'
'       External static loads
'
'  NOTE: icurin selects current case from IMPMOD for actual analysis
'
'       nlcomp    icurin    curfac     iwindin
        1         7         1.0          0
'
'-----------------------------------------------------------
'   Top tension: Riser end is at node 3 of line 3, segment 1
' -----------------------------------------------------------
'
'       ilin      ilseg    ilnode     ildof  rlmag      chicoo
        3         2        2          7      5950.0     LOCAL
'       lcons     isolvr
        1         1
'
'-----------------------------------------------------
       COMPUTATIONAL PROCEDURE
'
' -----------------------------------------------------
'       ameth
```

```
        FEM
'
        FEM ANALYSIS PARAMETERS DEFINE LOADING SEQUENCE
'
'-------------------------------------------------------
'
   LOAD GROUP DATA
'      nstep    maxit   racu
          5     30     1.E-7
'      LOTYPE
        TENS
        SFOR
' ------
   LOAD GROUP DATA
'      nstep   maxit    racu
         10      100     1.E-7
'      LOTYPE
       VOLU
'       SFOR
' -------
   LOAD GROUP DATA
'      nstep   maxit    racu
         30      100    1.E-7
'      LOTYPE
       DISP
       CURR
'
'  END
'
' -------------------------------------------------------
'   Definition of offset by use of parameter variation option
'
'
'
'    PARAMETER VARIATION DEFINITION
'
'   nstvar   iofpos   icurvar   ifovar   maxipv racupv
'    1        1        0         0        15     1.E-5
'
'    STATIC OFFSET INCREMENTS
'
'   iref   dxoff   dyoff    dzoff   irot   drot
'    0      0      0        0       0
'
'   Mandatory data when parameter variation:
'    STAMOD PRINT CONTROL
'
'   istep  isfor  ispos
'    1      1      1
'-------------------------------------------------------
    END
_
```

B.1.3 VIVANA

```
' ************************************************************
' #                                                          #
' #  Inputfile for test of VIVANA                            #
' #                                                          #
' #  Test case : 321 m in-marine drilling riser with buoyancy, #
' #              XMT                                         #
' #                                                          #
' #  Module    : VIVANA                                      #
' #                                                          #
' #  VIVANA input file  : med_staggared_vivana.inp            #
' #                                                          #
' #  RIFLEX input files : med_staggared_inpmod.inp            #
' #                       med_staggared_stamod.in            #
' #  Date        : 10/4 - 2012   GMK                         #
' ************************************************************
'
'
    VIVANA CONTROL INFORMATION 3.8
'
   - VIVANA Test case.
   - Drilling riser with staggared buoyant/bare joints
   - 321 m water depth, upper end above water
'
'   idris    idstat   idenv   temp      irstyp
    VERTIC   STVERT   ENV22    5.0      1
' ------------------------------------------------------------
'
    WORK ARRAY DIMENSION
'   nwiwa
    19000000
'
' ------------------------------------------------------------
'
    EIGENVALUE ANALYSIS PARAMETERS
'   neig  nvec
    200   200
'   eps1  eps2  eps3  ksr  maxit  kex  shift  maxniv
    0.0   0.0   0.0   1    7      0    0.0    0
'
' ------------------------------------------------------------
'
    EIGENVALUE PRINT OPTIONS
'   npeig  npvec
    150     15
'
' ------------------------------------------------------------
'
     SECTION PROPERTY SPECIFICATION
' nsegp
    19
' isegp  iexczo  iaddma  iliftc  idampg  istrou    iaddma2     iexcit2
    1      1        0       1      0       0         0           0
    2      1        0       1      0       0         0           0
    3      1        0       1      0       0         0           0
    4      1        0       1      0       0         0           0
    5      1        0       1      0       0         0           0
    6      1        0       1      0       0         0           0
    7      1        0       1      0       0         0           0
    8      1        0       1      0       0         0           0
    9      1        0       1      0       0         0           0
    10     1        0       1      0       0         0           0
    11     1        0       1      0       0         0           0
    12     1        0       1      0       0         0           0
    13     1        0       1      0       0         0           0
    14     1        0       1      0       0         0           0
    15     1        0       1      0       0         0           0
    16     1        0       1      0       0         0           0
```

```
    17     1        0       1      0       0         0           0
    18     1        0       1      0       0         0           0
    19     1        0       1      0       0         0           0
'
' ------------------------------------------------------------
'
     PROPERTY EXCITATION ZONE
' nexzon
    2
' iprono   cprpid      fhmin   fhmax
     1     Exc_norm    0.12     0.31
     2     Excit_stra  0.0625   0.33
'
'
' ------------------------------------------------------------
'
'
     PROPERTY DAMPING FACTORS
' ndpfac
    4
' iprono   cprpid     fstill   flowv   fhighv
     1     Dmp_norm     1.0     1.0      1.1
     2     Damp_01      1.0     0.8      1.14
     3     Damp_02      1.0     0.9      1.13
     4     Damp_03      1.2     0.3      1.12
'
'------------------------------------------------------------
'     PROPERTY STROUHAL SPECIFICATION
' nstrsp
'    3
' iprono   cprpdi   npudsc   strou
'     1     Strou_01  16       0.19
'     reynum      strnum
'        40.        0.1
'       100.        0.18
'       200.        0.19
'       400.        0.195
'      1000.        0.20
'      4000.        0.205
'     10000.        0.21
'     40000.        0.215
'    100000.        0.22
'    200000.        0.4
'    300000.        0.45
'    500000.        0.45
'    800000.        0.25
'   1000000.        0.23
'   4000000.        0.25
'  10000000.        0.27
'
' iprono   cprpdi   npudsc   strou
'     2     Strou_02  16       -1.
'     reynum      strnum
'        40.        0.1
'       100.        0.18
'       200.        0.19
'       400.        0.195
'      1000.        0.20
'      4000.        0.205
'     10000.        0.21
'     40000.        0.215
'    100000.        0.22
'    200000.        0.4
'    300000.        0.45
'    500000.        0.45
'    800000.        0.25
'   1000000.        0.23
'   4000000.        0.25
```

```
'  10000000.        0.27
'
' iprono   cprpdi   npudsc   strou
'     3     Strou_03  16       0.27
'     reynum      strnum
'        40.        0.1
'       100.        0.18
'       200.        0.19
'       400.        0.195
'      1000.        0.20
'      4000.        0.205
'     10000.        0.21
'     40000.        0.215
'    100000.        0.22
'    200000.        0.4
'    300000.        0.45
'    500000.        0.45
'    800000.        0.25
'   1000000.        0.23
'   4000000.        0.25
'  10000000.        0.27
'
' ------------------------------------------------------------
'
     PROPERTY ADDED MASS
' nadcur
    3
' iprono   cprpid    nampt
     1     Admas_01   12
' fhat   addmco
   0.0    -0.6
   0.15   -0.6
   0.16   -0.3
   0.17    1.7
   0.18    2.0
   0.2     2.2
   0.21    2.0
   0.24    1.7
   0.27    1.5
   0.33    1.2
   0.40    1.0
   0.5     1.0
'
' iprono  cprpid    nampt
     2    Admas_02    10
' fhat   addmco
   0.0    -0.4
   0.16   -0.2
   0.17    1.5
   0.18    2.0
   0.2     2.2
   0.21    2.0
   0.24    1.7
   0.27    1.5
   0.33    1.2
   0.5     1.2
'
' iprono  cprpid    nampt
     3    strakes     4
'  fhat   addmco
   0.028   2
   0.2     2
   0.5     2
   0.95    2
'
' ------------------------------------------------------------
'
     PROPERTY EXCITATION COEFFICIENT
```

```
' nlct01   nlct02
    1        1
' iprono   cprpid     nlcpt
    1     Test_211    17
' fhat     acl0   aclmax    clmax   cla0
  0.120   0.200   0.100   0.100   0.050
  0.125   0.400   0.200   0.100   0.060
  0.135   0.500   0.270   0.100   0.080
  0.140   0.550   0.350   0.140   0.110
  0.150   0.600   0.450   0.200   0.180
  0.160   0.700   0.500   0.350   0.240
  0.165   0.800   0.500   0.500   0.300
  0.170   0.900   0.430   0.800   0.400
  0.175   0.820   0.400   0.700   0.200
  0.180   0.780   0.400   0.500   0.150
  0.185   0.750   0.400   0.550   0.160
  0.190   0.650   0.400   0.600   0.170
  0.200   0.580   0.380   0.650   0.200
  0.210   0.550   0.350   0.600   0.250
  0.250   0.400   0.200   0.350   0.200
  0.300   0.200   0.100   0.200   0.150
  0.310   0.180   0.090   0.100   0.150
'
'-------------------------------------------------------------
' Strakes15D AIMS
' iprono cprpid     nft02
   4  STK15D    14
' fhtyp2   npoint
  0.33       8
'  ad     cl
  0       0
  0.100   -0.390
  0.200   -1
  0.300   -1.85
  0.390   -2.94
  0.490   -4.25
  0.600   -5.80
  0.700   -7.58
'
' fhtyp2   npoint
  0.250       8
'  ad     cl
  0   0
  0.100   -0.270
  0.200   -0.640
  0.300   -1.12
  0.390   -1.70
  0.490   -2.39
  0.600   -3.18
  0.700   -4.08
'
' fhtyp2   npoint
  0.20     8
'  ad     cl
  0   0
  0.100   -0.240
  0.200   -0.530
  0.300   -0.870
  0.390   -1.26
  0.490   -1.71
  0.600   -2.20
  0.700   -2.75
'
' fhtyp2   npoint
  0.16670       8
'  ad     cl
  0   0
  0.100   -0.210
```

```
  0.200   -0.440
  0.300   -0.710
  0.390   -1.01
  0.490   -1.34
  0.600   -1.70
  0.700   -2.10
'
' fhtyp2   npoint
  0.14290       8
'  ad     cl
  0   0
  0.100   -0.170
  0.200   -0.360
  0.300   -0.590
  0.390   -0.850
  0.490   -1.14
  0.600   -1.47
  0.700   -1.83
'
' fhtyp2   npoint
  0.1250        8
'  ad     cl
  0   0
  0.100   -0.190
  0.200   -0.400
  0.300   -0.630
  0.390   -0.880
  0.490   -1.16
  0.600   -1.46
  0.700   -1.79
'
' fhtyp2   npoint
  0.1110        8
'  ad     cl
  0   0
  0.100   -0.190
  0.200   -0.390
  0.300   -0.600
  0.390   -0.830
  0.490   -1.08
  0.600   -1.33
  0.700   -1.61
'
' fhtyp2   npoint
  0.10        8
'  ad     cl
  0   0
  0.100   -0.180
  0.200   -0.360
  0.300   -0.550
  0.390   -0.740
  0.490   -0.940
  0.600   -1.15
  0.700   -1.36
'
' fhtyp2   npoint
  0.09090       8
'  ad     cl
  0   0
  0.100   -0.150
  0.200   -0.310
  0.300   -0.480
  0.390   -0.660
  0.490   -0.840
  0.600   -1.03
  0.700   -1.23
'
' fhtyp2   npoint
```

```
  0.08330       8
'  ad     cl
  0   0
  0.100   -0.110
  0.200   -0.230
  0.300   -0.370
  0.390   -0.530
  0.490   -0.700
  0.600   -0.890
  0.700   -1.09
'
' fhtyp2   npoint
  0.07690       8
'  ad     cl
  0   0
  0.100   -0.0700
  0.200   -0.160
  0.300   -0.270
  0.390   -0.410
  0.490   -0.560
  0.600   -0.740
  0.700   -0.930
'
' fhtyp2   npoint
  0.07140       8
'  ad     cl
  0   0.0100
  0.100   -0.0300
  0.200   -0.0900
  0.300   -0.180
  0.390   -0.300
  0.490   -0.450
  0.600   -0.620
  0.700   -0.820
'
' fhtyp2   npoint
  0.06670       8
'  ad     cl
  0   0.0100
  0.100   -0.0200
  0.200   -0.0800
  0.300   -0.150
  0.390   -0.260
  0.490   -0.380
  0.600   -0.530
  0.700   -0.710
'
' fhtyp2   npoint
  0.06250       8
'  ad     cl
  0   0.0100
  0.100   -0.0500
  0.200   -0.120
  0.300   -0.210
  0.390   -0.300
  0.490   -0.400
  0.600   -0.510
  0.700   -0.630
'
'------------------------------------------------------------
'------------------------------------------------------------
'
    RESPONSE ANALYSIS PARAMETERS
'
'   reldam gives damping as fraction of critical damping
'
'   reldam     iopfrc    iprint
    0.01         0         1
```

```
'
'   ifrit      maxitr    ilim     conlim
     1          30         1       0.0001
'
'   ioptsh      nuddf
      1           0
'
' ------------------------------------------------------------
'
    VIVRESPONSE FATIGUE DAMAGE
'   nsect   npcs   ioppr   tslen    dt   irsno    tsioppr    chtsprn
    0       4      0        0        0    31415      0
'   dscfa   dscfy   dscfz  asi      wsti      thi    rfact
    1.0     1.0     1.0    0.0       0.0       0.0   0.001
'
' NOTE: rfact scales stresses from kPa (STAMOD) to MPa for
'       fatigue analysis using SN curves
'
'    Select Sn curves for calculation
'
'     nofc
      1
'     chidsn    chidsn
      SNC01
'
'------------------------------------------------------------
'
' SN curve data
'    nofc
      1
'    chidsn    nosl    limind    fatlim    tref    kexp
     SNC01      1        0         0        0.0     0.0
'
'    rmi1    rci1
     3.0     11.63
' ------------------------------------------------------------
'
     VIVANA RESULT PRINT
'
'    iprelf   iprstr    iprdrg     iprrsp    iprcng
        1       1          1         1          1
'
'------------------------------------------------------------
'
     VIVANA RMPF PRINT
'
'    iprcrv
       1
'
'
'------------------------------------------------------------
     END
```

B.2 Input files top strakes configuration, 1300 m water depth

B.2.1 INPMOD

```
'
' ************************************************************
' #                                                          #
' #  Inputfile for test of VIVANA                            #
' #                                                          #
' #  Test case  : 1300 m in-marine riser system              #
' #               no XMT, top 50% of riser straked           #
' #                                                          #
' #  Module     : RIFLEX INPMOD                              #
' #                                                          #
' #  VIVANA input file  : deep_strakes_top_50_vivana.inp     #
' #                                                          #
' #  RIFLEX input files : deep_strakes_top_50_inpmod.inp     #
' #                       deep_strakes_top_50_stamod.inp     #
' #  Date        : 06/2 - 2012   GMK                         #
' ************************************************************
'
'-----------------------------------------------------------
        INPMOD IDENTIFICATION TEXT  3.8
'-----------------------------------------------------------
   - VIVANA Test case
   - Drilling riser with buoyancy, top 50% of riser length straked
   - 1300 m water depth, upper end above water
'-----------------------------------------------------------
        UNIT NAME SPECIFICATION
         s   m   Mg  kN  9.81  1.
'-----------------------------------------------------------
        NEW SINGLE RISER
'-----------------------------------------------------------
         AR     VERTIC
         ARBITRARY SYSTEM AR
'        nsnod  nlin nsnfix  nves nricon  nspr  nakc
         4      3    2       0    0       0     0
'        ibtang  zbot     ibot3d
         0       -1300.    0
'
'-----------------------------------------------------------
'        ilinty   isnod1     isnod2
          1         1          2
          2         2          3
          3         3          4
'-----------------------------------------------------------
'
'    BOTTOM NODE COORDINATES AND BC
'    isnod  ipos   ix      iy     iz     irx    iry      irz    chref
     1      0      1       1      1      1      1        1      GLOBAL
'    xo     yo     zo      x1     y1     z1      rot     dir
     0.0    0.0    -1300.0  0.0    0.0   -1300.0  0.0     0.0
'
'    TOP NODE COORDINATES AND BC
'    isnod  ipos   ix      iy     iz     irx    iry      irz    chref
     4      0      1       1      0      1      1        1      GLOBAL
'    xo     yo     zo      x1     y1     z1     rot      dir
     0.0    0.0    35.885  0.0    0.0    35.885 0.0      0.0
'
'
' BOUNDARY CONDITIONS : Free supernodes
'
'ISNOD       X0      Y0      Z0
  2          0.      0.     -1283.6
  3          0.      0.      31.56
'
' -----------------------------------------------------------
'       LINE AND SEGMENT SPECIFICATION
```

```
'
        NEW LINE DATA
'
'       ilinty  nseg  icnlty  ifluty
        1       4     0       13
'
'   segment data
'   NOTE: Segment 1 is at seafloor
'
'      icmpty  icn1ty  iexwty  nelseg    slgth nstrps nstrpd slgth0
        1       0       0       2         3.0
       2      0      0      3        8.2
        3       0       0       2         3.675
        44      0       0       1         1.525
'
      NEW LINE DATA
'
'       ilinty  nseg    icnlty  iflty
        2       7       0       13
'
'       icmty   icn1ty  iexwty  nelseg   slgth  nstrps  nstrpd  slgth0
        5       0       0       12       23.86
        6       0       0       100      251.46
        7       0       0       100      251.46
        8       0       0       200      101.94
        9       0       0       300      629.58
       10      0       0       12       22.86
        11      0       0       8        34
'
       NEW LINE DATA
'
'       ilinty  nseg    iclnty  iflty
        3       2       0       13
'
'       icmty   icn1ty  iexwty  nelseg   slgth  nstrps  nstrpd  slgth0
        55      0       0       1        1.525
       12     0      0      2       2.8
'-------------------------------------------------------------
'             Total length : 1335.885 m
'=============================================================
'
'          C O M P O N E N T     D A T A
'  ---------------------------------------------------------
'       Pipe cross sections.  Only one component
'       definition is used
'  ---------------------------------------------------------
'
        NEW COMPONENT CRS1
'       Wellhead
'      icmpty  temp   alpha   beta
        1       5.0    0.0     0.0
'
'       ams    ae       ai       rgyr   ast   wst   dst   thst   r-extcnt   r-
intcnt
        20     0.7854   0.1605   0.0    /      /     /     /      0.0        0.0
'
'       iea    iej    igt   ipress   imf    harpar
        1      1      1      0        0       0
'
'       ea
        1.649e+08
'
'       ei
        9.88e+06
'
'       gt
        1.0e+08
'
```

```
'       dh is the hydrodynamic diameter used by VIVANA
'
'      cqx      cqy      cax     cay     clx   cly   icode   dh
        0.0      1.0      0.      1.0    0.     0.     1       1.0
'
'      tb      ycurmx
        14380.   0.4329
'
' ---------------------------------------------------------------------
'
        NEW COMPONENT CRS1
'       BOP
'      icmpty  temp   alpha   beta
        2       5.0    0.0     0.0
'
'       ams      ae       ai        rgyr   ast   wst   dst   thst   r-extcnt   r-
intcnt
        27.317   0.4266   0.1780    0.0    /      /     /     /      0.0        0.0
'
'       iea    iej    igt   ipress   imf    harpar
        1      1      1      0        0       0
'
'       ea
        8.959e+07
'
'       ei
        2.51e+06
'
'       gt
        1.0e+08
'
'       dh is the hydrodynamic diameter used by VIVANA
'
'      cqx      cqy      cax     cay    clx  cly   icode     dh
        0.0      1.0      0.      1.0    0.    0.     1       2.154
'
'      tb      ycurmx
        14380.   0.4329
'
' ---------------------------------------------------------------------
'
        NEW COMPONENT CRS1
'       LMRP
'      icmpty  temp   alpha   beta
        3       5.0    0.0     0.0
'
'       ams    ae       ai       rgyr   ast   wst   dst   thst   r-extcnt   r-
intcnt
        20     0.7854   0.1605   0.0    /      /     /     /      0.0        0.0
'
'       iea    iej    igt   ipress   imf    harpar
        1      1      1      0        0       0
'
'       ea
        8.959e+07
'
'       ei
        2.51e+06
'
'       gt
        1.0e+08
'
'       dh is the hydrodynamic diameter used by VIVANA
'
'      cqx      cqy      cax     cay     clx   cly    icode   dh
        0.0      1.0      0.      1.0    0.    0.     1       2.633
'
'      tb      ycurmx
```

```
       14380.   0.4329
'
' ------------------------------------------------
'
       NEW COMPONTENT CRS1
'      Lower flex joint
'
'      icmpty   temp
         44      5.0
'
'      ams        ae       ai      rgyr     ast    wst
       11.4615  1.45366  0.0       0.0      /       /
'
'      iea    iej    igt   ipress    imf
        1      1      1      0        0
'
'      ea
       5.5e+06
'
'      ei
       8.038e+03
'      gt
       1.0e+07
'
'      cqx     cqy    cax    cay    clx    cly   icode   dh
       0       1.0     0     1.0    0.0    0.0     1     1.36046
'
'      tb     ycurmx
        /      /
'
' ------------------------------------------------
'
       NEW COMPONTENT CRS1
'      Upper flex joint
'
'      icmpty   temp
         55      5.0
'
'      ams        ae       ai      rgyr     ast    wst
       11.4615  1.45366  0.0     0.0        /       /
'
'      iea    iej    igt   ipress    imf
        1      1      1      0        0
'
'      ea
       3.0e+06
'
'      ei
       1.136e+03
'      gt
       1.5e+05
'
'      cqx     cqy    cax    cay    clx    cly   icode   dh
       0       1.0     0     1.0    0.0    0.0     1     1.0
'
'      tb     ycurmx
        /      /
'
'-----------------------------------------------------------------
'
       NEW COMPONENT CRS0
'      riser joint bare
'     icmpty  temp
       5       5.0
'
'      diast   thst   densst  thex     densex
       0.533     0.0205  18   0.0      0.0
'      metkind emod       gmod
```

```
       1       210000000. 80000000.
'
'       dh is the hydrodynamic diameter used by VIVANA
'
'      cqx      cqy      cax     cay     clx   cly    icode   dh
        0.0      1.0      0.      1.0    0.    0.     1       0.533
'
'      tb      ycurmx
        14380.   0.4329
'
' ------------------------------------------------
'
        NEW COMPONENT CRS0
'       riser joint buoyant 5000ft
'      icmpty  temp
        6       5.0
'
'       diast   thst   densst  thex     densex
        0.533    0.0205  18    0.432      0.6051
'       metkind emod       gmod
        1       210000000. 80000000.
'
'       dh is the hydrodynamic diameter used by VIVANA
'
'      cqx      cqy      cax     cay     clx   cly    icode   dh
        0.0      1.0      0.      1.0    0.    0.     1       1.397
'
'      tb      ycurmx
        14380.   0.4329
'
' ------------------------------------------------
'
        NEW COMPONENT CRS0
'       riser joint buoyant 5000ft
'      icmpty  temp
        7       5.0
'
'       diast   thst   densst  thex     densex
        0.533    0.0205  18    0.432      0.6051
'       metkind emod       gmod
        1       210000000. 80000000.
'
'       dh is the hydrodynamic diameter used by VIVANA
'
'      cqx      cqy      cax     cay     clx   cly    icode   dh
        0.0      1.0      0.      1.0    0.    0.     1       1.397
'
'      tb      ycurmx
        14380.   0.4329
'
' ------------------------------------------------
'
        NEW COMPONENT CRS0
'       riser joint buoyant 2500ft
'      icmpty  temp
        8       5.0
'
'       diast   thst   densst  thex     densex
        0.533    0.0205  18    0.432      0.5561
'       metkind emod       gmod
        1       210000000. 80000000.
'
'       dh is the hydrodynamic diameter used by VIVANA
'
'      cqx      cqy      cax     cay     clx   cly    icode   dh
        0.0      1.0       0.     1.0    0.    0.     1       1.397
'
'      tb      ycurmx
```

```
       14380.   0.4329
'
' ------------------------------------------------
'
       NEW COMPONENT CRS0
'      riser joint buoyant 2500ft, straked
'     icmpty  temp
       9       5.0
'
'      diast   thst   densst  thex     densex
       0.533    0.0205  18    0.432      0.5561
'      metkind emod       gmod
       1       210000000. 80000000.
'
'      dh is the hydrodynamic diameter used by VIVANA
'
'     cqx      cqy      cax     cay     clx   cly    icode   dh
       0.0      1.35      0.     1.02    0.    0.     1       1.397
'
'     tb      ycurmx
       14380.   0.4329
'
' ------------------------------------------------
'
       NEW COMPONENT CRS0
'      riser joint bare, straked
'     icmpty  temp
       10      5.0
'
'      diast   thst    densst  thex     densex
       0.533   0.0205  18      0        0.0
'      metkind emod       gmod
       1       210000000. 80000000.
'
'      dh is the hydrodynamic diameter used by VIVANA
'
'     cqx      cqy      cax     cay     clx   cly    icode   dh
       0.0      1.35     0.      1.02    0.    0.     1       0.533
'
'     tb      ycurmx
       14380.   0.4329
'
' ------------------------------------------------
'
       NEW COMPONENT CRS0
'      telescopic joint
'     icmpty  temp
       11      5.0
'
'      diast   thst   densst  thex     densex
       0.60    0.0250  19.63    0      0.0
'      metkind emod       gmod
       1       210000000. 80000000.
'
'      dh is the hydrodynamic diameter used by VIVANA
'
'     cqx      cqy      cax     cay     clx   cly    icode   dh
       0.0      1.0      0.      1.0    0.    0.     1       0.60
'
'     tb      ycurmx
       14380.   0.4329
'
' ------------------------------------------------
'
'
       NEW COMPONENT CRS0
'      diverter
'     icmpty  temp
```

```
        12       5.0
'
'       diast   thst   densst  thex     densex
        1.575    0.032  7.85   0        0.0
        1       210000000. 80000000.
'
'       dh is the hydrodynamic diameter used by VIVANA
'
'      cqx      cqy      cax     cay     clx   cly    icode   dh
        0.0      1.0      0.      1.0    0.    0.     1        1.575
'
'      tb      ycurmx
        14380.   0.4329
'  ------------------------------------------------------
'
        NEW COMPONENT FLUID
'       icmpty
        13
'       rhoi    vveli    pressi    dpress    idir
        1.5     0        0         0         1
'
' ------------------------------------------------------
'
         ENVIRONMENT IDENTIFICATION
'
         Current conditions
'        idenv
         ENV0
'
         WATERDEPTH AND WAVETYPE
'        wdepth   noirw  norw    ncusta
         1300.0    0      0       8
'
         ENVIRONMENT CONSTANTS
'        airden   watden   wakivi
         .0013    1.000    1.188e-6
'
'
'
'Note: Current profiles are extreme current profiles
'
'
'              --------------- Case 1
         NEW CURRENT STATE
'        icusta   nculev
         1        7
'        curlev   curdir  curvel
         0.0      0.      1.44
        -200    0.     0.97
        -400    0.     0.78
        -600    0.     0.76
        -800    0.     0.83
        -1000   0.     0.50
        -1297   0.     0.55
'
'              -------------- Case 2
         NEW CURRENT STATE
'        Uniform current velocity
'        icusta   nculev
         2        7
'        curlev   curdir  curvel
         0.0      0.      1.0
         -200   0.     1.0
        -400    0.     1.0
        -600    0.     1.0
        -800    0.     1.0
        -1000   0.     1.0
        -1297   0.     1.0
```

```
'
'            --------------- Case 3
         NEW CURRENT STATE
'        Linearly sheared
'        icusta   nculev
         3        7
'        curlev   curdir  curvel
         0.0      0.      1.0
         -200   0.     0.769
        -400    0.     0.615
        -600    0.     0.462
        -800    0.     0.308
        -1000   0.     0.154
        -1300   0.     0.0
'
'           ------------------ Case 4
         NEW CURRENT STATE
'        Bidirectional
'        icusta   nculev
         4        7
'        curlev   curdir  curvelV
         0.0      0.      1.0
         -200   0.     0.615
        -400    0.     0.308
        -650    0.     0.0
        -800    180.   0.308
        -1000   180.          0.615
        -1300   180.          1.0
'
'            ----------------- Case 5
         NEW CURRENT STATE
'        Gulf of Mexico no. 1
'        icusta   nculev
         5        10
'        curlev   curdir  curvel
         0.0      0.      1.0
         -120   0.     0.8
        -240    0.     0.5
        -360    0.     0.25
        -480    0.     0.2
        -600    0.     0.2
        -720    0.     0.2
         -840     0.      0.2
         -960     0.      0.2
         -1300    0.      0.2
'
'            ----------------- Case 6
         NEW CURRENT STATE
'        Gulf of Mexico no. 2
'        icusta   nculev
         6        10
'        curlev   curdir  curvel
         0.0      0.      1.0
         -120   0.     0.4
        -240    0.     0.18
        -360    0.     0.15
        -480    0.     0.3
        -600    0.     0.4
        -720    0.     0.45
         -840     0.      0.55
         -960     0.      0.65
         -1300    0.      0.65
'
'            ----------------- Case 7
         NEW CURRENT STATE
'        Ormen Lange no. 1
'        icusta   nculev
         7        4
```

```
'         curlev   curdir  curvel
          0.0      0.      1.0
         -480    0.     0.65
          -840     0.      0.65
          -1300    0.      0.0
'
'            ----------------- Case 8
          NEW CURRENT STATE
'         Ormen Lange no. 2
'         icusta   nculev
          8        11
'         curlev   curdir  curvel
          0.0      0.      1.15
          -50      0.      1.15
          -100     0.      1.15
          -200     0.      1.10
          -300     0.      1.05
          -400     0.      1.0
          -500     0.      0.95
          -600     0.      0.75
          -750     0.      0.55
          -850     0.      0.55
          -1300    0.      0.55
'
'
'
'
'
     END
```

B.2.2 STAMOD

```
' ************************************************************
' #                                                          #
' #  Inputfile for test of VIVANA                            #
' #                                                          #
' #  Test case :  1300 m drilling riser system               #
' #               no XMT, top 50% of riser straked           #
' #                                                          #
' #  Module    : RIFLEX STAMOD                               #
' #                                                          #
' #  VIVANA input file  : deep_strakes_top_50_vivana.inp     #
' #                                                          #
' #  RIFLEX input files : deep_strakes_top_50_inpmod.inp     #
' #                       deep_strakes_top_50_stamod.inp     #
' #  Date        : 06/2 - 2012    GMK                       #
' ************************************************************
'
' ------------------------------------------------------------
       STAMOD CONTROL INFORMATION 3.8
' ------------------------------------------------------------
   - VIVANA Test case.
   - Drilling riser with buoyancy, top 50% of riser length straked
   - 1300 m water depth, upper end above water
' ------------------------------------------------------------
'
'       irunco   idris    ianal iprdat iprcat  iprfem  ipform iprnor
        1        VERTIC   1     5      1       1       1      1
'
' ------------------------------------------------------------
       RUN IDENTIFICATION
' ------------------------------------------------------------
'       idsta
        STVERT
'
' ------------------------------------------------------------
'
       ENVIRONMENT REFERENCE IDENTIFIER
'       idenv
        ENV0
'
' ------------------------------------------------------------
'            STATIC ANALYSIS WITH FIXED PARAMETERS
' ------------------------------------------------------------
       STATIC CONDITION INPUT
'
'       External static loads
'
'  NOTE: icurin selects current case from IMPMOD for actual analysis
'
'       nlcomp    icurin    curfac    iwindin
        1         1         1.0          0
'
'-------------------------------------------------------
'   Top tension: Riser end is at local node 2 of segment 1 in line 3
' -------------------------------------------------------
'
'       ilin      ilseg    ilnode     ildof  rlmag    chicoo
        3         2        2          7      6050     LOCAL
'       lcons     isolvr
        1         1
'
'-------------------------------------------------------
       COMPUTATIONAL PROCEDURE
'
' -------------------------------------------------------
'       ameth
        FEM
```

```
'
        FEM ANALYSIS PARAMETERS DEFINE LOADING SEQUENCE
'
'-------------------------------------------------------
'
   LOAD GROUP DATA
'      nstep    maxit   racu
          5      30     1.E-7
'      LOTYPE
        TENS
        SFOR
' ------
   LOAD GROUP DATA
'      nstep   maxit    racu
         10      100     1.E-7
'      LOTYPE
       VOLU
'       SFOR
' -------
   LOAD GROUP DATA
'      nstep   maxit    racu
         30      100     1.E-7
'      LOTYPE
       DISP
       CURR
'
' END
'
' ------------------------------------------------------
'   Definition of offset by use of parameter variation option
'
'
'    PARAMETER VARIATION DEFINITION
'
'   nstvar   iofpos   icurvar   ifovar   maxipv racupv
'    1        1        0         0        15     1.E-5
'
'    STATIC OFFSET INCREMENTS
'
'   iref   dxoff   dyoff    dzoff   irot   drot
'    0      0      0        0       0
'
'   Mandatory data when parameter variation:
'    STAMOD PRINT CONTROL
'
'   istep  isfor  ispos
'    1      1      1
'-------------------------------------------------------------------------
'
'Updating static analysis from increased drag force under VIV conditions
'
'    DRAG AMPLIFICATION INPUT
'
'   chfdrg                          chiop
'    deep_in_marine_drag_vivana            MPF
'
'-------------------------------------------------------------------------
    END
_
```

B.2.3 VIVANA

```
'
' ************************************************************
' #                                                          #
' #  Inputfile for test of VIVANA                            #
' #                                                          #
' #  Test case : 1300 m in-marine riser system               #
' #              no XMT, top 50% of riser straked            #
' #                                                          #
' #  Module    : VIVANA                                      #
' #                                                          #
' #  VIVANA input file  : deep_strakes_top_50_vivana.inp     #
' #                                                          #
' #  RIFLEX input files : deep_strakes_top_50_inpmod.inp     #
' #                       deep_strakes_top_50_stamod.inp     #
' #  Date        : 07/2 - 2012   GMK                         #
' ************************************************************
'
'
    VIVANA CONTROL INFORMATION  3.8
'
   - VIVANA Test case.
   - Drilling riser with buoyancyy, top 50% of riser length straked
   - Buoyancy zone with extended diameter
'
'   idris    idstat   idenv   temp    irstyp
    VERTIC   STVERT   ENV0     5.0     1
' ------------------------------------------------------------
'
    WORK ARRAY DIMENSION
'   nwiwa
    19000000
'
' ------------------------------------------------------------
'
    EIGENVALUE ANALYSIS PARAMETERS
'   neig  nvec
    150    150
'   eps1  eps2  eps3  ksr  maxit  kex  shift  maxniv
    0.0   0.0   0.0   1    7      0    0.0    0
'
' ------------------------------------------------------------
'
    EIGENVALUE PRINT OPTIONS
'   npeig  npvec
    150     15
'
' ------------------------------------------------------------
'
     SECTION PROPERTY SPECIFICATION
' nsegp
    13
' isegp  iexczo  iaddma  iliftc  idampg  istrou   iaddma2   iexcit2
    1      1        0       1       0       0        0          0
    2      1        0       1       0       0        0          0
    3      1        0       1       0       0        0          0
    4      1        0       1       0       0        0          0
    5      1        0       1       0       0        0          0
    6      1        0       1       0       0        0          0
    7      1        0       1       0       0        0          0
    8      1        0       1       0       0        0          0
    9      2        3       4       0       0        0          0
    10     2        3       4       0       0        0          0
    11     1        0       1       0       0        0          0
    12     1        0       1       0       0        0          0
    13     1        0       1       0       0        0          0
'
' ------------------------------------------------------------
```

```
'
     PROPERTY EXCITATION ZONE
' nexzon
    2
' iprono   cprpid    fhmin   fhmax
     1     Exc_norm  0.120     0.31
     2     Excit_02  0.0625    0.33
'
'
' ------------------------------------------------------------
'
'
     PROPERTY DAMPING FACTORS
' ndpfac
    4
' iprono   cprpid     fstill   flowv   fhighv
     1     Dmp_norm     1.0     1.0      1.1
     2     Damp_01      1.0     0.8      1.14
     3     Damp_02      1.0     0.9      1.13
     4     Damp_03      1.2     0.3      1.12
'
'
' ------------------------------------------------------------
'
     PROPERTY STROUHAL SPECIFICATION
' nstrsp
    3
' iprono   cprpdi   npudsc   strou
     1     Strou_01  16       0.19
'     reynum      strnum
        40.        0.1
       100.        0.18
       200.        0.19
       400.        0.195
      1000.        0.20
      4000.        0.205
     10000.        0.21
     40000.        0.215
    100000.        0.22
    200000.        0.4
    300000.        0.45
    500000.        0.45
    800000.        0.25
   1000000.        0.23
   4000000.        0.25
  10000000.        0.27
'
' iprono   cprpdi   npudsc   strou
     2     Strou_02  16       -1.
'     reynum      strnum
        40.        0.1
       100.        0.18
       200.        0.19
       400.        0.195
      1000.        0.20
      4000.        0.205
     10000.        0.21
     40000.        0.215
    100000.        0.22
    200000.        0.4
    300000.        0.45
    500000.        0.45
    800000.        0.25
   1000000.        0.23
   4000000.        0.25
  10000000.        0.27
'
' iprono   cprpdi   npudsc   strou
```

```
     3     Strou_03  16       0.27
'     reynum      strnum
        40.        0.1
       100.        0.18
       200.        0.19
       400.        0.195
      1000.        0.20
      4000.        0.205
     10000.        0.21
     40000.        0.215
    100000.        0.22
    200000.        0.4
    300000.        0.45
    500000.        0.45
    800000.        0.25
   1000000.        0.23
   4000000.        0.25
  10000000.        0.27
'
' ------------------------------------------------------------
'
     PROPERTY ADDED MASS
' nadcur
    3
' iprono   cprpid    nampt
     1     Admas_01   12
' fhat   addmco
   0.0    -0.6
   0.15   -0.6
   0.16   -0.3
   0.17    1.7
   0.18    2.0
   0.2     2.2
   0.21    2.0
   0.24    1.7
   0.27    1.5
   0.33    1.2
   0.40    1.0
   0.5     1.0
'
' iprono  cprpid    nampt
     2    Admas_02    10
' fhat   addmco
   0.0    -0.4
   0.16   -0.2
   0.17    1.5
   0.18    2.0
   0.2     2.2
   0.21    2.0
   0.24    1.7
   0.27    1.5
   0.33    1.2
   0.5     1.2
'
'iprono  cprpid    nampt
    3    strakes     4
'fhat    addmco
   0.08    2
   0.2     2
   0.5     2
   0.95    2
'
' ------------------------------------------------------------
'
     PROPERTY EXCITATION COEFFICIENT
' nlct01   nlct02
    1        1
' iprono   cprpid     nlcpt
```

```
    1     Test_211    17
' fhat     acl0   aclmax    clmax   cla0
   0.120   0.200   0.100   0.100   0.050
   0.125   0.400   0.200   0.100   0.060
   0.135   0.500   0.270   0.100   0.080
   0.140   0.550   0.350   0.140   0.110
   0.150   0.600   0.450   0.200   0.180
   0.160   0.700   0.500   0.350   0.240
   0.165   0.800   0.500   0.500   0.300
   0.170   0.900   0.430   0.800   0.400
   0.175   0.820   0.400   0.700   0.200
   0.180   0.780   0.400   0.500   0.150
   0.185   0.750   0.400   0.550   0.160
   0.190   0.650   0.400   0.600   0.170
   0.200   0.580   0.380   0.650   0.200
   0.210   0.550   0.350   0.600   0.250
   0.250   0.400   0.200   0.350   0.200
   0.300   0.200   0.100   0.200   0.150
   0.310   0.180   0.090   0.100   0.150
'--------------------------
' Strakes15D AIMS
' iprono cprpid     nft02
   4  STK15D    14
' fhtyp2   npoint
  0.33       8
'  ad     cl
  0       0
  0.100   -0.390
  0.200   -1
  0.300   -1.85
  0.390   -2.94
  0.490   -4.25
  0.600   -5.80
  0.700   -7.58
'
' fhtyp2   npoint
  0.250       8
'  ad     cl
  0   0
  0.100   -0.270
  0.200   -0.640
  0.300   -1.12
  0.390   -1.70
  0.490   -2.39
  0.600   -3.18
  0.700   -4.08
'
' fhtyp2   npoint
  0.20     8
'  ad     cl
  0   0
  0.100   -0.240
  0.200   -0.530
  0.300   -0.870
  0.390   -1.26
  0.490   -1.71
  0.600   -2.20
  0.700   -2.75
'
' fhtyp2   npoint
  0.16670       8
'  ad     cl
  0   0
  0.100   -0.210
  0.200   -0.440
  0.300   -0.710
  0.390   -1.01
  0.490   -1.34
```

```
  0.600   -1.70
  0.700   -2.10
'
' fhtyp2   npoint
  0.14290       8
'  ad     cl
  0   0
  0.100   -0.170
  0.200   -0.360
  0.300   -0.590
  0.390   -0.850
  0.490   -1.14
  0.600   -1.47
  0.700   -1.83
'
' fhtyp2   npoint
  0.1250        8
'  ad     cl
  0   0
  0.100   -0.190
  0.200   -0.400
  0.300   -0.630
  0.390   -0.880
  0.490   -1.16
  0.600   -1.46
  0.700   -1.79
'
' fhtyp2   npoint
  0.1110        8
'  ad     cl
  0   0
  0.100   -0.190
  0.200   -0.390
  0.300   -0.600
  0.390   -0.830
  0.490   -1.08
  0.600   -1.33
  0.700   -1.61
'
' fhtyp2   npoint
  0.10        8
'  ad     cl
  0   0
  0.100   -0.180
  0.200   -0.360
  0.300   -0.550
  0.390   -0.740
  0.490   -0.940
  0.600   -1.15
  0.700   -1.36
'
' fhtyp2   npoint
  0.09090       8
'  ad     cl
  0   0
  0.100   -0.150
  0.200   -0.310
  0.300   -0.480
  0.390   -0.660
  0.490   -0.840
  0.600   -1.03
  0.700   -1.23
'
' fhtyp2   npoint
  0.08330       8
'  ad     cl
  0   0
  0.100   -0.110
```

```
  0.200   -0.230
  0.300   -0.370
  0.390   -0.530
  0.490   -0.700
  0.600   -0.890
  0.700   -1.09
'
' fhtyp2   npoint
  0.07690       8
'  ad     cl
  0   0
  0.100   -0.0700
  0.200   -0.160
  0.300   -0.270
  0.390   -0.410
  0.490   -0.560
  0.600   -0.740
  0.700   -0.930
'
' fhtyp2   npoint
  0.07140       8
'  ad     cl
  0   0.0100
  0.100   -0.0300
  0.200   -0.0900
  0.300   -0.180
  0.390   -0.300
  0.490   -0.450
  0.600   -0.620
  0.700   -0.820
'
' fhtyp2   npoint
  0.06670       8
'  ad     cl
  0   0.0100
  0.100   -0.0200
  0.200   -0.0800
  0.300   -0.150
  0.390   -0.260
  0.490   -0.380
  0.600   -0.530
  0.700   -0.710
'
' fhtyp2   npoint
  0.06250       8
'  ad     cl
  0   0.0100
  0.100   -0.0500
  0.200   -0.120
  0.300   -0.210
  0.390   -0.300
  0.490   -0.400
  0.600   -0.510
  0.700   -0.630
'--------------------------
'
' ------------------------------------------------------------
'
    RESPONSE ANALYSIS PARAMETERS
'
'   reldam gives damping as fraction of critical damping
'
'   reldam   iopfrc    iprint
    0.01     1         1
'
'   ifrit    maxitr    ilim    conlim
     1        30        1      0.0001
'
```

```
'   ioptsh   nuddf
      1       0
'
' ------------------------------------------------------------
'
    VIVRESPONSE FATIGUE DAMAGE
'   nsect   npcs   ioppr   tslen   dt   irsno   tsioppr   chtsprn
    0       4      0        0      0     31415     0
'   dscfa   dscfy   dscfz  asi     wsti    thi     rfact
    1.0     1.0     1.0    0.0      0.0    0.0      0.001
'
' NOTE: rfact scales stresses from kPa (STAMOD) to MPa for
'       fatigue analysis using SN curves
'
'
'    Select SN curves for calculation
'
'    nofc
     1
'    chidsn    chidsn
     SNC01
'
'
'    SN curve data
'    nofc
     1
'    chidsn    nosl    limind    fatlim    tref    kexp
     SNC01     1       0         0         0.0     0.0
'    rmi1      rci1
     3.0       11.63
'
'------------------------------------------------------------
'
    VIVANA RESULT PRINT
'
'   iprelf    iprstr    iprdrg    iprrsp    iprcng
       1         1         1         1         1
'
'------------------------------------------------------------
'
    VIVANA RMPF PRINT
'
'   iprcrv
      1
'
'------------------------------------------------------------
      END
_
```